École des Ponts

ParisTech

2023

# Projet de Fin d'Études


Département Génie Civil et Construction

Theodora Grosomanidi

Elève ingénieur, double diplôme

Tuteur professionnel : Will Laufs

Tuteur académique : Daniel Weisz-Patrault


# Modular free-form system for immersive entertainment spaces - Structural study of 3D printed metal connector nodes


Projet réalisé au sein de Laufs Engineering Design LLC

46-01 5th St Long Island City, New York NY 11101, USA

March 1, 2023 - August 31, 2023

# Acknowledgements

I would like to acknowledge and give thanks to my supervisor Will Laufs, who made this thesis possible. I would like to thank my academic advisors Professor Charis Gantes from NTUA and Professor Daniel Weisz-Patrault from ENPC for their support and guidance throughout this research project.

I would also like to express my appreciation for the support and patience of my colleagues at the office, with special thanks to Alexey Nefedov for his willingness to answer my numerous questions and share his knowledge.

Last but not least, I would like to thank my family, without whose support I would not be here today.

# Abstract

This report summarizes the study carried out on the design of the nodes of a digital theater space truss dome, as well as the study of variations on the possible attachment methods of the interior insulation panels and loudspeakers to the main structure. This work was completed in the New York office of Laufs Engineering Design within a six-month period.

The missions entailed first doing research on the different typologies of domes and nodes (Mero, Triodetic, Stamped, Unistrut, etc.) with the aim to gain understanding of their pros and cons. Then developing the sub frame structure supporting the insulation panels and studying different variations to connect to the main structure (existing or new). Also, the global model of the dome theater geometry was analyzed. Finally, the new node geometry has been studied in detail and verified structurally under the loads from the global model.

This thesis shows an original node design for space trusses, tested for the requirements of the Limes360 digital theater. It focuses on the node's verification and lastly its weight optimization within the capacity of the FEM software used. Finally, the required 1:1 testing was not available to be performed during the time of the thesis, but it is necessary and will be done before the construction phase of the project.

Keywords: steel, nodes, freeform dome, space truss, attachment details

# Résumé

Ce document présente une vue d'ensemble analytique de certaines parties et détails de la conception de Limes360. Limes360 est un espace de spectacle numérique avec plusieurs configurations de taille en fonction de la typologie de la scène du théâtre. Il est composé d'une structure en treillis métallique 3D avec une surface de projection intérieure courbe connectée en forme de dôme libre. Les dimensions approximatives de la structure varient : longueur = 10 à 40 m, largeur = 10 à 40 m, hauteur = 10 à 30 m. L'objectif de ce PFE est la conception et le développement des nœuds métalliques pour un treillis spatial modulaire de forme libre, y compris une étude de leur comportement structurel pour les configurations de géométrie de treillis variables.

En premier lieu, différentes typologies de géométries de dômes et de nœuds de treillis 3D sont présentées dans le but de gagner en compréhension de leurs avantages et inconvénients. Ensuite, différentes variations géométriques pour le système global ont été étudiées en ce qui concerne la connexion de la "peau" intérieure à la structure principale, ainsi que les techniques et méthodes appropriées de systèmes de liaison. Ensuite, après un retour à l'analyse globale du dôme et l'obtention des résultats, nous nous concentrons sur l'analyse par éléments finis des nœuds, les schémas de contraintes et les déformations observées. Enfin, nous proposons une optimisation de la forme du nœud basée sur les schémas de contraintes observés et l'utilisation de chaque zone.

**Cadres spatiaux et dômes**

L'un des avantages les plus importants d'une structure en treillis spatial est son poids léger. Cela est principalement dû au fait que le matériau est réparti spatialement de manière à ce que le mécanisme de transfert de charges soit principalement axial, en traction ou en compression. Par conséquent, tout le matériau dans un élément donné est utilisé à sa pleine mesure. Les unités des treillis spatiaux sont généralement produites en série en usine afin de tirer pleinement parti d'un système de construction industrialisé. Les treillis spatiaux peuvent être construits à partir d'unités préfabriquées simples, qui sont souvent de taille et de forme standard. De telles unités peuvent être facilement transportées et assemblées rapidement sur site par une main-d'œuvre semi-qualifiée. Par conséquent, les treillis spatiaux peuvent être construits à moindre coût.

Bien que les géométries de grille carrée et radiale (ou des combinaisons de celles-ci) soient parfois utilisées dans les dômes, la géométrie en surface du dôme doit toujours être entièrement triangulée afin de tirer pleinement parti de l'action en coque rigide. Un dôme avec des motifs carrés à la surface entraînera généralement une structure plus lourde. Par conséquent, les motifs triangulés sont plus efficaces.

*Dômes nervurés* : Les dômes nervurés sont le premier type de dômes renforcés qui ont été construits. Un dôme nervuré se compose d'un certain nombre de solides goussets ou treillis

méridiens identiques, interconnectés au sommet par un anneau de compression. Les nervures sont également reliées par des anneaux concentriques pour former des grilles en forme de trapèze. Le dôme nervuré est généralement renforcé par un anneau de tension en acier ou en béton armé à sa base.

*Dôme en dentelle* : Cette géométrie est générée à partir d'une grille triangulaire uniforme coupée pour créer une forme de dodécagone, puis étirée pour former un cercle, et enfin enroulée sur la surface de révolution. La géométrie résultante est structurellement efficace. Elle maintient également des triangles presque équilatéraux et a une base uniforme.

*Dômes lamellaires* : Les dômes lamellaires sont générés avec des anneaux concentriques, où chaque anneau suivant est tourné d'un demi-module. Cela réduit la longueur des tubes de l'anneau à mesure que la géométrie progresse vers le sommet. Lorsque les tubes des anneaux deviennent horizontaux, ils forment une sorte de clé de voûte à l'intérieur du dôme. Les dômes lamellaires sont généralement couronnés par un anneau de compression.

*Kiewitt* : Les dômes Kiewitt sont également générés avec des anneaux concentriques. La génération commence à partir de la base avec un nombre spécifique de divisions rendant les modules d'une longueur raisonnable. Ensuite, les anneaux suivants réduisent le nombre de divisions du nombre de segments dans le dôme. Généralement, le nombre de segments est compris entre 5 et 8. Comme pour les dômes à lamelles, les anneaux de Kiewitt horizontaux permettent un contrôle facile pendant la construction, mais le motif donne lieu à beaucoup plus de pièces différentes.

*Géodésique* : Un « dôme géodésique » dépose un certain nombre de points sur la surface d'une sphère et les relie par des lignes droites pour définir un polyèdre. Ces lignes sont des approximations des « courbes géodésiques » qui relieraient les points. La géométrie géodésique comporte des triangles presque équilatéraux.

*Schwedler* : Cette géométrie est générée en disposant les éléments principaux le long des méridiens et des anneaux, puis en introduisant des diagonales pour trianguler les modules rectangulaires. C'est facile à générer, mais pas très efficace. Les éléments diagonaux sont nettement plus longs que les barres annulaires ou méridiennes et doivent donc être plus robustes pour résister au flambement.

Couches structurelles

La couche structurelle affecte les nœuds dans le sens où elle détermine l'angle selon lequel les éléments s'y connectent. Chaque typologie de nœud, comme nous le verrons dans la partie suivante, possède un angle de connexion minimum/maximum.

- Les géométries monocouches sont utilisées pour les portées modérées, pour les applications architecturales et pour les applications à longue portée lorsqu'elles sont utilisées avec des tubes ovales ou rectangulaires.

- Les géométries de treillis à double couche sont utilisées chaque fois qu'il y a des charges importantes ou concentrées, des supports de colonnes ou pour des portées extrêmement longues.
- Les géométries de couches Vierendeel peuvent être utilisées pour la plupart des dômes. Il s'agit de treillis à double couche avec des nœuds parallèles dans chaque couche reliée à des poteaux perpendiculaires à la surface du dôme.
- Les géométries de couches nervurées sont également utilisées dans les dômes. Ils sont faciles à installer car la plupart des travaux d'assemblage peuvent être effectués au sol et mis en place.

Dômes de forme libre

Les dômes de forme libre offrent tous les avantages des dômes circulaires, mais avec un plan non circulaire et des supports irréguliers. En utilisant la résistance inhérente des surfaces doublement courbées, les dômes de forme libre peuvent dégager des portées allant jusqu'à 1000 pieds (300 m) et sont souvent conçus pour être la structure la plus légère pour couvrir une zone de forme libre spécifique. En tant que dômes circulaires, les dômes de forme libre peuvent avoir des motifs en surface lamellaire, de Kiewitt ou de dentelle et des couches structurelles simples ou doubles. Là où les dômes de forme libre diffèrent des dômes circulaires, c'est dans leur forme générale. Le dôme Limes360 appartient à cette catégorie.

**Nœuds de treillis 3D**

Les nœuds d'une ferme spatiale sont très importants car ils peuvent représenter 30 % du coût de la structure. Les joints doivent être solide et rigide, simple structurellement et mécaniquement, et pourtant facile à fabriquer. L'excentricité au niveau d'un joint doit être réduite au minimum, mais les détails du joint doivent prévoir les tolérances nécessaires qui peuvent être requises lors de la construction. Enfin, les joints des cadres spatiaux doivent être conçus pour permettre un entretien facile et efficace. Un système préfabriqué réussi nécessite des joints qui doivent être répétitifs, produits en série, simples à fabriquer et capables de transmettre toutes les forces dans les éléments interconnectés au niveau du nœud.

Certaines des conceptions de nœuds les plus utilisées et les plus réussies sont les suivantes :

- Méro
- Triodétique
- Estampillé
- Unistrut

LaufsED a développé deux conceptions de nœuds originales. Une option est un nœud composé de trois parties distinctes serrées ensemble par l'élément latéral passant par le milieu. Les éléments sont à nouveau des sections creuses circulaires. Les extrémités sont des formes coniques solides soudées aux membres. Ce nœud facilite la fixation des panneaux plus facilement. Il ne nécessite pas l'utilisation de fixations supplémentaires, mais simplement un

écrou bloquant le tout en place. Il est adapté aux fermes double couche et peut s'adapter à différents angles. Pour ces raisons, c'est la solution qui a été choisie pour le dôme Limes360.

La raison pour laquelle nous envisageons la possibilité de l'impression 3D en acier dans ce projet est que chaque nœud a une géométrie différente en fonction de sa position dans le dôme. Au total il y a environ 1500 pièces mais elles sont différentes car les angles changent. L'impression 3D permettrait également d'introduire un niveau de porosité dans les zones peu utilisées, et ainsi d'économiser de la matière. La tolérance géométrique générale d'impression est généralement de +/- 0,1 mm mais peut varier selon l'imprimante. En impression 3D métal, le coût reste constant quel que soit le volume. Il ne s'agit pas de la méthode de fabrication la plus rentable pour tous les volumes : pour des volumes élevés, la plupart des autres processus de fabrication sont nettement plus abordables. Cependant, pour une part importante de la production en volume faible à moyen, l'impression 3D métal peut être le moyen le plus abordable de fabriquer des pièces. Pour la majorité des processus de fabrication, une complexité accrue signifie un coût supplémentaire. Pour l'impression 3D métal, ce n'est pas le cas. Le coût dépend de la taille des pièces plutôt que de leur complexité. En résumé, il est difficile de déterminer avec ces seules informations générales si la fabrication additive est la meilleure solution pour notre projet. Une étude du marché plus détaillée, incluant une communication avec les fabricants, serait nécessaire pour comparer les coûts et le temps requis pour produire toutes les pièces.

**Étude de connexion du revêtement Limes360**

L'une des premières tâches consistait à proposer schématiquement différentes idées d'attachement. Les dimensions supposées des panneaux sont de 2,4m x 2,4m, déterminées par la portée maximale du matériau isolant. La composition du panneau est constituée de mousse de verre acoustique (granulés de verre expansé 500 kg/m$^3$) de 25 mm d'épaisseur et d'une couche de plâtre cellulosique pulvérisé de 3 à 5mm. Le panneau est collé avec du silicone ou des vis sur la sous-structure (sub-frame). Le poids de l'isolant est de 0,125 kN/m$^2$ et le poids de l'enduit supposé mouillé de 0,05 kN/m$^2$. Ici, l'isolation la plus lourde en verre mousse est prise en compte (0,125 kN/m$^2$). L'équipe d'architecture avait une autre option, l'isolant PET (composition de polymères) qui pèse environ 200 kg/m$^3$. L'analyse est faite pour le cas le plus lourd.

Les différentes variantes prises en compte pour le développement des fixations sont les inclinaisons de 0 degré, 45 degrés et 90 degrés, la position de l'enceinte, les points de fixation au cadre principal ou au mur. La structure des panneaux comporte des sections en T en aluminium afin de maintenir son poids autour de 23 kg total en limitant les déflexions à 1-2 mm.

**Analyse globale du dôme**

Le dôme étudié mesure 38m (longueur) x32m (largeur) x16m (hauteur), et il est constitué d'une double couche décalée de 1m. La typologie des dômes ne correspond exactement à aucune de celles existantes. Il est similaire au type lamellaire et au Schwedler.

Analyse statique

La section des membrures est une section HSS (Hollow Structural Section) circulaire de 60 mm de diamètre et 4,1 mm d'épaisseur en aluminium 6060 T6. Étant donné que l'emplacement exact du dôme n'est pas déterminé car il est destiné à être construit n'importe où (à l'intérieur à priori), certaines hypothèses générales de charge ont été faites concernant la pression du vent et le poids des panneaux acoustiques :

- Charge du vent (directions x,y) : 0,10 kPa
- Charge permanente : 0,20 kPa

Les efforts internes observés dans le pire des cas pour l'état limite ultime (1,35G+1,5Wy) sont de 5,83 kN de traction et de 15,53 kN de compression. Comme prévu, nous constatons les valeurs de tension les plus élevées sur les éléments de l'anneau horizontal, qui sont activés lorsque le dôme tente de s'ouvrir vers la base. Les valeurs de compression les plus élevées sont observées au niveau de l'anneau supérieur et à la base aux méridiens, en particulier là où se trouvent les ouvertures de porte.

**Analyse structurelle des nœuds de treillis 3D**

L'analyse par éléments finis a été réalisée pour les nœuds de treillis 3D. Les résultats ont montré les déformations et les schémas de contraintes dans les nœuds. Ces résultats ont été utilisés pour optimiser la forme des nœuds afin de minimiser les contraintes locales et d'améliorer la performance structurelle globale.

Hypothèses de modélisation

Le nœud est composé de trois parties distinctes. Ils partagent des points communs (nœuds) dans la zone centrale mais sont décalés les uns des autres au niveau du périmètre extérieur d'une distance de 0,5 mm. Le nœud a été modélisé de cette façon car près du centre, les trois parties sont maintenues ensemble (comprimées) par le boulon précontraint, elles sont donc en plein contact. Près des bords, l'effet de la prétension du boulon est moins important donc si un élément est en tension, il est probable que le nœud s'ouvre et que les différentes pièces se détachent les unes des autres. Idéalement, les interfaces devraient être modélisées comme un solide de contact mince qui ne peut transférer que la compression (pas de tension) et présente le frottement matériel approprié. Dans le logiciel utilisé pour cette étude (RFEM) par contre, les surfaces de contact non planes ne peuvent pas être modélisées, c'est la raison pour laquelle la technique de modélisation précédente a été suivie.

Les supports de surface sont situés autour de la zone de contact de la tige centrale. Mais en réalité, les conditions de support du nœud sont plus complexes que cela. Le nœud n'est pas seulement soutenu par la tige centrale, il est également soutenu par tous les éléments qui s'y connectent, et la direction de support dépend de l'inclinaison du nœud dans le dôme et de l'angle de connexion de chaque élément. Il s'agit essentiellement d'un équilibre où chaque membre joue

un rôle. La condition de support intermédiaire suffira aux besoins de cette analyse car il est nécessaire de disposer de certains supports pour que le modèle fonctionne.

Dans un premier temps, un nœud proche de la base du dôme a été choisi pour être étudié, car dans cette zone nous observons certaines des valeurs de compression les plus élevées. On choisit de partir de là pour comprendre le comportement des contraintes en compression.

Comme nous pouvons le constater, la limite d'élasticité est ici dépassée. Nous pouvons observer à partir de ce cas de chargement que les modèles de contraintes des nœuds sont indépendants par fente de barre. Par conséquent, nous testerons ensuite les emplacements individuels pour les pires scénarios de chargement. On note cependant qu'en réalité, des interactions peuvent se produire dans le nœud même si le modèle 3D n'en montre aucune. C'est pourquoi des tests en laboratoire sont nécessaires en plus de cette analyse.

Sous charge de compression maximale, il est évident que la contrainte dépasse la capacité de l'acier supposée (S235).

Le diamètre total initial de la pointe de l'élément était de 6,69 mm, correspondant à une surface de 35,1 mm2. Cette hypothèse initiale incluait également les coins arrondis. Nous voyons que même en supposant cette plus grande surface, le nœud est surcontraint. En réalité cependant, un contact complet sur les coins arrondis ne peut pas être obtenu. Pour affiner ce calcul et déterminer la surface de contact exacte autour du bord, nous allons utiliser les équations hertziennes et déterminer la surface exacte nécessaire.

Notre pression donnée sous tension est bien inférieure à la capacité d'élasticité, il n'y a donc aucun souci de plastification sous tension dans le nœud. Lorsqu'il est en tension, le nœud sur son interface solide a tendance à s'ouvrir. La déformation correspondante pour la tension de 5,9 kN est de 0,0031 mm, ce qui est négligeable.

D'autres scénarios de chargement incluent les charges de moment et les charges de cisaillement provenant des panneaux. Les cônes des éléments en aluminium ont également été vérifiés en traction et en compression.

Optimisation

Le poids initial du nœud était supérieur à 6 kg, ce qui est très lourd pour la construction du dôme et excessif en termes d'utilisation de matériaux. La zone située entre les cônes n'est utilisée ni en traction ni en compression, une option consiste donc à augmenter la porosité lors de l'impression 3D pour cette zone. Ceci est cependant très difficile à simuler dans le logiciel FE et devrait donc être vérifié par des tests 1:1.

La charge de compression active uniquement la zone autour du centre du nœud. Nous notons que la zone est déjà utilisée à hauteur de 90 % à environ 20 %, donc la réduire davantage créerait des contraintes et des peaks plus élevés.

Comme nous le voyons dans les diagrammes de résultats, la zone entre les cônes n'est pas vraiment utilisée. La longueur actuelle du cône peut également être réduite pour diminuer cette zone inutilisée en raccourcissant les cônes.

Réduire le diamètre de 140,1 mm à 108,1 mm en minimisant la zone autour des côtés du cône ne semble pas avoir d'impact sur les contraintes maximales dues aux charges de traction. Le poids du nœud dans ce cas est réduit de 58% à 2,5 kg.

**Conclusion**

Limes360 est un projet ambitieux qui vise à créer un espace théâtral numérique innovant avec une structure en treillis spatial modulaire. La conception des nœuds de treillis 3D et leur analyse structurelle sont des éléments essentiels de ce projet. Différentes géométries de dômes ont été explorées pour déterminer la plus efficace du point de vue de la performance structurelle et de la légèreté du début. L'analyse par éléments finis des nœuds a permis d'optimiser leur forme pour minimiser les contraintes locales.

Concernant l'analyse nodale, nous pouvons dire que même si la conception initiale du nœud était satisfaisante en termes de géométrie et d'ajustement de l'angle, certains changements étaient nécessaires pour qu'il fonctionne dans ce treillis spatial. L'idée générale du nœud était d'avoir un système simple, sans beaucoup de pièces ni de fixations, et de pouvoir l'assembler rapidement.

Les changements requis impliquent les dimensions de la pointe des fentes du cône où les éléments se connectent et la diminution du diamètre du nœud afin de réduire le poids total à un niveau raisonnable.

Avant de passer à la phase de construction, des tests en laboratoire à grande échelle seraient nécessaires afin de vérifier cette analyse. En effet, un tel produit est innovant, n'a jamais été utilisé auparavant et possède des caractéristiques complexes. Les tests garantiraient donc que le comportement et les limites sont tels que prédits ci-dessus.

Limes360 représente un exemple fascinant de la convergence de l'architecture, de l'ingénierie et de la technologie pour créer un espace de spectacle unique en son genre.

Mots-clés : acier, nœuds, dôme, treillis spatial, détails de fixation

# Table of contents


1. Introduction 16
2. Space frames & domes 16
   2.1 Patterns 16
   2.2 Structural Layers 20
   2.3 Freeform domes 22
   2.4 Methods of Fabrication and Erection 22
3. Nodes 23
   3.1 Mero 26
   3.2 Triodetic 29
   3.3 Stamped 33
   3.4 Unistrut 35
   3.5 PNST (Pin Node Space Truss System) 37
   3.6 Bearing Joints 41
4. Original nodes by LaufsED 42
   4.1 Option 1 42
   4.2 Option 2 45
5. 3D Printing methods 49
   Benefits 50
6. LIMES 360 Cladding Connection Study 51
   Attachment options 55
      Option A.1 55
      Option A.2 57
      Option B.1 59
      Option B.2 63
7. Dome global analysis 72
   7.1 Static Analysis 72
   7.2 Stability analysis 77
   7.3 Preliminary dynamic frequency check 77
8. Nodal analysis 78
   8.1. Modeling assumptions 80
   8.2. First case study - base of dome 80

8.3. Maximum compression case study 81
8.4. Stress distribution patterns 85
8.5. Maximum tension 87
8.6. Case of interior node 89
8.7. Case with moment load 90
9. Member verification 91
10. Optimization 95
11. Environmental self-assessment 99
12. Conclusions 100
References 101
APPENDIX 102
1. Dynamic analysis – 30 first modes 102
2. Temperature loading 107

# Table of figures

Figure 1 : Dome patterns 16
Figure 2: Santa Maria del Fiore - Firenze 17
Figure 3 : Ruwais dome in the UAE 17
Figure 4: Mustafa Center, Singapore 18
Figure 5: Marchwood dome in the UK 18
Figure 6: Montreal Biosphere 19
Figure 7: Gas Reservoir Roof, F.W. Schwedler, Berlin, 1874 19
Figure 8: Dome layers 20
Figure 9: a. Single layer - British Museum 21
Figure 10: b. Double layer - UABJ Arena in Oaxaca, Mexico 21
Figure 11: c. Vierendeel double layer - Mexico City's Velodrom 21
Figure 12: d. Ribbed layer - Heydar Aliyev Cultural Centre 22
Figure 13: Geometry of a freeform dome 22
Figure 14: Assembly on the ground with temporarily pinned joints 23
Figure 15: Table of typologies 26
Figure 16: Mero node 27
Figure 17: Node sections 27
Figure 18: Deformed shape under compression 27
Figure 19: Member critical section 28
Figure 20: Buckling length 28
Figure 21: Annotated values for diameter formula 29
Figure 22: Zaha Hadid's Heydar Aliyev Cultural Centre 29
Figure 23: Triodetic node 30
Figure 24: Plan view and elevation 30
Figure 25: Tear-out critical areas 31
Figure 26: Compressive forces, critical area 31
Figure 27: Inclined force - disk bending 31
Figure 28: Inclined force 32
Figure 29: Photo of triodetic node 32
Figure 30: Stress-strain diagram 33
Figure 31: Twin domes Herradura (70m dia., 35m height) 33
Figure 32: Eccentricity in stamped node 34
Figure 33: Steel spacer 34
Figure 34: Bending moment and deformation 34
Figure 35: Flattened and unflattened cross-sections 35
Figure 36: Forces on bolt 35
Figure 37: Unistrut node 36
Figure 38: Truss with unistrut nodes 36
Figure 39: Unistrut cross-section 36
Figure 40: Plate critical area under tear-off 37
Figure 41: Tension in bolts due to U-channel member 37
Figure 42: PNST node 38
Figure 43: PNST plans and elevations 39
Figure 44: Member cross-sections 39
Figure 45: Tear-off and buckling critical areas 40
Figure 46: Bending of node plate due to member axial force 40
Figure 47: Examples of bearing joints (MERO) 41
Figure 48: Photo of printed node 42
Figure 49: Front and back perspective views of node 43
Figure 50: Elevation and section drawings 43
Figure 51: Member to node connection - section 43
Figure 52: Member tear-off failure - section 44

Figure 53: Node cross sections S1 and S2 44
Figure 54: Moment couple in bolts - section 44
Figure 55: Node tear-off mechanism under member tension - plan view 45
Figure 56: Perspective #1 node and member assembly 45
Figure 57: Perspective #2 node and member assembly 46
Figure 58: Front and side cross-sections of node geometry 46
Figure 59: Member tear-off mechanism under member tension 47
Figure 60: Node tear-off mechanism under member tension - cross section 48
Figure 61: DMLS procedure diagram by Protolabs 50
Figure 62: Cost – Volume diagrams by Markforged 50
Figure 63: Option 1 - elevations and cross sections 51
Figure 64: Option 2 - elevations and cross sections 52
Figure 65: Option 3 - elevations and cross sections 52
Figure 66: Option 4 - elevations and cross sections 53
Figure 67: Corners vs middle alignment 53
Figure 68: Numerical and physical models of the mock-up 54
Figure 69: Schematic diagram of attachment options 55
Figure 70: Cross-sections 55
Figure 71: Panel to existing main structure configurations 56
Figure 72: SLS deflection 1.1mm 56
Figure 73: SLS deflection 1.0mm 57
Figure 74: SLS deflection 1.3mm 57
Figure 75: SLS deflection 9.1mm 58
Figure 76: SLS deflection 1.8mm 58
Figure 77: SLS deflection 6.5mm 59
Figure 78: Panel to space truss configurations 59
Figure 79: SLS deflection 1.8mm 60
Figure 80: SLS deflection 2.1mm 60
Figure 81: SLS deflection 2.0mm 61
Figure 82: SLS deflection 2.2mm 61
Figure 83: SLS deflection 2.3mm 62
Figure 84: SLS deflection 2.5mm 62
Figure 85: SLS deflection 1.5mm 63
Figure 86: SLS deflection 1.6mm 63
Figure 87: SLS deflection 11mm 64
Figure 88: SLS deflection 7.9mm 64
Figure 89: SLS deflection 1.2mm 65
Figure 90: Speaker to node attachment via plates 65
Figure 91: Speaker to node attachment via extended rod 66
Figure 92: Speaker attachment to additional diagonal 66
Figure 93: Details - speaker to additional diagonal attachment 67
Figure 94: Speaker to member attachment 67
Figure 95: Details - speaker to member attachment 68
Figure 96: Vertical configuration 68
Figure 97: Overhead & 45d configuration 69
Figure 98: Overhead configuration 69
Figure 99: Vertical configuration attachment 70
Figure 100: Scaffold clip connection detail 71
Figure 101: Panel to panel connection detail 71
Figure 102: Panel members connections 72
Figure 103: HSS member cross-section 72
Figure 104: Perspective view of dome 73
Figure 105: Internal forces under ULS 1.35G+1.5Wy 73
Figure 106: Deflection 3mm under self-weight 74
Figure 107: Deflection 8.4mm under D+SDL 74
Figure 108: Deflection 8.6mm under D+SDL+Wx 75
Figure 109: Deflection 9.4mm under D+SDL+Wy 75

Figure 110: Member utilization ratios 76
Figure 111: Weld check sketch from EC9 76
Figure 112: RFEM stability analysis results 77
Figure 113: 2nd mode shape - sway in y direction 78
Figure 114: Max and min axial internal forces 79
Figure 115: Load paths for domes 79
Figure 116: Perspective view of model with boundary conditions 80
Figure 117: High compression effect 81
Figure 118: Top compression ring of dome 82
Figure 119: Von Mises stress 82
Figure 120: Rounded edge 82
Figure 121: Spherical contact in cavity 83
Figure 122: Cylindrical contact in cavity 84
Figure 123: New stresses on increased surface 84
Figure 124: Boussinesq's distribution under square load 85
Figure 125: Boussinesq's distribution under circular loaded surface 86
Figure 126: σz stress distribution x-z plane 86
Figure 127: σz stress distribution y-z plane 87
Figure 128: τxz stress distribution 87
Figure 129: Von Mises stresses 88
Figure 130: Deformation under tension 88
Figure 131: Interion layer node 89
Figure 132: Von Mises stresses 89
Figure 133: Point local peaks 90
Figure 134: VM stresses due to 0.02kNm moment 91
Figure 135: Local stress peaks 91
Figure 136: VM stresses under 15.5kN compression 92
Figure 137: Initial and modified cone shape 93
Figure 138: Expansion 93
Figure 139: VM stresses for tension 94
Figure 140: Cross-section in tension 94
Figure 141: VM stresses for cone in tension 95
Figure 142: Initial geometry under tension - VM stresses 95
Figure 143: Geometry under maximum compression 96
Figure 144: 120.1mm diameter node in tension 96
Figure 145: 108.1mm node geometry in tension 97
Figure 146: Initial minimum angle between members 97
Figure 147: 35d angle variation under compression loads 98
Figure 148: 35º angle variation under tensile loads 98
Figure 149: Stresses under 39kN tensile load 99

# 1. Introduction

This document presents an analytical overview of certain parts and details of the design of Limes360.

Limes360 is a digital theater space with multiple size configurations depending on the typology of the theater stage. It is made of a 3D metal grid shell with a connected interior curved projection surface in the shape of a freeform dome. The approximate dimensions of the structure can vary: length= 10 to 40m, width= 10 to 40m, height=10 to 30m. The objective of this PFE is the conception and development of the metal nodes for a free-form modular space truss, including a study of the panels' structural behavior for the varying truss geometry configurations.

As a first step, different typologies of dome geometries and 3D truss nodes are presented for the purpose of gaining insight and understanding of their advantages and disadvantages. Then, different geometrical variations for the global system were studied in terms of the connection of the interior "skin" to the main structure, as well as the appropriate techniques and methods of joining systems. Next, after returning to the global analysis of the dome and obtaining the results we focus on the Finite Element Analysis of the nodes, the stress patterns and deflections observed. Lastly, we propose an optimization of the shape of the node based on the stress patterns observed and the utilization of each zone.

# 2. Space frames & domes

One of the key benefits of a space frame structure lies in its lightweight design. This is predominantly attributed to the way materials are arranged in space, facilitating primary load transfer through axial forces such as tension or compression. As a result, every element within the structure is effectively utilized. Space frame components are typically manufactured in mass production facilities, allowing for efficient utilization of an industrialized construction system. Space frames can be constructed using readily available, standardized prefabricated units, which are often of uniform size and shape. These units can be easily transported and swiftly assembled on-site, even by semi-skilled labor, resulting in cost-effective construction of space frame structures.

Furthermore, the advantage of the space truss is that there is no requirement for bending stiffness in the nodes. The stability of the truss is achieved by the configuration of the members.

## 2.1 Patterns

While square-grid and radial configurations (or a mix of both) are occasionally employed in dome structures, it is crucial to ensure that the internal surface geometry of the dome is fully triangulated to maximize the advantages of shell-like behavior. Opting for square patterns on the dome's surface typically leads to a heavier framework, making triangulated patterns a more efficient choice for achieving desired outcomes.

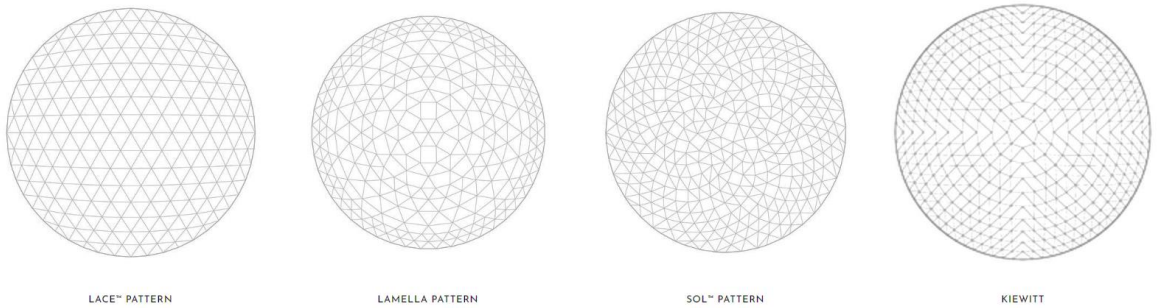


*Figure 1 : Dome patterns*

**Ribbed**: Ribbed domes represent one of the earliest types of braced dome structures. Such a dome is composed of multiple identical meridional solid girders or trusses, linked together at the apex by a compression ring. These ribs are additionally interconnected by concentric rings to create a grid pattern, often taking on a trapezoidal configuration. To enhance its structural rigidity, a ribbed dome typically incorporates a steel or reinforced concrete tension ring at its lowermost part. A classic example of the ribbed dome is Santa Maria del Fiore in Italy.

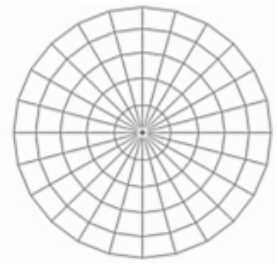

*Figure 2: Santa Maria del Fiore - Firenze*

**Lace**: This geometric configuration is derived by first taking a uniform triangular grid and adjusting it to fit within a dodecagon shape. Subsequently, this modified grid is stretched to assume a circular form and then applied to the surface of a revolution. The resulting geometry exhibits structural efficiency, preserves almost-equilateral triangles, and maintains a uniform base throughout its design. Some of the largest domes in the world, such as the 133 m Ruwais dome in the UAE, the 142m San Cristobal dome in Bolivia, and the 122m JEA domes in Florida, are built with the Lace geometry, or with a lamella-lace combination geometry.

*Figure 3 : Ruwais dome in the UAE*

**Lamella:** Lamella domes are created through the arrangement of concentric rings, where each subsequent ring is rotated by half a module's length. This rotation gradually reduces the length of the ring tubes as the geometry progresses towards the apex. As the tubes of the rings reach a certain diminutive size, typically half the length of the initial tubes, they seamlessly merge with the adjoining ring, uniting the two segments into a single entity. The distance between the rings in Lamella domes can be adjusted to create equilateral triangles within each ring. Because the tubes of every ring are equal, the manufacturing process is swift, and assembly is straightforward. Lamella domes are renowned for their aesthetic appeal and are a preferred choice for various architectural applications.

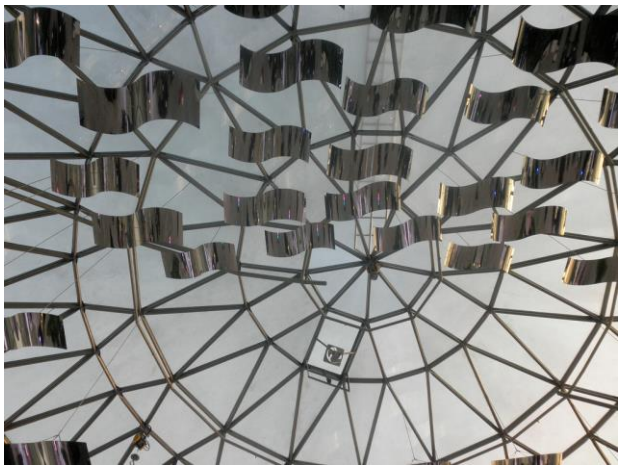

*Figure 4: Mustafa Center, Singapore*

**Kiewitt:** Kiewitt domes, like Lamella domes, employ a concentric ring structure. The process commences at the base with an initial division count, ensuring that module lengths remain manageable. Subsequent rings progressively decrease the division count by the number of segments in the dome, typically ranging between 5 and 8. While the horizontal Kiewitt rings offer a convenient reference point during construction, this approach results in a greater variety of component parts compared to Lamella domes. Kiewitt domes include the 112m Marchwood dome in the UK (32m high).

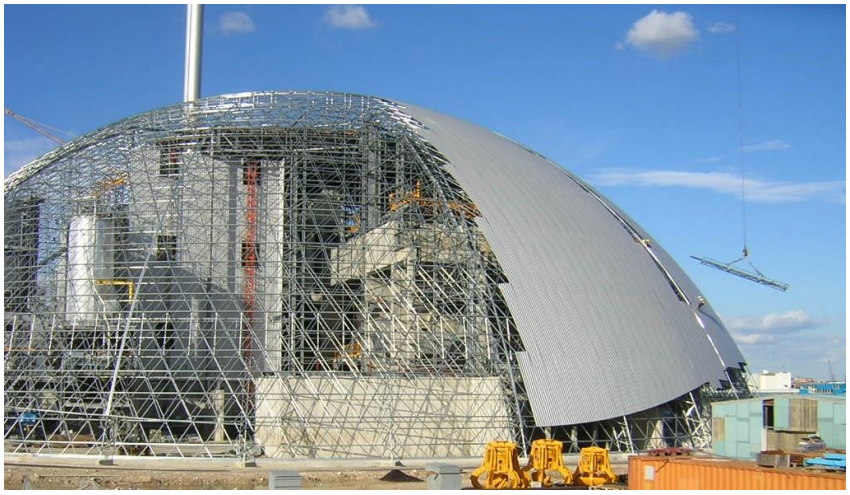

*Figure 5: Marchwood dome in the UK*

**Geodesic:** A "geodesic dome" is constructed by positioning several points on the surface of a sphere and connecting them with straight lines, essentially outlining a polyhedron. These lines serve as approximations to the "geodesic curves" that would naturally connect these points. This geodesic geometry primarily consists of nearly-equilateral triangles and is typically employed in the construction of spherical domes. While R. Buckminster Fuller utilized icosahedrons as the basis for the polyhedron, it's important to note that any other polyhedron, whether regular or irregular in shape, can be employed to create geodesic domes. An example of this dome typology is the Montreal Biosphere, designed by Fuller, boasting a diameter of 76 meters and a height of 62 meters.

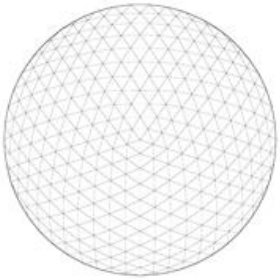

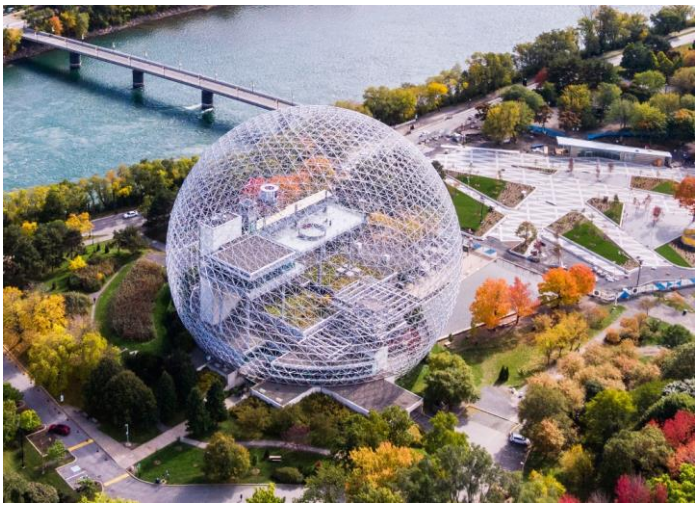

*Figure 6: Montreal Biosphere*

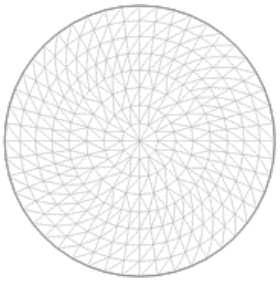

**Schwedler:** This geometric configuration is created by placing primary structural elements along meridians and rings, and subsequently adding diagonal elements to create triangles within the rectangular modules. While it is a straightforward design to produce, it lacks efficiency. Diagonal members in this configuration are considerably longer than the ring or meridian bars, necessitating greater strength to withstand buckling loads. It does find some utility in glass-covered domes, as trapezoidal glazing tends to be more cost-effective than triangular glazing. However, for other applications, this geometry results in structures that are 20 to 30% heavier than those employing alternative geometric configurations.

*Figure 7: Gas Reservoir Roof, F.W. Schwedler, Berlin, 1874*

## 2.2 Structural Layers

The structural layer plays a role in the maximum span of the dome. It also affects the nodes in the sense that it determines the angle by which the members connect to it. Each node typology, as we will see in the following part, has a minimum/maximum connection angle.

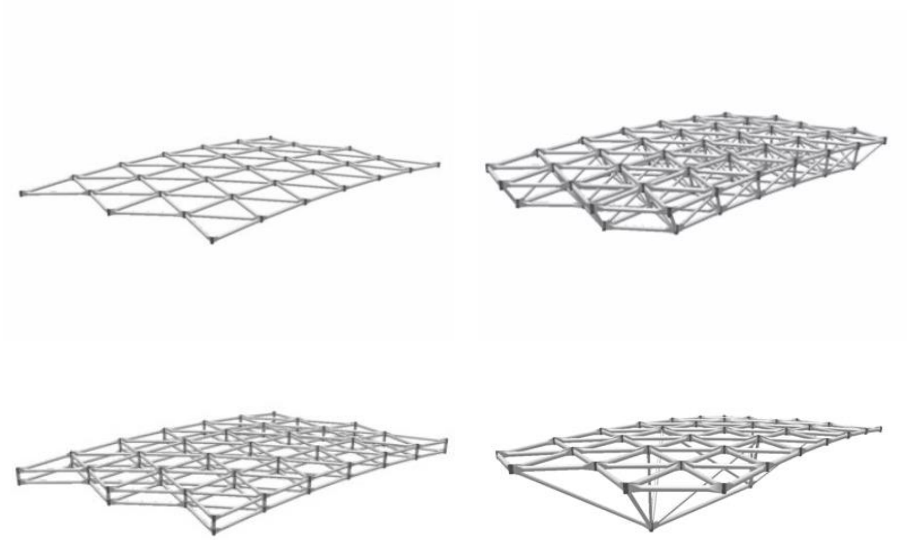

*Figure 8: Dome layers*

**Single layer** configurations are typically employed for moderate spans, architectural purposes, and in cases where long spans are needed and oval or rectangular tubes are utilized.

**Double layer** truss configurations come into play when there are substantial or concentrated loads, the need for column support, or when exceptionally long spans are required.

**Vierendeel layer** configurations can be applied to a wide range of dome designs. These configurations consist of double-layer frames with parallel nodes in each layer, connected by post members perpendicular to the dome's surface. The inclusion of a second layer enhances bending strength and buckling resistance without introducing unnecessary web elements.

**Ribbed layer** configurations also find use in dome construction. They are convenient to install because much of the assembly work can be completed on the ground before being lifted into position. Both double layer truss and ribbed geometries may benefit from increased chord density.

*Figure 9: a. Single layer - British Museum*

*Figure 10: b. Double layer - UABJ Arena in Oaxaca, Mexico*

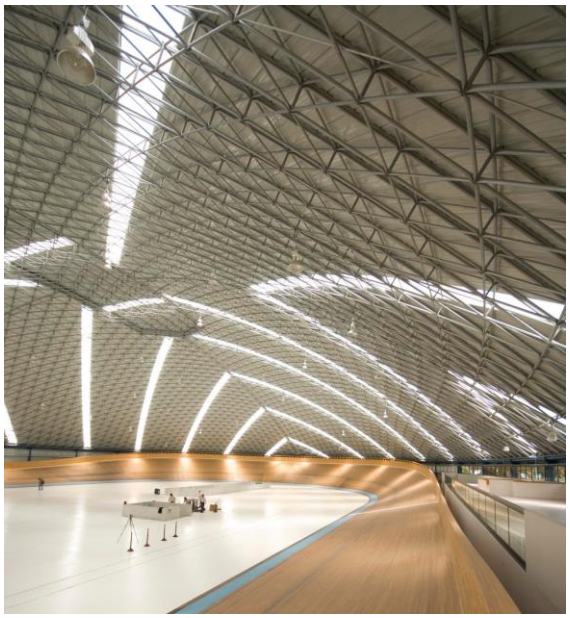

*Figure 11: c. Vierendeel double layer - Mexico City's Velodrom*

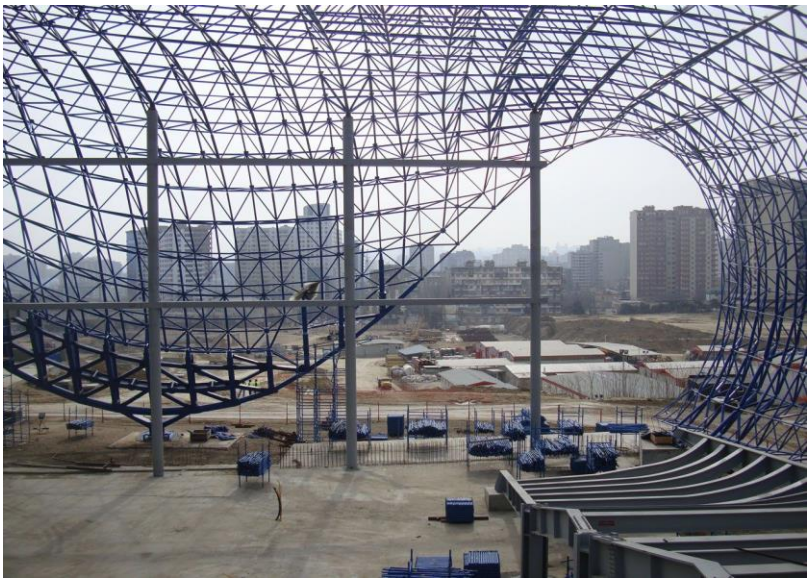

*Figure 12: d. Ribbed layer - Heydar Aliyev Cultural Centre*

## 2.3 Freeform domes

Freeform domes offer the same benefits as circular domes but come with a non-circular layout and irregular supports. Leveraging the intrinsic strength of doubly curved surfaces, freeform domes can span up to 1000 feet (300 meters) and are often designed to be the most lightweight structure for a particular free-form area. Similar to circular domes, freeform domes may feature lamella, kiewitt, or lace patterns on their surfaces and can have either single or double structural layers. The primary distinction between freeform and circular domes lies in their overall shape.

To accommodate the changing perimeter of the dome, the meridian varies as it is assessed from different angles. Additionally, the dome may incorporate an integrated tension ring to withstand the horizontal forces generated by gravitational loads. An example of the freeform dome is Zaha Hadid's Heydar Aliyev Center.

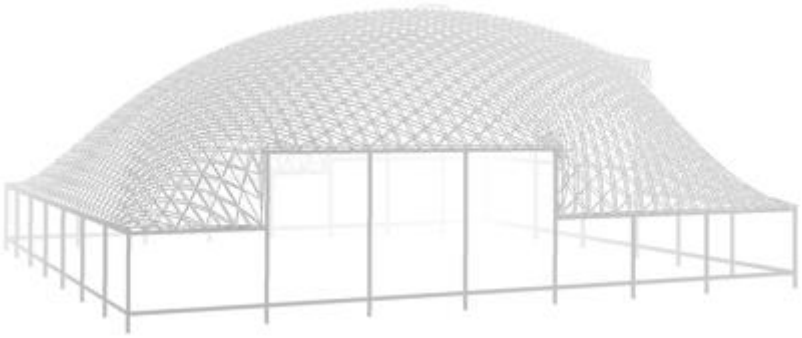

*Figure 13: Geometry of a freeform dome*

## 2.4 Methods of Fabrication and Erection

The methods employed can be classified into three categories as follows:

a. Individual member assembly: This involves raising and connecting separate members one by one to the existing assembly.

b. Sub-assembly installation: At an intermediate stage, members are joined together in sub-assemblies, either in a factory setting or on the site. These sub-assemblies are then lifted into their final positions and connected to the pre-existing structure.

c. Lifting of the entire spatial structure: The complete structure is assembled on the ground at the construction site and is then lifted into place. Various approaches may be considered, including the use of vertical construction components as lifting masts or the utilization of cranes.

The selection of one of these three methods hinges on several factors, including:

- Project Characteristics: This encompasses the type and size of the structure being constructed.
- Operational Considerations: Factors like the actual site layout, available lifting equipment, transportation expenses, and the level of expertise play a pivotal role in the decision-making process.
- Safety: Ensuring the safety of construction operations is of paramount importance.

In cases (a) and (b), it's crucial to anticipate the potential requirement for temporary supports, especially when the structure only attains stability upon completion. Careful assessment of the multiple phases in the erection process is necessary to avoid interim structural behaviors that are less favorable than the final state of the structure.

Hoisting the entire space frame offers several advantages:

- Most of the construction work is conducted on the ground, allowing for better control of the operation, particularly when it comes to welding joints.
- Heavy lifting equipment is required for a shorter duration, potentially leading to reduced overall costs.
- In some scenarios, it's possible to lift the structure along with other attached equipment or components.

The hoisting phase is a critical step in the erection process. Careful consideration should be given to the placement of lifting points. Ideally, lifting should occur under optimal weather conditions, avoiding windy conditions. Once in place, the structure needs to be securely connected to the already erected sections. It's advisable to plan and incorporate precise regulating devices in advance to simplify the connection and fixation process. The lifting phase can significantly influence the overall design of the structure.

A novel approach was implemented in Barcelona for erecting the dome of the Olympic Palace. It involved constructing the dome on the ground in five segments temporarily pinned together. The central portion was then lifted into position, and the remaining dome segments were locked into their final locations.

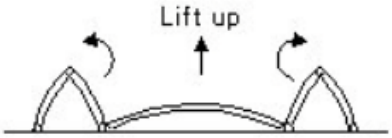


*Figure 14: Assembly on the ground with temporarily pinned joints*

## 3. Nodes

The nodes of a space truss are very important as they can make up 30% of the structure's cost. They must be strong and stiff, simple structurally and mechanically, and yet easy to fabricate. The eccentricity should be kept to a minimum, yet the joint detailing should provide for the necessary tolerances that may be required during the construction. Finally, the nodes of space trusses must be designed to allow for easy and effective maintenance. The cost of their production is one of the most important factors affecting the final economy of the finished structure. Therefore, a successful prefabricated system requires joints that must be repetitive, mass produced, simple to fabricate, and able to transmit all the forces in the members interconnected at the node.

Effective Buckling Lengths

Effective buckling lengths are a crucial consideration for compression members in spatial structures. Members with flattened (crimped or coined) ends, like the Triodetic system, typically exhibit the highest effective length factors for buckling, especially around the crimped areas. Conversely, in spatial structures where members retain their full sections at the nodes, such as when welded ends are employed, the design typically employs the smallest effective length factors. Systems with different end conditions typically fall somewhere between these two extremes.

Therefore, for the three possible cases, the following effective length factors are recommended:

- systems with full section ends (welded ends) k=0.7
- systems with reduced section ends (such as Mero System) k=0.9
- systems with flattened section ends (such as Triodetic System) k=0.95

The following table found in "*Space Frame Structures" Structural Engineering Handbook* by Lan, T.T. summarizes schematically some existing typologies:

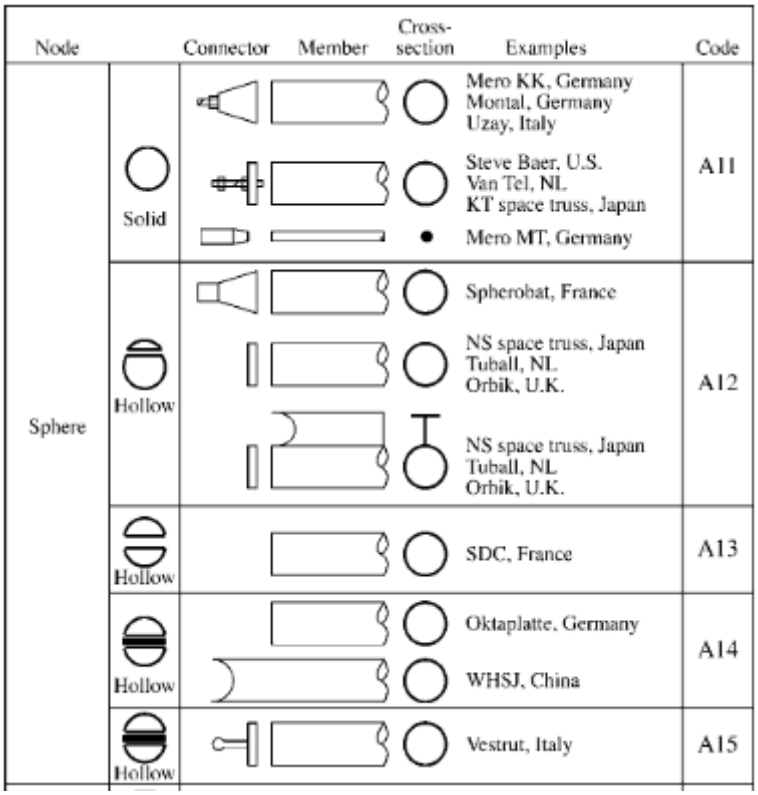

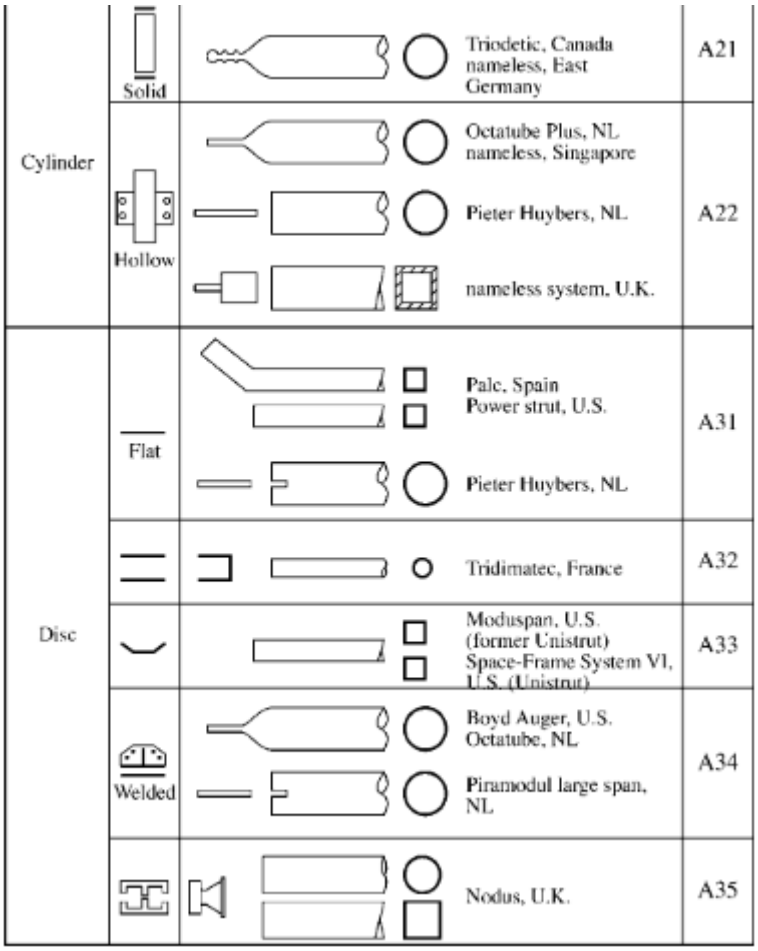


| Node | | Connector | Member | Cross-section | Examples | Code |
|---|---|---|---|---|---|---|
| Prism | Solid | | | | Montal, Germany<br>Mero BK, Germany | A41 |
| | Hollow | | | | Mero TK and ZK, Germany<br>Mero NK, Germany<br>Satterwhite, U.S. | A42 |

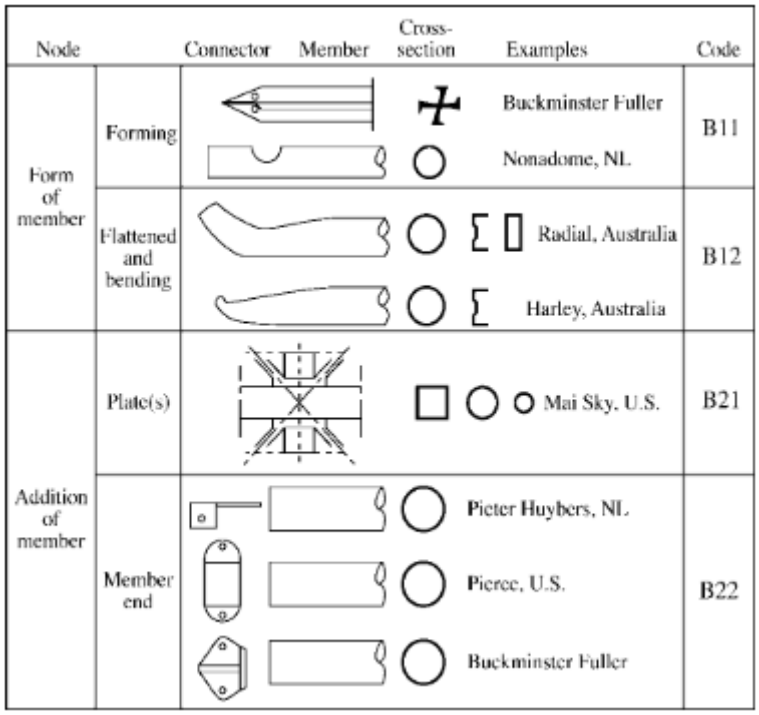


*Figure 15: Table of typologies*

In the following section, we are going to look into more detail some of the most widely used and innovative node designs (Mero, Triodetic, Stamped, Unistrut, PNST).

## 3.1 Mero

Approximately five decades ago, Dr. Mengeringhausen introduced the Mero connector, which swiftly gained widespread popularity and has since been utilized in a multitude of both temporary and permanent structures. This connector comprises a node, which is a spherical hot-pressed steel forging featuring flat facets and threaded holes. The structural members are circular hollow sections, each equipped with cone-shaped steel forgings at their ends to accommodate connecting bolts. Remarkably, a joint can accommodate up to 18 members with no eccentricity. The manufacturer offers nodes in various sizes, ranging in diameter from 46.5 mm to 350 mm, with corresponding bolts spanning from M12 to M64.

The standard node boasts 18 surfaces, positioned at connecting angles of 45, 60, 90 degrees, and their multiples. Meanwhile, the regular node offers 10 surfaces. For more specialized requirements, there are custom nodes with holes positioned at any desired angle, with the caveat that the minimum angle between two adjacent holes is 35 degrees.

The Mero connector has the advantage that the axes of all members pass through the center of the node, eliminating eccentricity loading at the joint. Thus, the joint is only stressed under the axial forces (no bending).

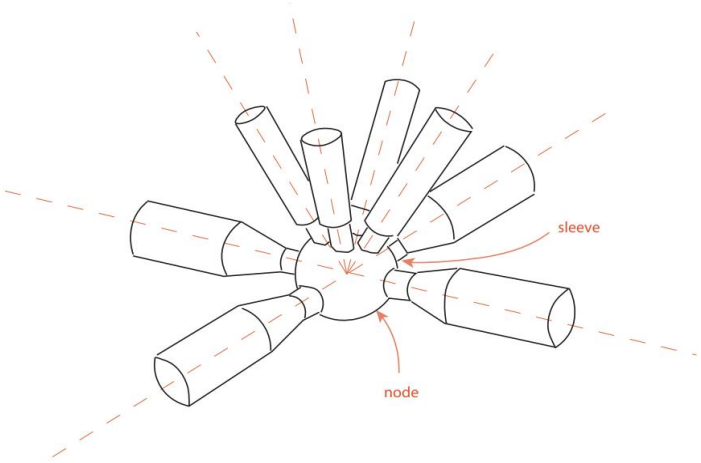


*Figure 16: Mero node*

## TYPES OF FAILURES

Node:

In tension the node may reach its yield or ultimate strength, first on its smaller net sections that are closer to its outer surface (S1) and then towards the center (S2).

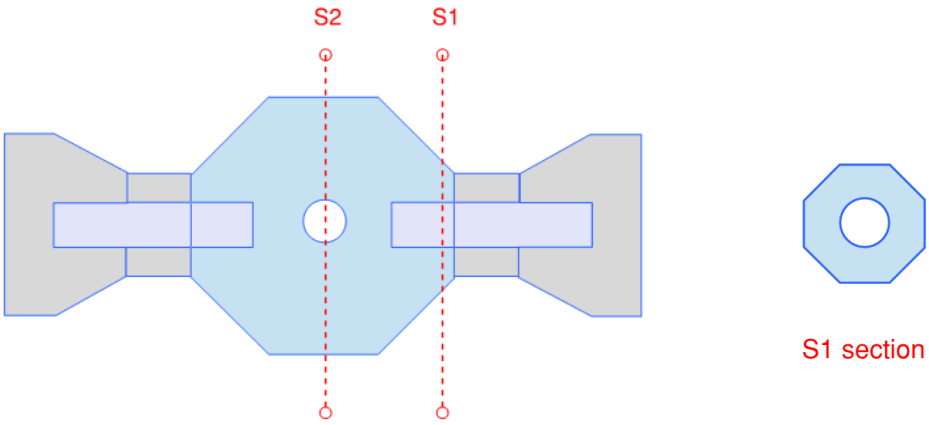


*Figure 17: Node sections*

In compression, the node may reach its yield or ultimate strength also, but it isn't under risk of buckling thanks to its spherical shape. It will deform according to the following shape.

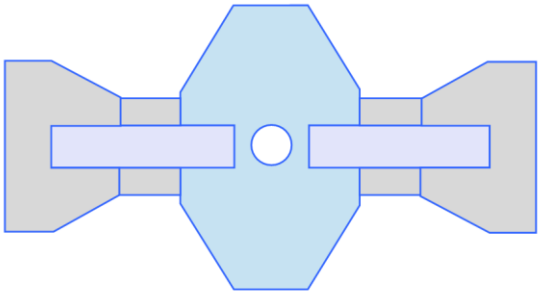

*Figure 18: Deformed shape under compression*

Bolt:

The bolts can work under tension only. Therefore, their diameter should provide sufficient tensile strength.

Members:

Member failure due to tension can occur in the net thinned end of the member, also known as the sleeve (S3).

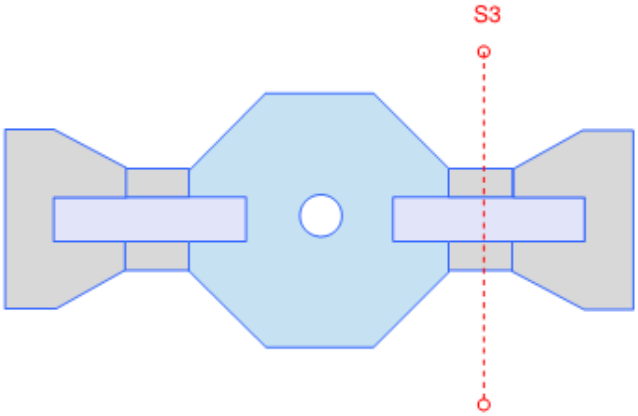


*Figure 19: Member critical section*

Member failure due to compression is also likely to occur in the same area as the member section gets reduced and local buckling is more likely to happen. The buckling length of the entire member is considered almost equal to their actual length as they are 90% hinged on the ends (k=0.90).

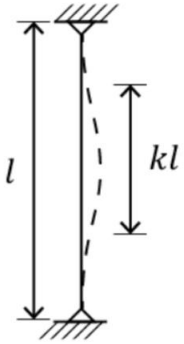


$k = 0.90$

*Figure 20: Buckling length*

DIAMETER

The diameter of a steel node may be determined by the following equation:

$$D \geq \sqrt{(\frac{d_2}{sin\theta} + d_1 ctg\theta + 2\xi d_1)^2 + \eta^2 {d_1}^2}$$

where,

D = diameter of steel ball (mm)
θ = the smaller intersecting angle between two bolts (rad)
d = diameter of bolts (mm)
ξ = ratio between the inserted length of the bolt into the steel ball and the diameter of the bolt
η = ratio between the diameter of the circumscribed circle of the sleeve and the diameter of the bolt

Normally ξ = 1.1 and η = 1.8.

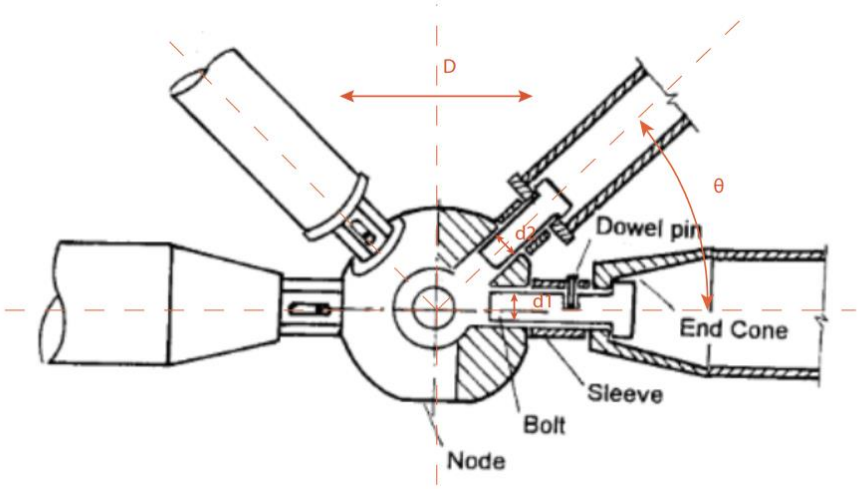


*Figure 21: Annotated values for diameter formula*

*Figure 22: Zaha Hadid's Heydar Aliyev Cultural Centre*

In case of need for member replacement, it is difficult to remove a member as that requires a translative movement on the axis of the member which is blocked by the back node.

In general, the Mero node offers an aesthetically pleasing solution that can be used in various architectural projects, and is easily assembled.

## 3.2 Triodetic

The node designed for the Triodetic system, originating in Canada and credited to Fentiman (see Geometrica reference), is comprised of an extruded connector hub featuring serrated keyways. To complete the node assembly, each member's end is pressed to create a coined edge that securely fits into the hub's keyway. This node is fully assembled when the members are inserted into the hub, washers are positioned at each end of the hub, and a screw bolt is passed through the center of the hub. Remarkably, up to 12 members can be connected to a single hub at a wide range of angles.

In comparison to the Mero system, the Triodetic node comes at a lower cost; however, it has some capability to transfer moments across the joint. Consequently, it becomes possible to affix cladding directly onto the members without requiring an additional supporting structure.

The failure mechanism in this system typically occurs at the thinned section of the members. Furthermore, accessibility to the node for member replacement is relatively straightforward, as members can easily slide out when necessary. Aesthetically it works well in projects.

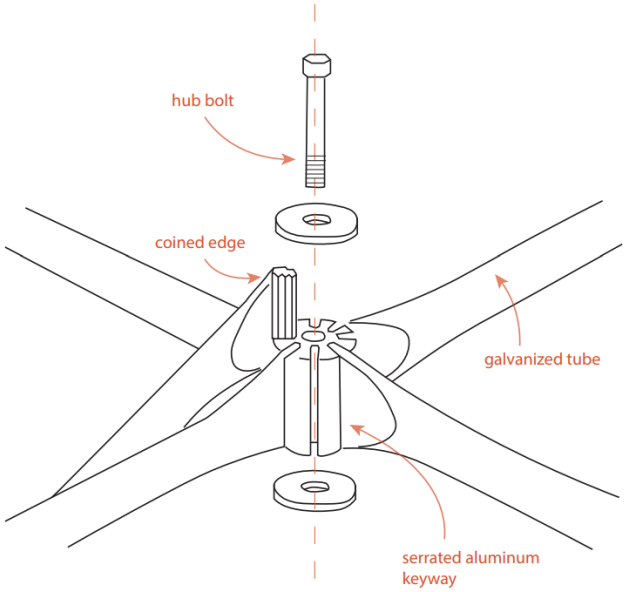


*Figure 23: Triodetic node*

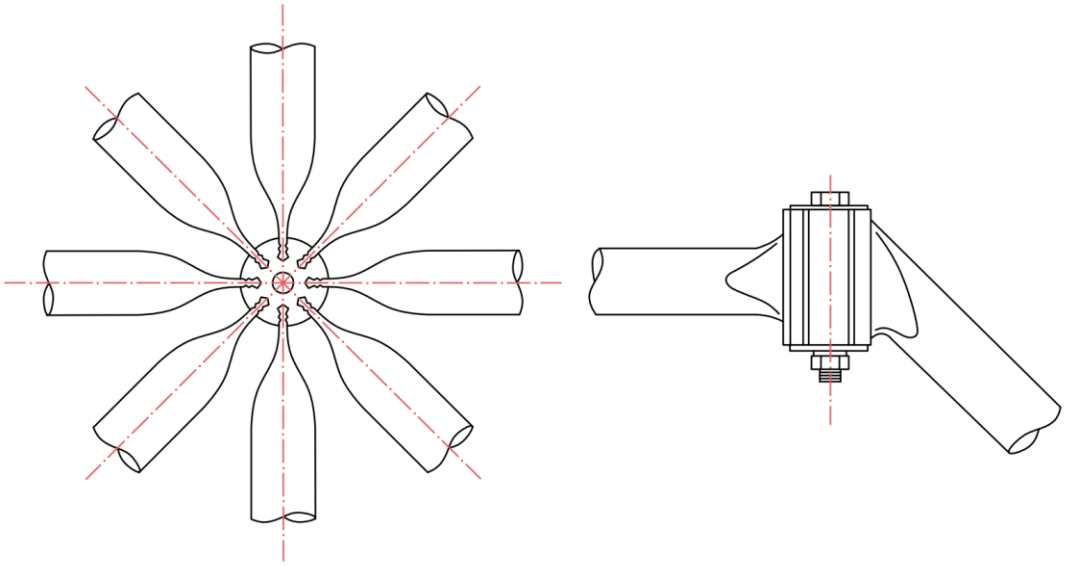

*Figure 24: Plan view and elevation*

## TYPES OF FAILURES

Node:

When a tensile force is applied to the node there is risk of local tear-off of the outer surface of the node holding the coined edge in place (see highlighted zones below). Therefore, the width of those zones needs to be sufficient to withstand the tensile force which causes shear.

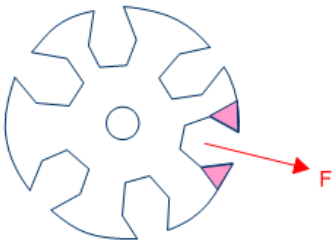


*Figure 25: Tear-out critical areas*

In compression, the inner part of the node may reach the yield or ultimate limit (see highlighted zone below).

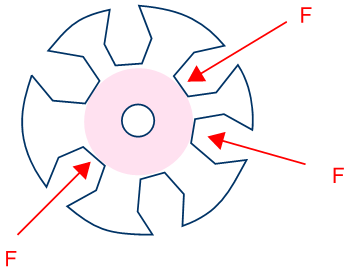


*Figure 26: Compressive forces, critical area*

Disks:

The disks prevent the members from sliding out of the node. Therefore, when the member forces are not in one plan (e.g. inclined members), there is shear applied on the disks as the member tries to slide out. The shear and bending failure can be prevented by having an adequate thickness for the disks that lock the members.

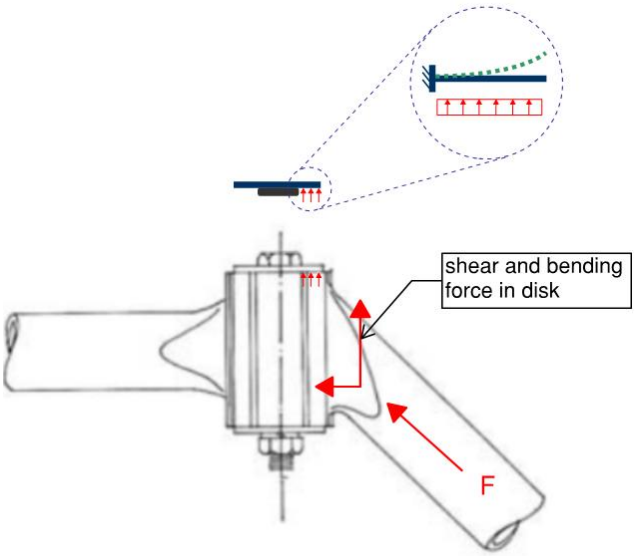


*Figure 27: Inclined force - disk bending*

Bolt:

The bolt can fail in tension when the members are inclined and exercising a pull-out force at the node. If all the members are in a horizontal plan (i.e. 0% inclination), the bolt is not under any stress (other than the self-weight).

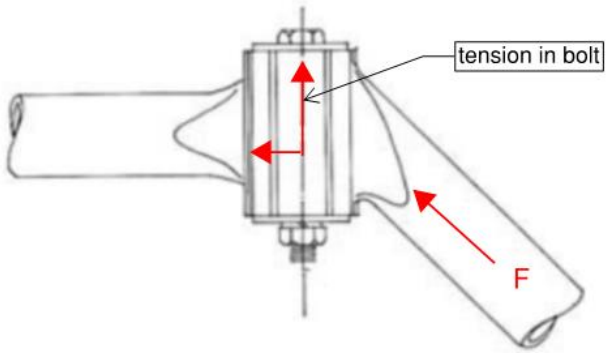


*Figure 28: Inclined force*

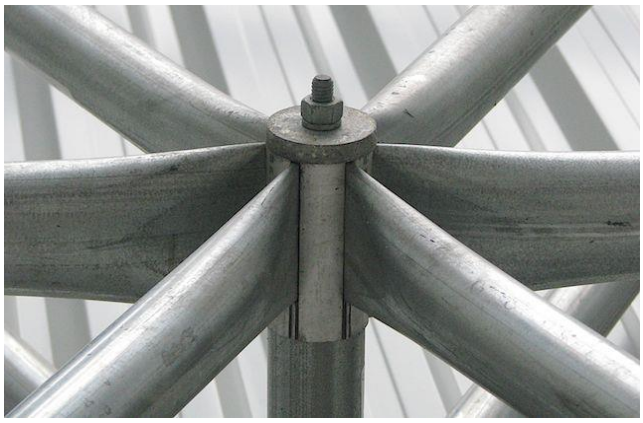

*Figure 29: Photo of triodetic node*

Members:

The members can buckle under compression, especially in their thinned end sections because the moment of inertia there is largely reduced along the vertical axis.

Under tension, the section can reach the yield or ultimate limit if it has not been adequately sized.

It should also be noted that the members' end sections have already plastified (plastic zone of the stress-strain curve) because of the permanent deformation they succumbed while cold pressing them. Therefore, the added load that makes the stress surpass the linear zone will cause even more permanent deformation. In other words, the plastification makes the sections more prone to larger deformations.

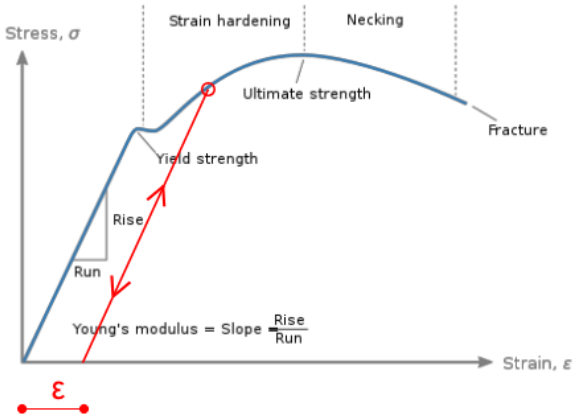


*Figure 30: Stress-strain diagram*

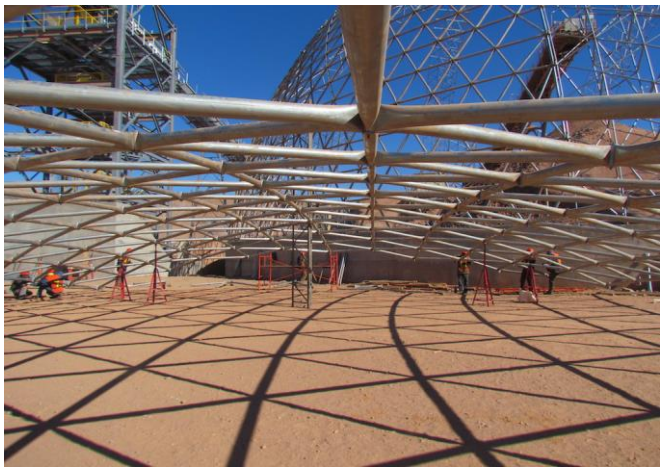

*Figure 31: Twin domes Herradura (70m dia., 35m height)*

## 3.3 Stamped

The primary drawbacks of the stacked end-flattened, often referred to as "stamped," connection are twofold:

1. Nodal eccentricities, denoted as E1 and E2.

2. Section flattening.

However, despite these disadvantages, these connections are widely used in many countries due to their simplicity and cost-effectiveness in manufacturing.

Nodal eccentricity results in the generation of additional bending moments at the ends of the tubular sections, while the end-flattening process reduces the stiffness of the tubes themselves. In this typology, the typical failure mechanism occurs when excessive distortion at the nodes surpasses the buckling limit.

One proposed solution to address the issue of vertical eccentricity involves inserting spacers between the elements, significantly enhancing the node's strength. Nevertheless, architects often refrain from adopting this solution as it may not align with their aesthetic preferences.

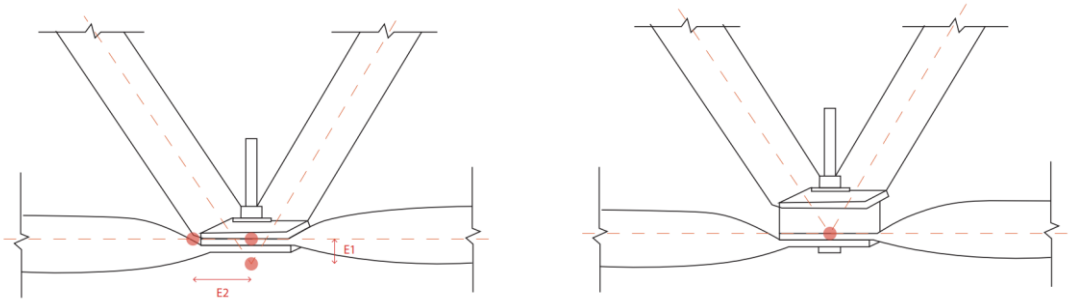


*Figure 32: Eccentricity in stamped node*


*Figure 33: Steel spacer*

## TYPES OF FAILURES

Members:

The members are likely to fail due to buckling in the flattened section (reduced moment of inertia). If there is eccentricity, it creates an additional bending moment to the members which can lead to failure also (see figure below). There is also the risk of tear-off of the ends when a member is in tension.

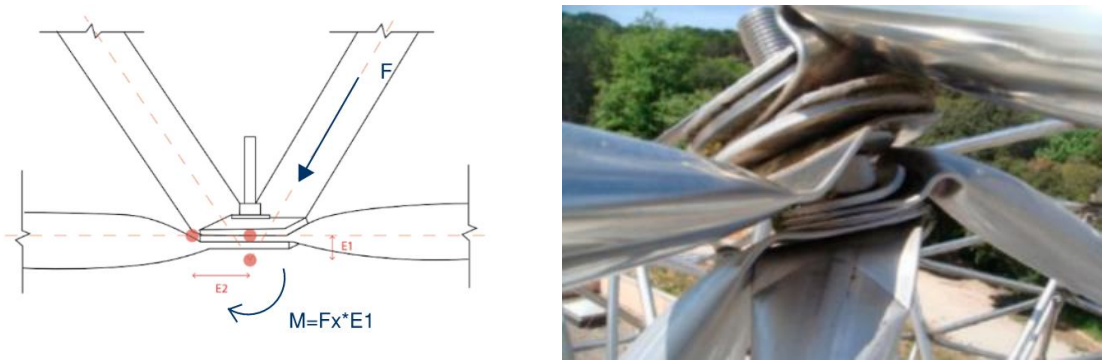


*Figure 34: Bending moment and deformation*

It should also be noted that the members have already reached the plastic zone of the stress-strain curve because of the permanent deformation they succumbed while flattening. Therefore, the added load that makes the stress surpass the linear zone will cause even more permanent deformation.

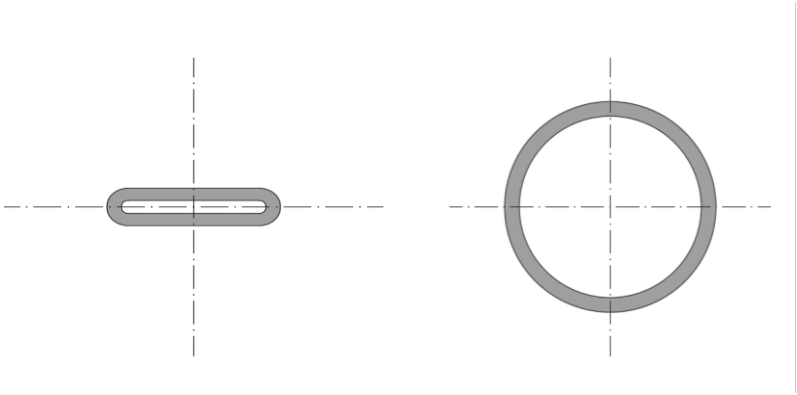

*Figure 35: Flattened and unflattened cross-sections*

Bolt:

The bolt can fail under shear or tension.

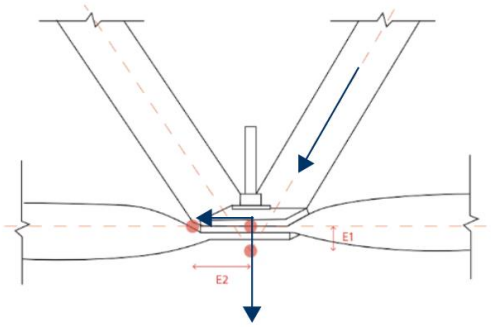


*Figure 36: Forces on bolt*

Spacer:

The spacer only works under compression, so it must have a sufficient size to withstand the compressive load. There isn't much risk of buckling because its length is very short.

## 3.4 Unistrut

The Unistrut system, originating in the United States during the early 1950s, features a joint configuration comprising a connector plate crafted through press-forming a steel plate. The structural members are shaped like U channels and are secured to the connector plate using a single bolt at each end. Notably, the connectors employed for both the upper and lower layers are identical, resulting in Unistrut double layer grids consisting of just four components: the connector plate, the strut, the bolt, and the nut. The maximum span achievable with this system typically reaches around 40 meters, utilizing standard modules of 1.2 meters and 1.5 meters. However, from an architectural perspective, this system may not be considered particularly aesthetically pleasing.

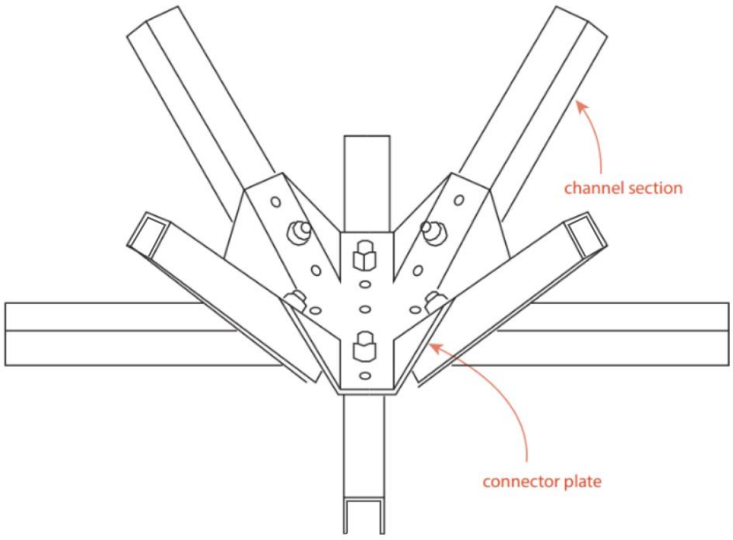


*Figure 37: Unistrut node*

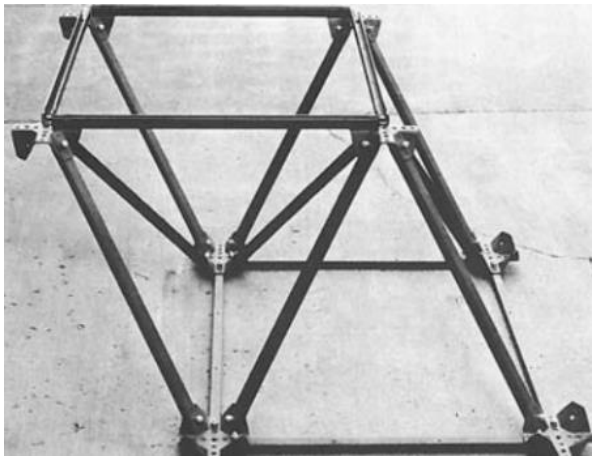

*Figure 38: Truss with unistrut nodes*

## TYPES OF FAILURES

Members:

The members are channel sections (U) and they work in tension/compression. Under tension, the net sections (where the bolts are located) must be checked. Under compression, there is risk of buckling around the weak axis.

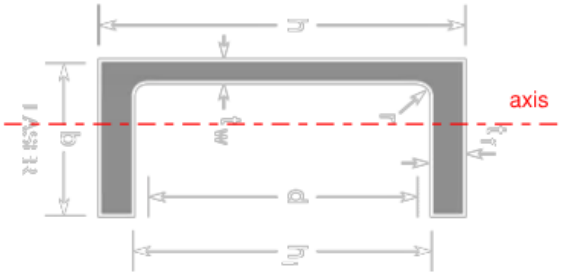


*Figure 39: Unistrut cross-section*

Connector plate:

The connector plate works in tension/compression but also in bending when there is an external load to it (e.g. weight of acoustic panel or a loudspeaker).

In case of tensile force in the member, there is risk of tear-off of the outer surface of the plate due to tension/shear in the plate.

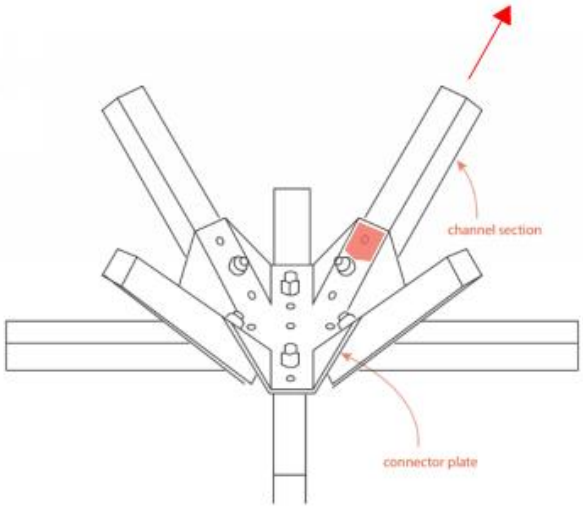


*Figure 40: Plate critical area under tear-off*

The inner plate, when the member force is compressive, is under risk of buckling. So, its thickness needs to be sufficient to withstand that stress.

Bolts:

The bolts principally work in shear as they are perpendicular to the members and the members only transfer axial loads. However, they may also work in tension as there is some eccentricity (e) between the neutral axis of the channel member and the connection point with the bolt, which creates a very small bending moment that is then taken by the bolts.

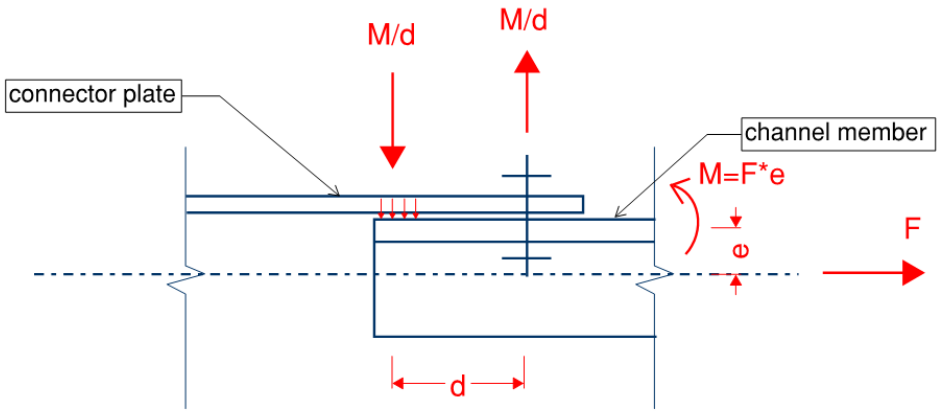


*Figure 41: Tension in bolts due to U-channel member*

## 3.5 PNST (Pin Node Space Truss System)

The PNST system presents a variety of geometric configurations, offering flexibility in its design approach. However, it carries a potential drawback, as it poses a risk of inducing local instabilities on the node plates, primarily arising

from compression forces. Additionally, this system may pose challenges when it comes to integrating acoustic or facade panels into its structure.

Despite these considerations, it's worth noting that the PNST system offers the advantage of accessibility, making it relatively straightforward to replace members when necessary, which can contribute to ease of maintenance and potential cost savings in the long run. It is also important to note that there are not eccentricities in the members' connecting axis.

While the theoretical merits of this system are evident, it's noteworthy that no practical built examples of this typology were discovered in the available data, suggesting that its implementation in real-world projects may require further exploration and experimentation.

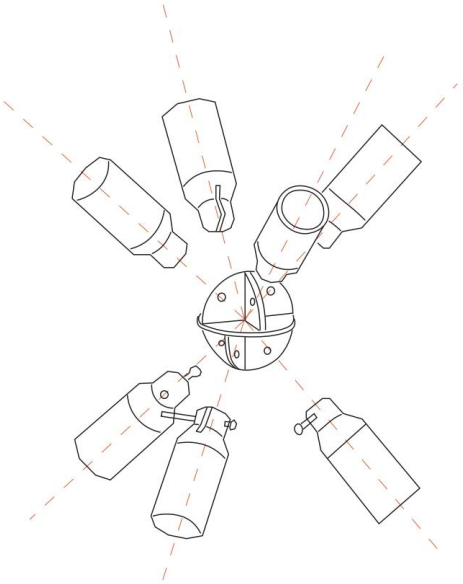

*Figure 42: PNST node*

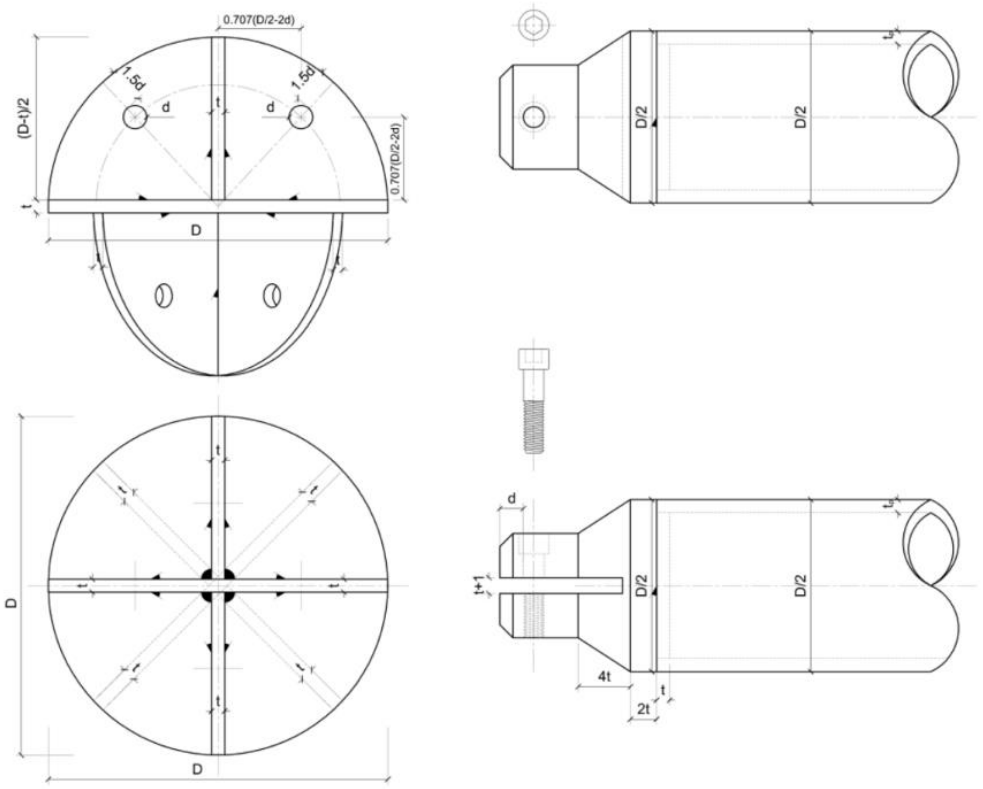


*Figure 43: PNST plans and elevations*

## TYPES OF FAILURES

Members:

The members are round hollow sections which are welded to a connecting edge with a smaller diameter. Failure can happen under compression or tension. In tension the critical net section would be on the end of the member where the slit and bolt are.

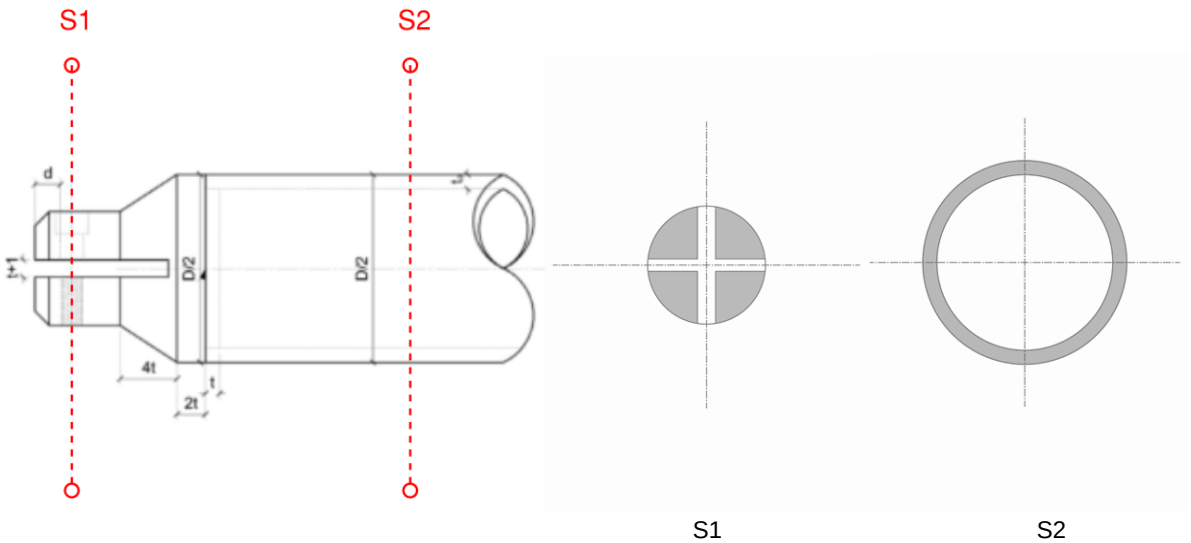


*Figure 44: Member cross-sections*

Node:

The node can be in either tension or compression depending on the member forces. In case of tensile force, the outer node plate surface is pulled out, so there is risk of being torn off. Having a sufficient distance from the end is therefore necessary.

In case of a member compressive force, it is the center of the node that is activated (compression) and is under risk of buckling if its thickness is not adequate.

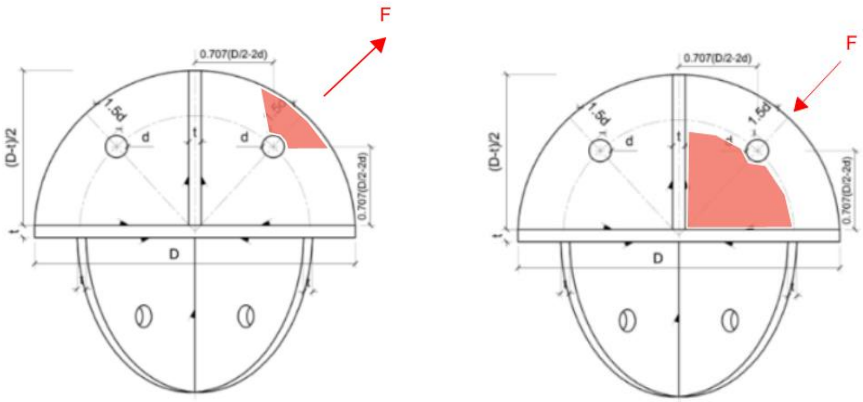


*Figure 45: Tear-off and buckling critical areas*

Another possible failure mechanism is under bending of the plates in the node caused by the bearing of the upper plates to the horizontal plate. As we can see in the drawings, the top and bottom plates are not necessarily in the same axis. They can be offset from each other by an angle. So, if a member is for example in compression, it could cause bending on the plate.

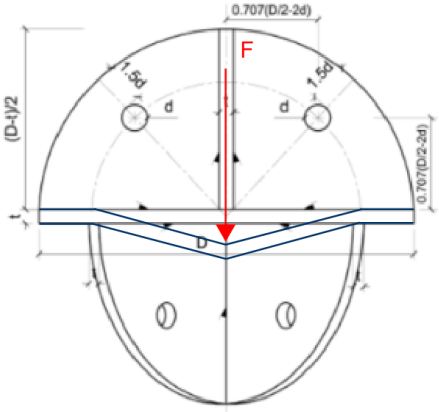


*Figure 46: Bending of node plate due to member axial force*

Bolt:

The bolt on this node only works in shear as it is perpendicular to the member axis.

All the above node typologies require prefabrication for the node part, and bolting on site to assemble with the members.

## 3.6 Bearing Joints

Space frames are upheld by columns or ring beams via bearing joints. These joints must possess sufficient strength and rigidity to effectively transmit the support reactions without compromising safety. Typically, under vertical loads, bearing joints are subjected to compression forces. However, in certain double-layer grids employing a diagonal layout, the bearing joints located at corners might need to withstand tension.

It's important to recognize that the level of restraint provided by a bearing joint significantly influences both the displacement of the joint and the forces experienced by the individual members. Therefore, it's imperative that the construction details of a bearing support closely align with the assumed restraint in the design. Failure to meet this requirement could potentially lead to alterations in the magnitude or even the direction of the member forces.

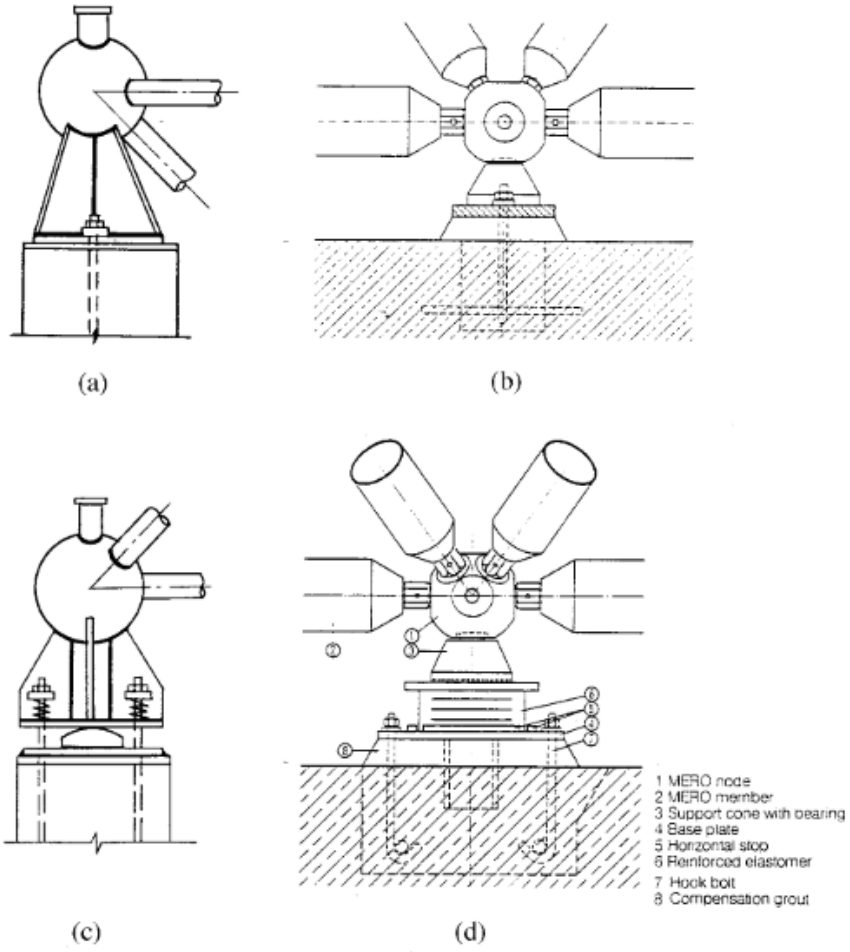


*Figure 47: Examples of bearing joints (MERO)*

# 4. Original nodes by LaufsED

Two node designs have been developed in the office, which can be either 3D printed or cast in steel.

## 4.1 Option 1

Within this particular configuration, it's worth noting that the member section remains consistent up to the node, where the members are securely bolted directly. However, it's important to highlight an aspect: the node lacks a flat front surface that can readily accommodate the attachment of panels or additional components.

A tangible illustration of this node design can be observed in the accompanying photograph, showcasing an instance employed in a single layer gridshell project at LaufsED's New York office. This specific node was fabricated using 3D printing technology and utilized plastic material, which was particularly suitable for the scale of the project, representing a fine example of the versatility of node design possibilities.


*Figure 48: Photo of printed node*

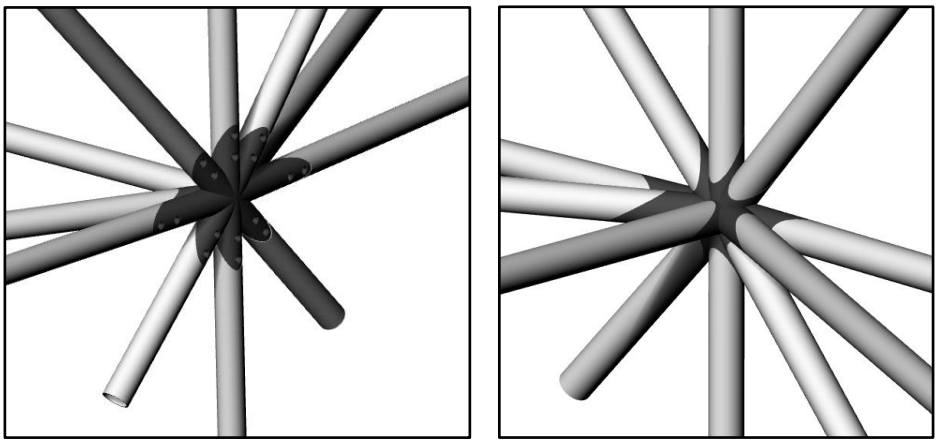

*Figure 49: Front and back perspective views of node*

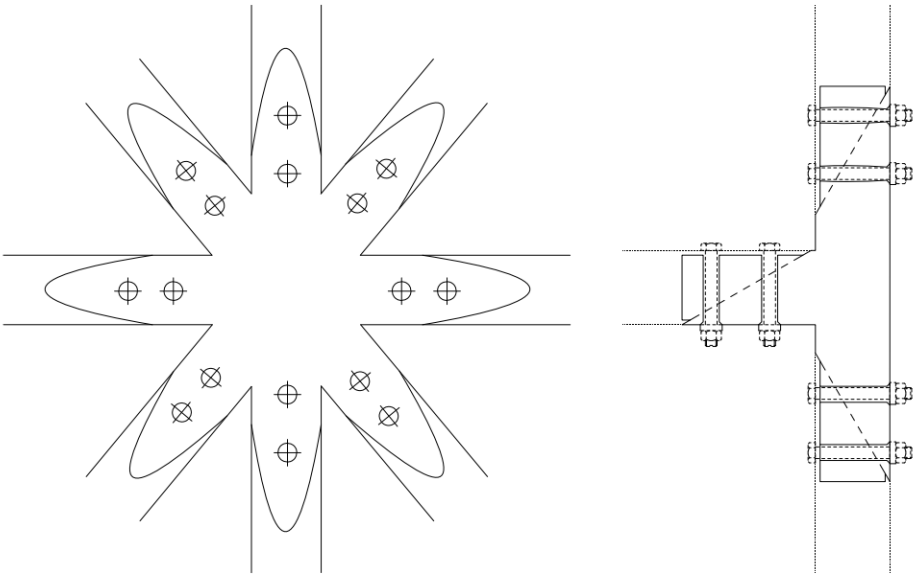

*Figure 50: Elevation and section drawings*

## TYPES OF FAILURES

Members:

The members are circular hollow sections that work in tension/compression. The section is constant throughout the member's length. It is prone to yield, and buckling failure under compression. Under tension it is prone to yielding or rupture.

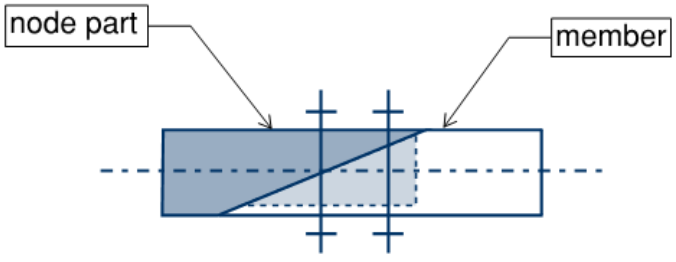


*Figure 51: Member to node connection - section*

The member end section is also prone to tear-off failure when in tension.

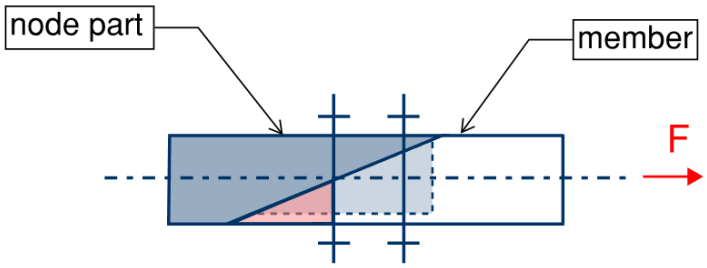


*Figure 52: Member tear-off failure - section*

The end reduced net section needs also to be checked for tensile yield failure.

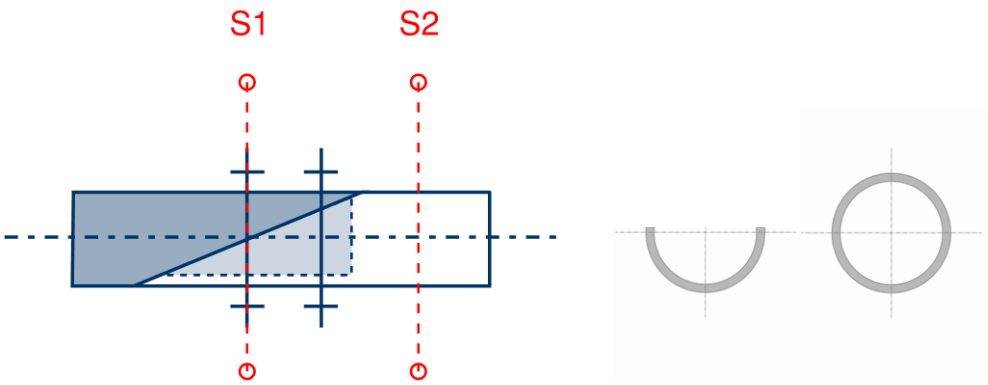


*Figure 53: Node cross sections S1 and S2*

Bolt:

The bolts only work in shear and tension. Shear occurs from the transfer of the member's axial forces to the node. Tension can occur when there is lateral load applied to the member or node. For instance, if there is a loudspeaker attached to the node, the moment created from the weight can be transferred to the bolts and analyzed as a couple.

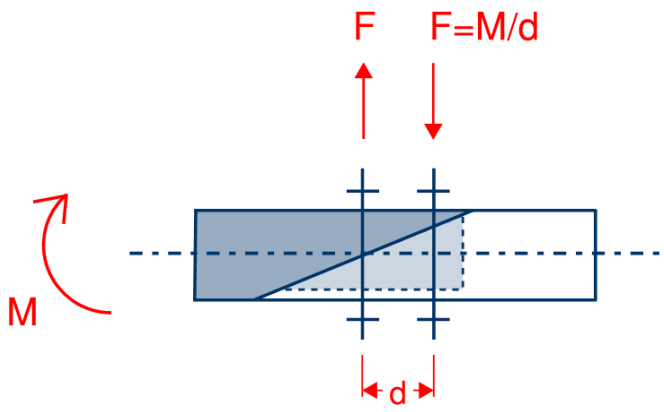


*Figure 54: Moment couple in bolts - section*

Node:

The node is a solid unit that is tensioned or compressed. There is no bending originating from the members thanks to the absence of eccentricity. The risk of node buckling is low if the members already pass that check, because the geometry of the node is the same as the members' with a solid section.

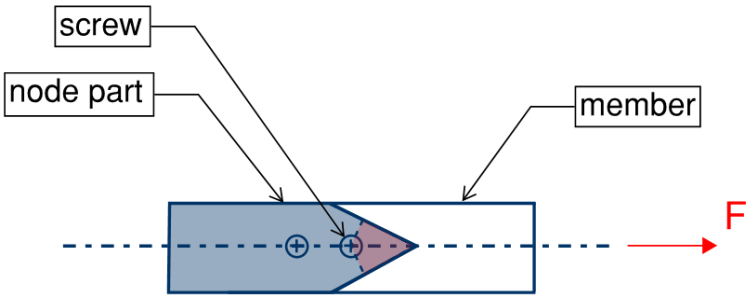


*Figure 55: Node tear-off mechanism under member tension - plan view*

## 4.2 Option 2

Another option is a node composed of three separate parts clamped together by the lateral member passing through the middle. The assembly is done in two steps:

1. Member to member end,
2. Members to node.

The members are again circular hollow sections. The ends are solid conical shapes welded to the members (step 1).

This node facilitates the attachment of panels more easily. It does not require the use of any additional fasteners, but simply one nut locking everything in place. It is adapted for double layer trusses and can accommodate different angles. For these reasons, this is the solution that has been chosen for the Limes360 dome.

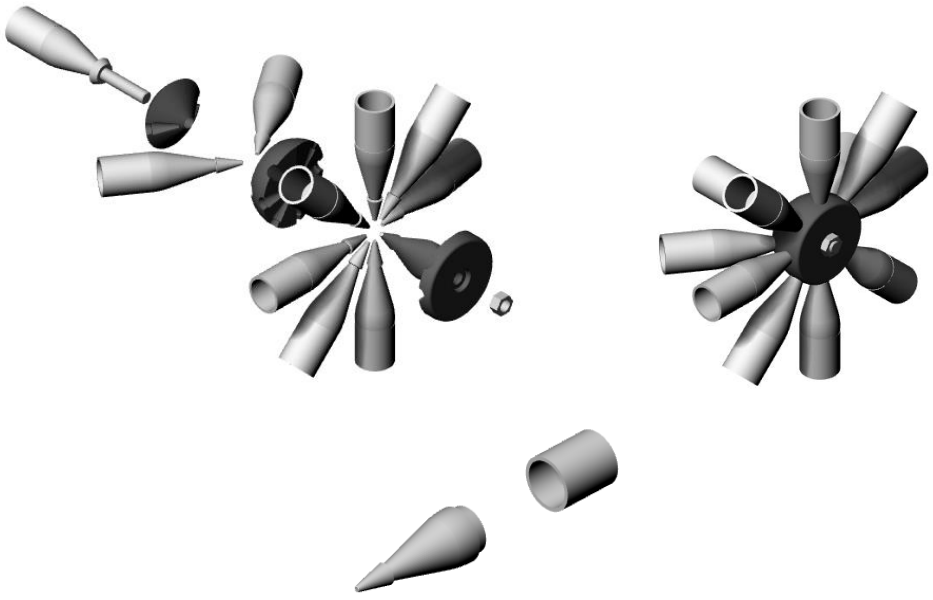

*Figure 56: Perspective #1 node and member assembly*

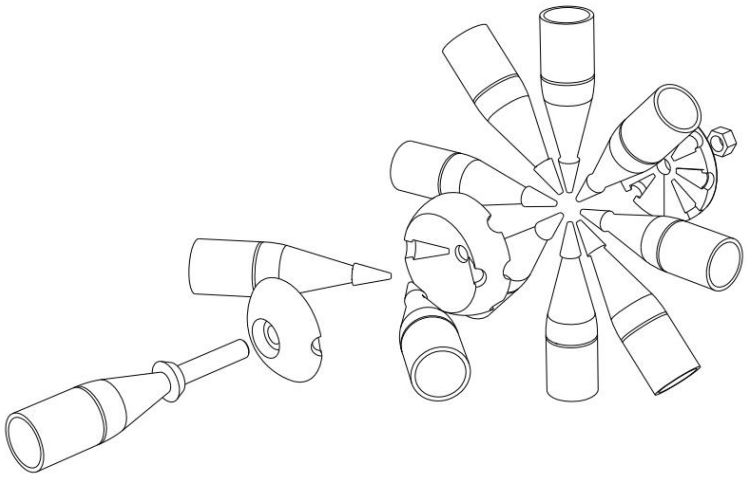

*Figure 57: Perspective #2 node and member assembly*

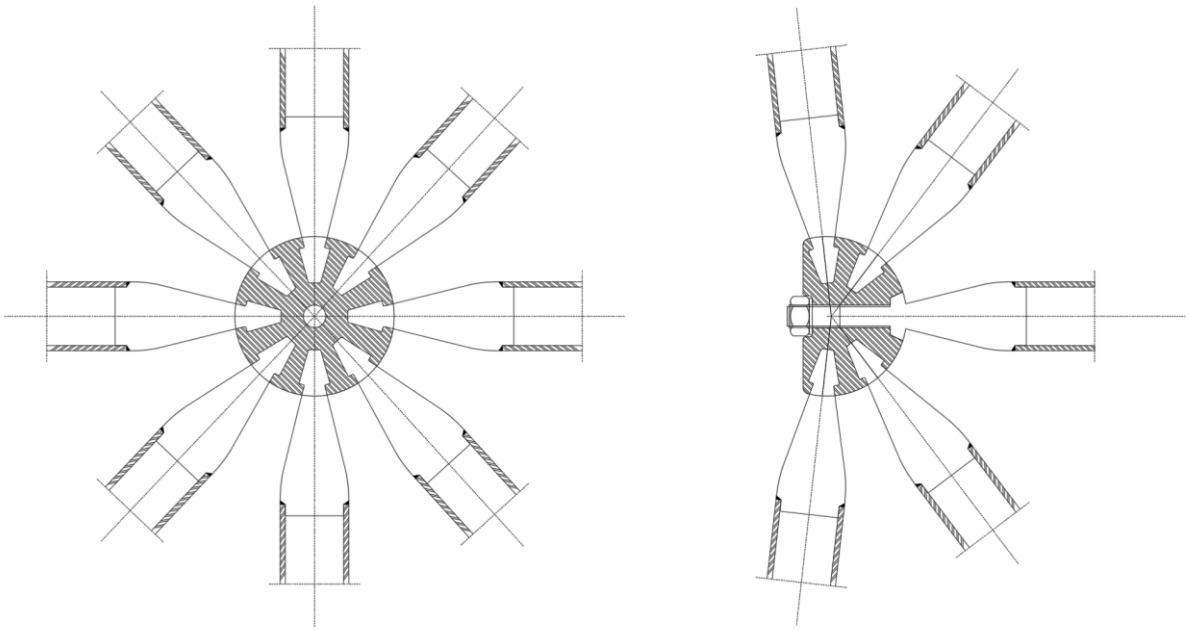

*Figure 58: Front and side cross-sections of node geometry*

## TYPES OF FAILURES

Members:

Members can fail under tension or compression. The thinned section on the ends of the members needs to be verified as it is the most critical one. When a member is in tension, the very edge that locks into the node is under risk of tearing off, therefore it needs to have adequate dimensions.

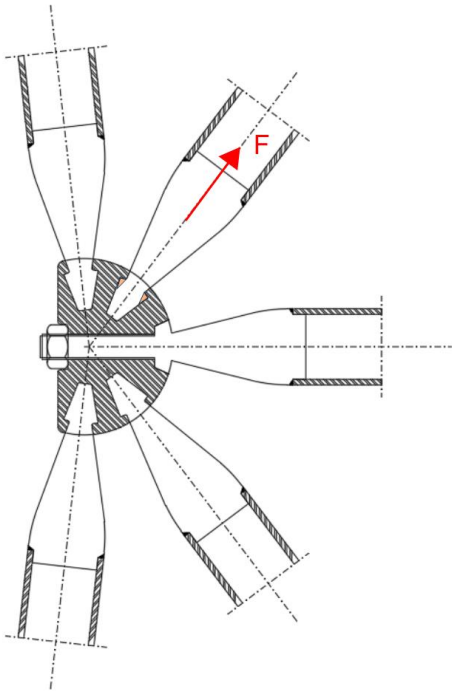


*Figure 59: Member tear-off mechanism under member tension*

The distance required to withstand tear-off is defined by the shear capacity of the active zone in section. A = length*thickness.

TEAR-OFF CHECK (MEMBER):

Aluminum 6060 T6: fo=160 MPa
fu=215 MPa
$\gamma_{M1}$=1.10
$\gamma_{M2}$=1.25

Considering a rectangular section around the perimeter of the ring of 1mm width and depth equal to the edge distance (9.3mm), we have:

$$N/L_{perimeter} = 5.83kN/76.4mm = 0.076\ kN/mm$$
$$\tau_{Ed} = \frac{V_{Ed}\,S}{I\,t} \leq f_o/(\sqrt{3}\gamma_{M1})$$
$$A = 9.3 * 1 = 9.3\ mm^2$$
$$\tau_{Ed} = 49\ MPa \leq 84\ MPa$$
$$utilization = \frac{49}{84} = 0.58$$

This result means the cone shape can be a bit further reduced.

Node:

The node works under tension/compression. The part of the node that holds the member in place needs to be adequately sized so that it doesn't tear off when a member is in tension. See figure below.

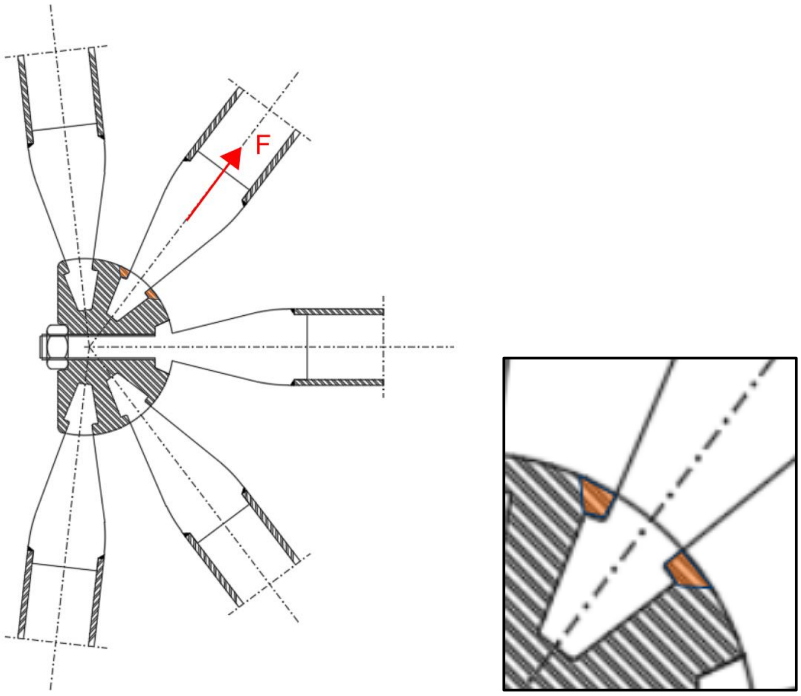


*Figure 60: Node tear-off mechanism under member tension - cross section*

The node is under biaxial stress because all the members have different directions. The stress shall be calculated by the Von Mises equation:

$$\sigma_v = \sqrt{1/2\,[(\sigma_1 - \sigma_2)^2 + (\sigma_2 - \sigma_3)^2 + (\sigma_3 - \sigma_1)^2]}$$

The distance required to withstand a pull-out force is defined by the shear capacity of the section.
A = length*thickness

$$V_{Ed}/V_{Rd} \leq 1$$
$$V_{pl,Rd} = A_v\,(f_y/\sqrt{3})/\gamma_{M0}$$

TEAR-OFF CHECK (NODE):

Steel S235: fy=235 MPa (t<40mm)
fu=360 MPa
$\gamma_{M0}$=1.00

$$N/L_{perimeter} = 5.83kN/76.4mm = 0.076\ kN/mm$$
$$\tau_{Ed} = \frac{V_{Ed}\,S}{I\,t} \leq f_y/(\sqrt{3}\gamma_{M0})$$
$$A = 1mm * t = 9.56\ mm^2$$
$$\tau_{Ed} = \frac{V_{Ed}\,S}{I\,t} = 45.7 * 0.076/(9.56 * 72.8 * 10^{-3}) = 48\ MPa \leq 135.7\ MPa$$
$$utilization = \frac{48}{135.7} = 0.35$$

This result means there is little risk of tear-off in the node. In the FEM model we will be able to see the total Von Mises stresses and determine how the areas can be optimized further.

Rod:

The rod connecting to the lateral member locks the node parts into place. The rod can be under tension/compression depending on the other forces enacting on the node. Bending may occur if panels or other objects are attached to the rod.

We note here that the analysis of the node has been done assuming steel S235 as material which would be galvanized. The aluminum members connecting to the node would be anodized and then powder coated to reduce risk of galvanic corrosion between metals. It is important to mention that the exact material of the members is not fully decided yet (could be steel also), which is why the S235 assumption for the node is acceptable. If the members remain aluminum, the ideal solution would be to have stainless steel for the node. 3D printers are capable of producing 316 SS.

# 5. 3D Printing methods

The reason we consider the possibility of 3D printing in this project is because each node has a different geometry depending on its position in the dome. In total there are approximately 1500 parts but they are different because the angles change. 3D printing would also allow introducing a level of porosity to the areas that are not highly utilized, and thus, save material. The general printing geometrical tolerance is typically +/- 0.1mm but can vary per printer. An overview of the principles of metal 3D printing is presented below.

Additive manufacturing or 3D printing of microstructures has anisotropic behavior. Therefore, the mechanical properties of the 3D printed steel may differ from those of the factory manufactured steel, which is why lab tests are a must.

Some additive manufacturing methods are namely the following:

- Binder jetting
- Directed energy deposition
- Material extrusion
- Material jetting
- Powder Bed Fusion - direct metal laser sintering (DMLS)
- Sheet Lamination
- Vat Photopolymerization

One of the most common methods is DMLS. The way it works is the machine begins sintering each layer with a laser aimed onto a bed of metallic powder. After a cross-section layer of powder is micro-welded, the build platform shifts down and a recoater blade moves across the platform to deposit the next layer of powder into an inert build chamber. The process is repeated layer by layer until the build is complete.

When the process finishes, an initial brushing is manually given to parts to remove the loose powder, followed by the appropriate heat-treat cycle while still fixtured in the support systems to relieve any stresses. Parts are removed from the platform and support structures are removed from the parts, then finished with any needed bead blasting and deburring. Final DMLS parts are nearly 100 percent dense.

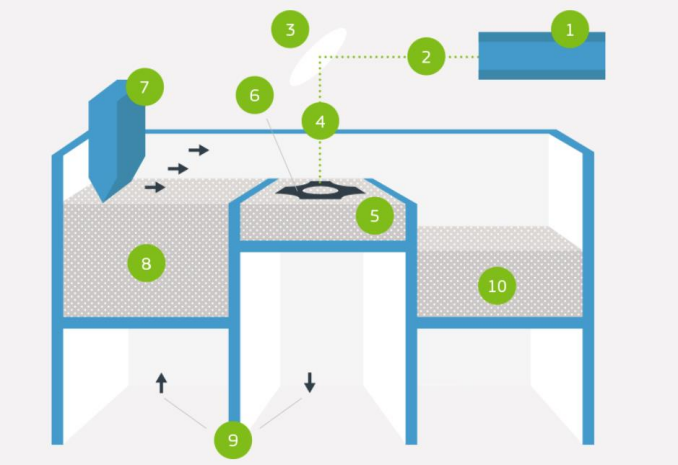


*Figure 61: DMLS procedure diagram by Protolabs*

## Benefits

Although most manufacturing methods are based on subtraction, additive manufacturing or 3D printing, as the name says, is based on addition. Therefore, there is no wasted material. Other advantages include:

1. The cost-effectiveness of fabrication methods typically improves as the volume or quantity of parts being produced increases. In contrast, when it comes to metal 3D printing, the cost remains relatively consistent, regardless of the production volume. It's essential to acknowledge that metal 3D printing isn't always the most economical manufacturing approach, especially for high-volume production, where many alternative manufacturing processes tend to be notably more cost-efficient. Nevertheless, for a substantial portion of low to medium volume production scenarios, metal 3D printing can emerge as the most economically viable method for producing parts.

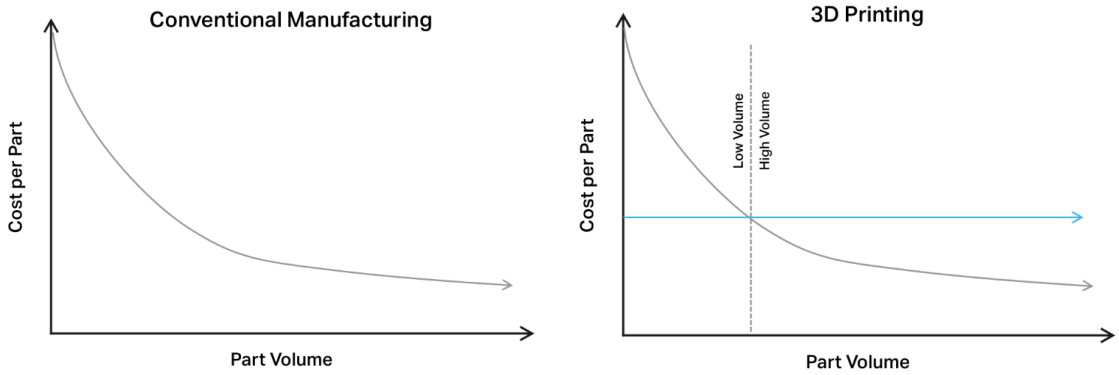


*Figure 62: Cost – Volume diagrams by Markforged*

2. For the majority of fabrication processes added complexity means added cost. For metal 3D printing that is not the case. Cost is driven by part size instead of complexity.

3. Because complexity is not an issue, metal 3D printing allows for topology optimization to be applied to the design of the parts. Therefore, more sustainable solutions are feasible by using less material.

It is difficult to determine solely with this general information whether additive manufacturing is the best solution in our project. A more detailed market research, including communication with manufacturers would be necessary to compare costs and time required to produce all parts.

# 6. LIMES 360 Cladding Connection Study

One of the first tasks was to schematically come up with different attachment ideas. The assumed panel sizes are 2.4m x 2.4m determined by the maximum span of the insulation material. The panel composition is acoustic foamglass (expanded glass granules 500 kg/m$^3$) 25mm thick and a 3-5mm cellulose spray plaster layer. The panel is glued with silicone or screws to the substructure. The weight of the insulation is 0.125 kN/m$^2$ and the weight of the plaster assumed when wet 0.05 kN/m$^2$. Here the heaviest insulation of foam glass is assumed (0.125 kN/m2). The architecture team had another option, the PET insulation which weighs around 200 kg/m$^3$. We are going to be dimensioning all the following options for the heaviest case.

- Option 1: In this case the panels don't require additional fasteners to be attached. They are held by a pressure attachment in the form of two convex disks that might be cast or 3D printed metal and inserted in the rod passing through the node. Parts of the rod could be threaded to allow this attachment.

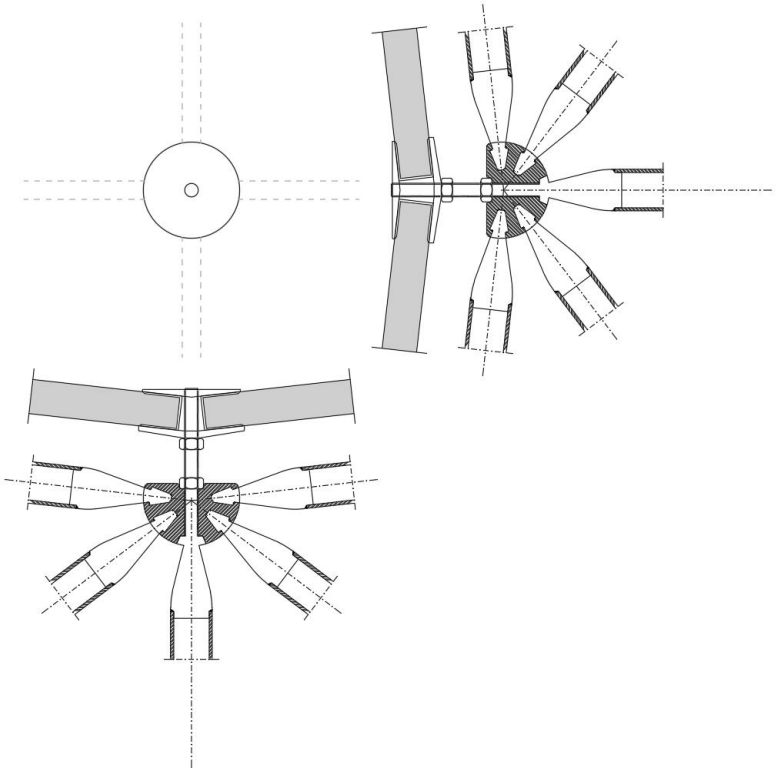

*Figure 63: Option 1 - elevations and cross sections*

- Option 2: A similar disk design is placed at the end of the rod and then the panel is attached to it with additional screws. The difficulty here is placing the self-drilling screws from the back. The back distance needs to be sufficient to allow space for a drill.

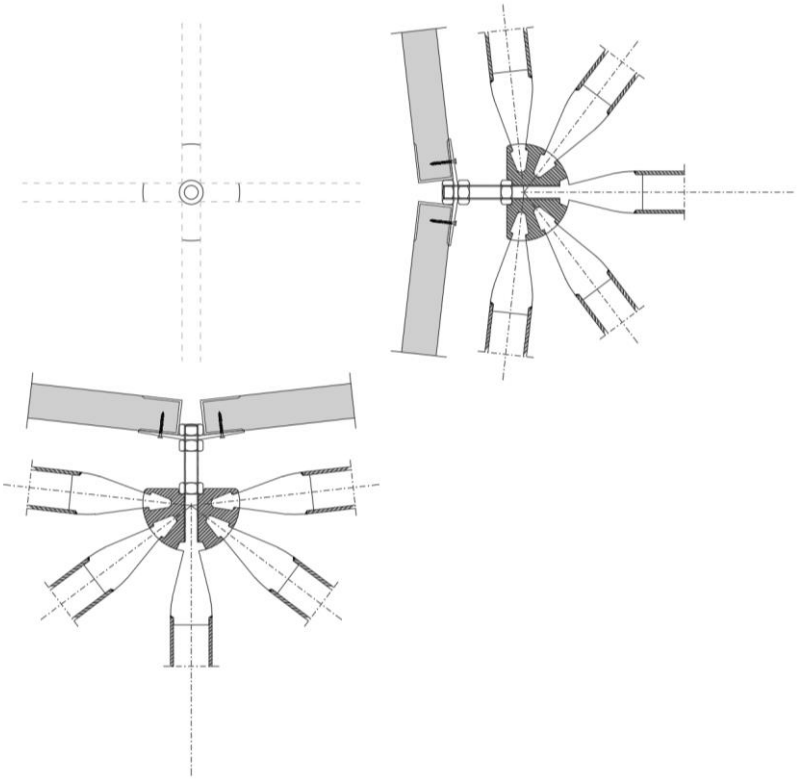

*Figure 64: Option 2 - elevations and cross sections*

- Option 3: The “spider” attachment is typically used for curtain wall connections. In this case the same idea can be used to support the acoustic panels in the interior with the extra use of screws.

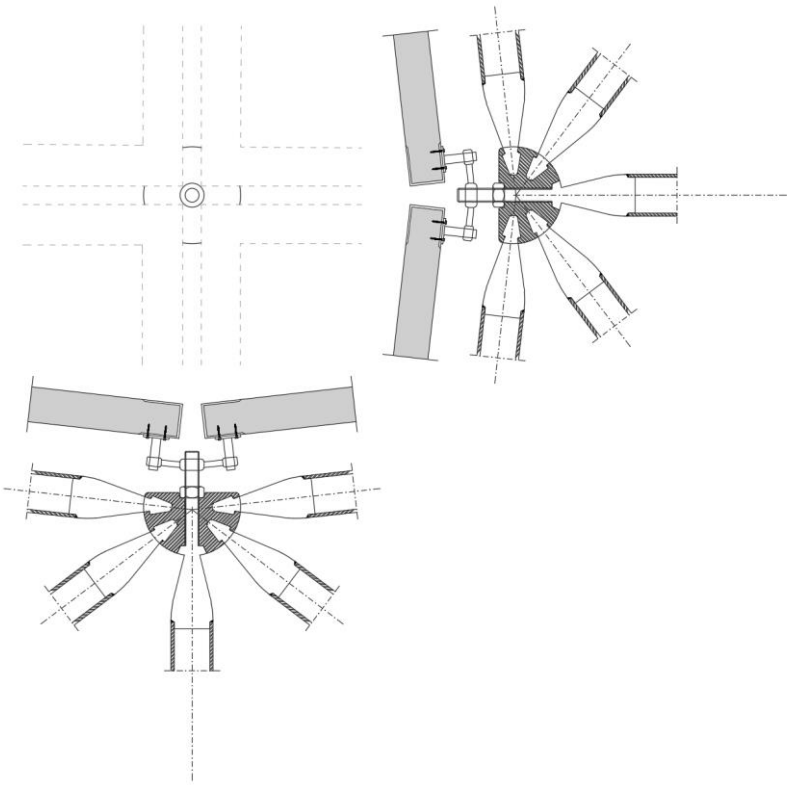

*Figure 65: Option 3 - elevations and cross sections*

- Option 4: If the panel subframe consists of aluminum mullions, the attachment can consist of five small plates hinge connected (to avoid the need for cold bending). A torsion spring clip, glue, or screws can be used for the subframe to panel connection.

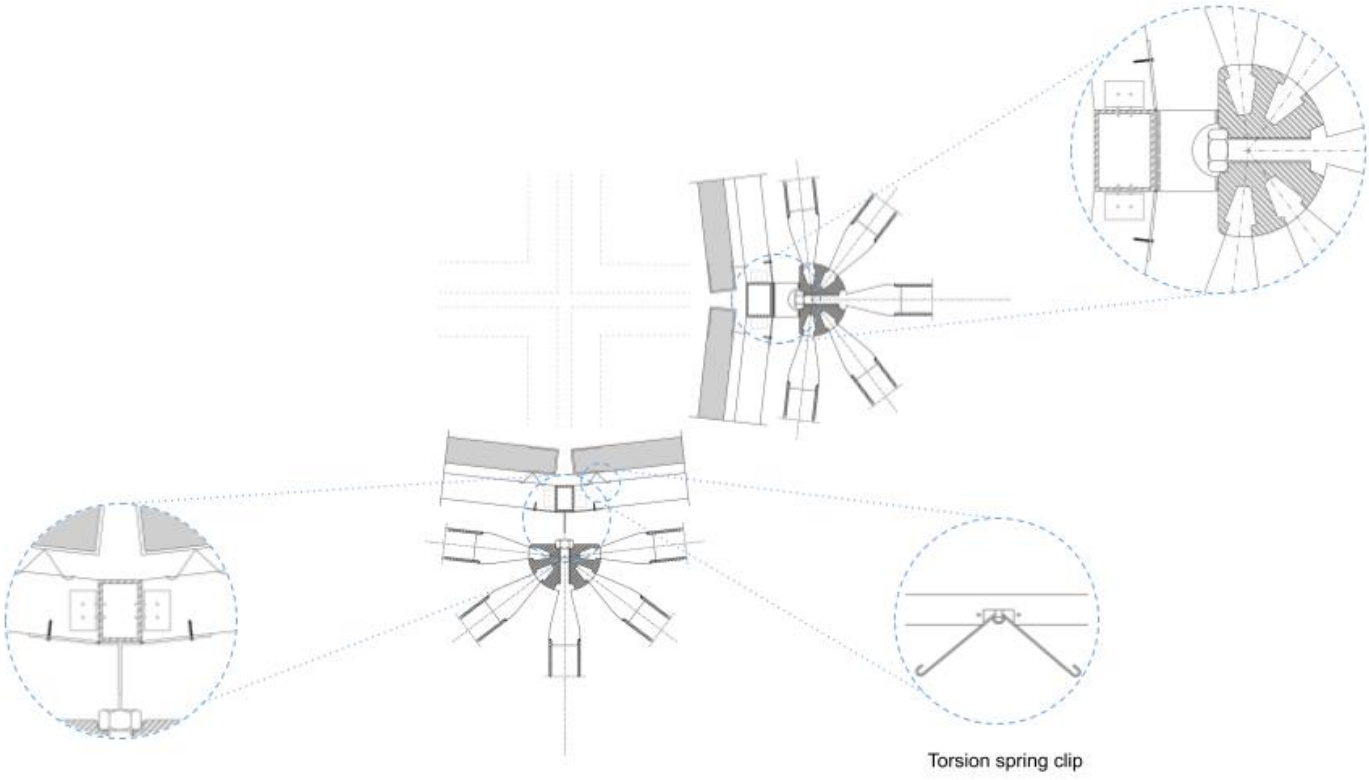


*Figure 66: Option 4 - elevations and cross sections*

It is always preferable to align the panel corners with the nodes of the space truss as this way the distance between truss and panels is minimized. If we were centering the panel at a node, then a bigger cantilevering distance would be required and the connection detail would therefore be bigger to have more rigidity.

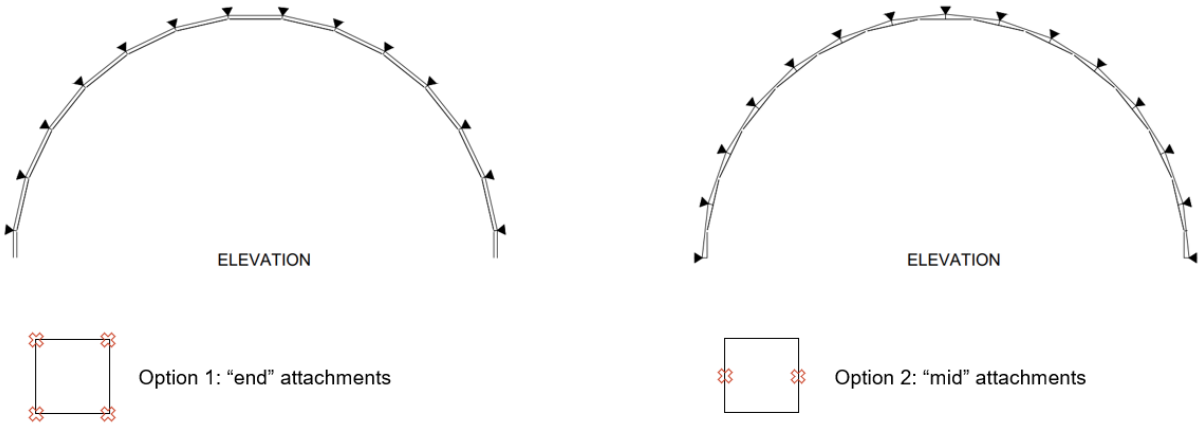


*Figure 67: Corners vs middle alignment*

Mockup:

A different approach was followed for the mock-up, where OSB framing was used instead. This was done because the architects wanted to test a new idea, and it was completed before I started working on this thesis.

*Figure 68: Numerical and physical models of the mock-up*

Rod sizing for Ultimate Limit State:

Verification of aluminum rod according to EN 1999, chapter 6.

**Tension**

$$N_{Ed} / N_{t,Rd} \leq 1.0$$

The design of plastic resistance of the gross cross-section:

$$N_{t,Rd} = N_{pl,Rd} = A_g f_o / \gamma_{M1}$$

**Shear**

The design value of the shear force at each cross section shall satisfy:

$$V_{Ed} / V_{c,Rd} \leq 1.0$$

Given the absence of torsion we may take the design plastic shear resistance:

$$V_{pl,Rd} = A_v (f_o / \sqrt{3}) / \gamma_{M1}$$

**Bending**

The design value of the bending moment $M_{Ed}$ at each cross section shall satisfy:

$$M_{Ed} / M_{c,Rd} \leq 1.0$$

Where $M_{c,Rd}$ is defined as:

$$M_{c,Rd} = M_{pl,Rd} = W_{pl} f_o / \gamma_{M1}$$

We verify that the effect of shear in bending can be neglected:

$$V_{Ed} \leq 0.5\, V_{Rd}$$

We also make sure the effect of axial force in bending can be neglected:

$$\left(\frac{N_{Ed}}{\omega_0 M_{y,Rd}}\right)^{\psi} + \left[\left(\frac{M_{y,Ed}}{\omega_0 M_{y,Rd}}\right)^{1.7} + \left(\frac{M_{z,Ed}}{\omega_0 M_{z,Rd}}\right)^{1.7}\right]^{0.6} \leq 1.00$$

where ψ = 2 for solid sections.

According to these checks we find that 1.7cm diameter is sufficient for the rod to cantilever the 20kg loudspeaker.

## Attachment options

Depending on the inclination, the geometry of the spaceframe, the position of attachment points, and the location of the loudspeaker, a list of options was developed and is summed up schematically on the following diagram.

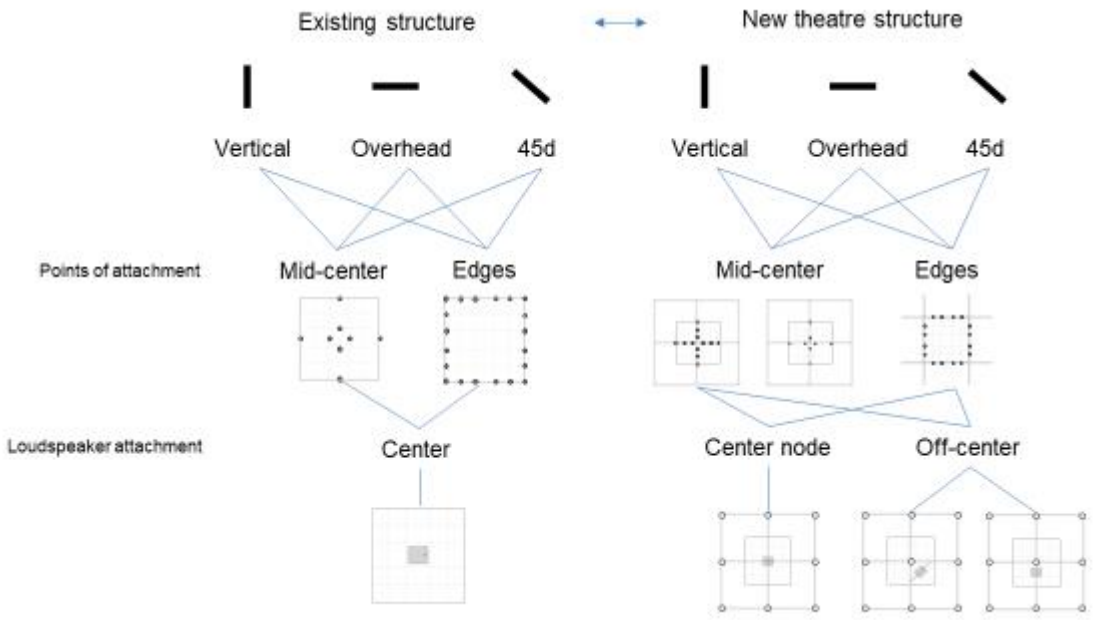


*Figure 69: Schematic diagram of attachment options*

The first task was to determine the panel frame geometry so that it is lightweight (less than ~25kg) and that it can accommodate the acoustic panels as necessary.

The profiles used for that purpose are the ones below. The total weight of the panel is 23kg.

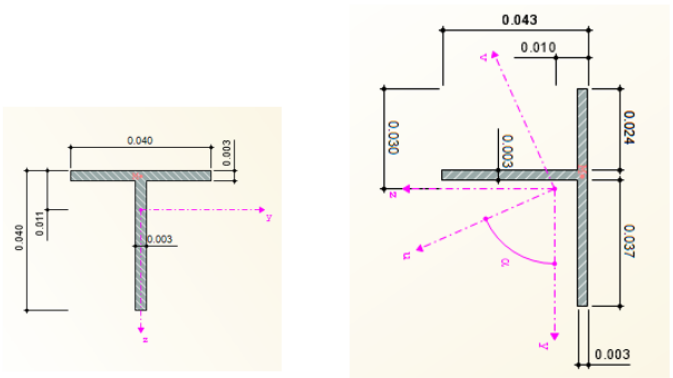


*Figure 70: Cross-sections*

Our criterion for accepting or rejecting each option was approximately 2 mm of deflection maximum as the final surface would be plastered and cracking needed to be avoided.

### Option A.1

Following the diagram of options, we consider the first scenario where the panels are attached to an existing main structure (wall or ceiling) at midspan. The number of suspender elements in this case needs to only be 8. Minimizing the number of suspenders is important because it means minimizing the number of connections there would have to be done on site.

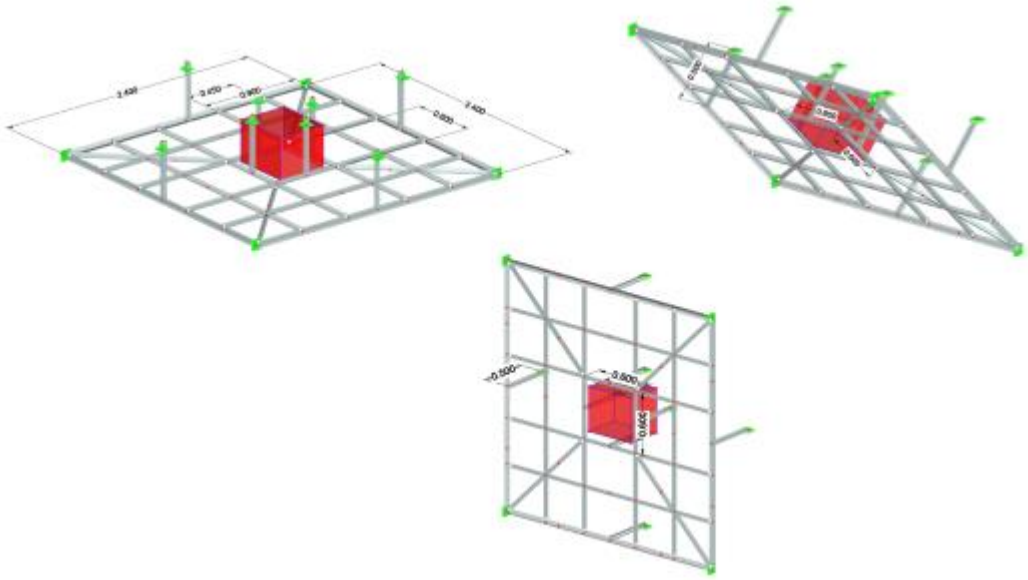

*Figure 71: Panel to existing main structure configurations*

For the overhead configuration the maximum deflection under service load (D+SDL) is 1.1mm.

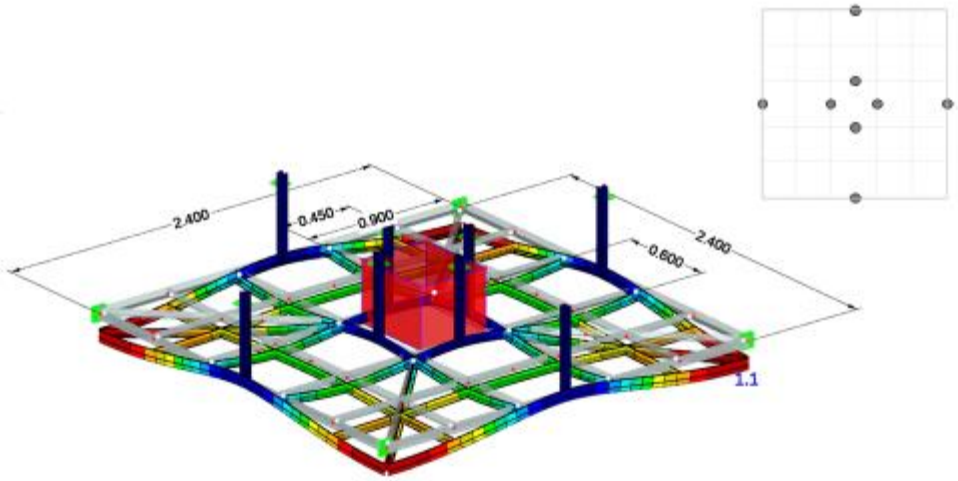


*Figure 72: SLS deflection 1.1mm*

For the vertical configuration the maximum deflection under service load (D+SDL) is 1.0mm.

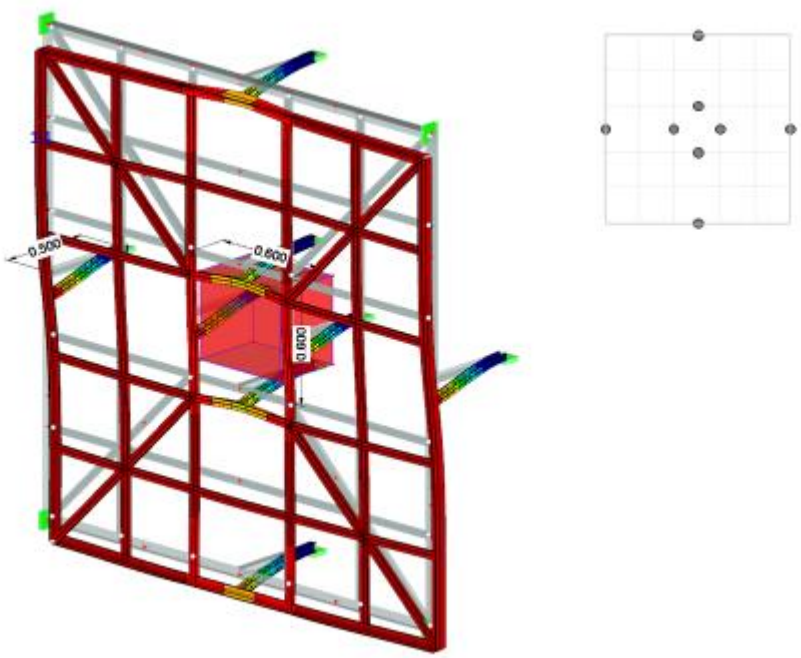

*Figure 73: SLS deflection 1.0mm*

For the 45º inclined configuration the maximum deflection under service load (D+SDL) is 1.3mm.

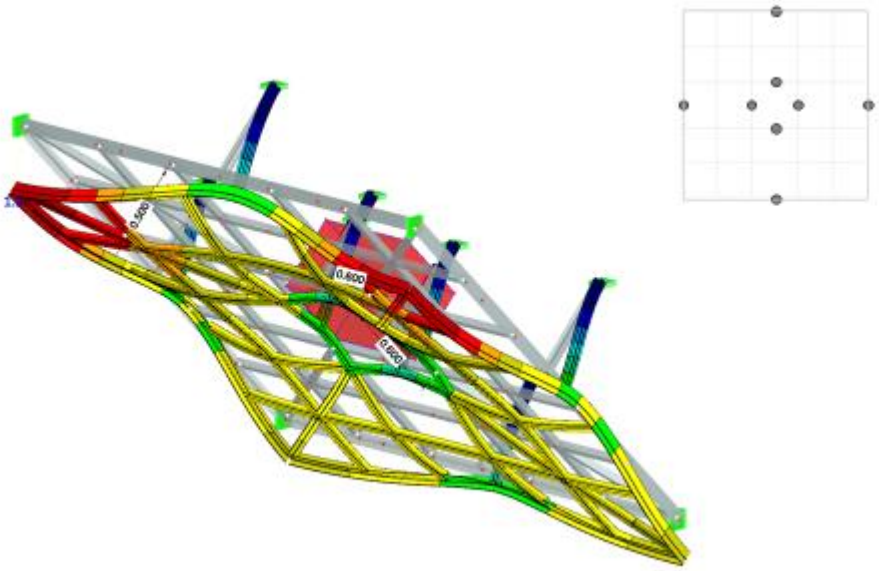

*Figure 74: SLS deflection 1.3mm*

### Option A.2

If the panels are supported only perimetrically, they do not pass the deflection criteria for the overhead and 45º options. The number of suspenders around the perimeter does not play a critical role, it is rather the absence of suspenders at midspan that causes the big deflections. This option is therefore not accepted.

For the overhead configuration the maximum deflection under service load (D+SDL) is 9.1mm.

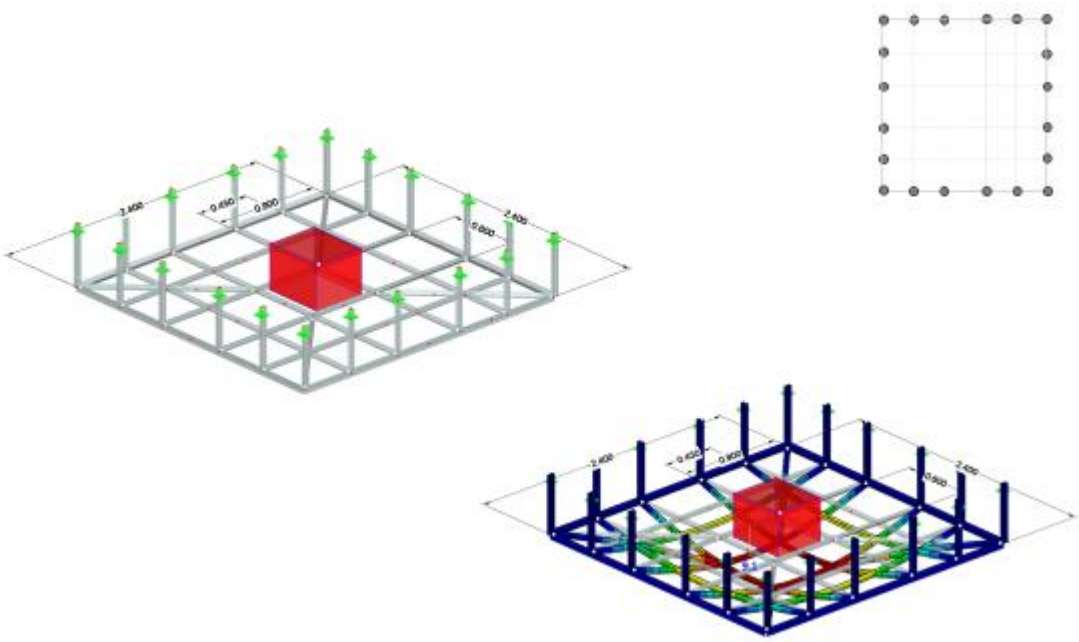

*Figure 75: SLS deflection 9.1mm*

For the vertical configuration the maximum deflection under service load (D+SDL) is 1.8mm where the support points are pinned. If the support points are fixed the deflection is 0.3mm. Having a fixed connection is possible, however more time consuming as it requires a larger number of fasteners to ensure rotation is blocked

.

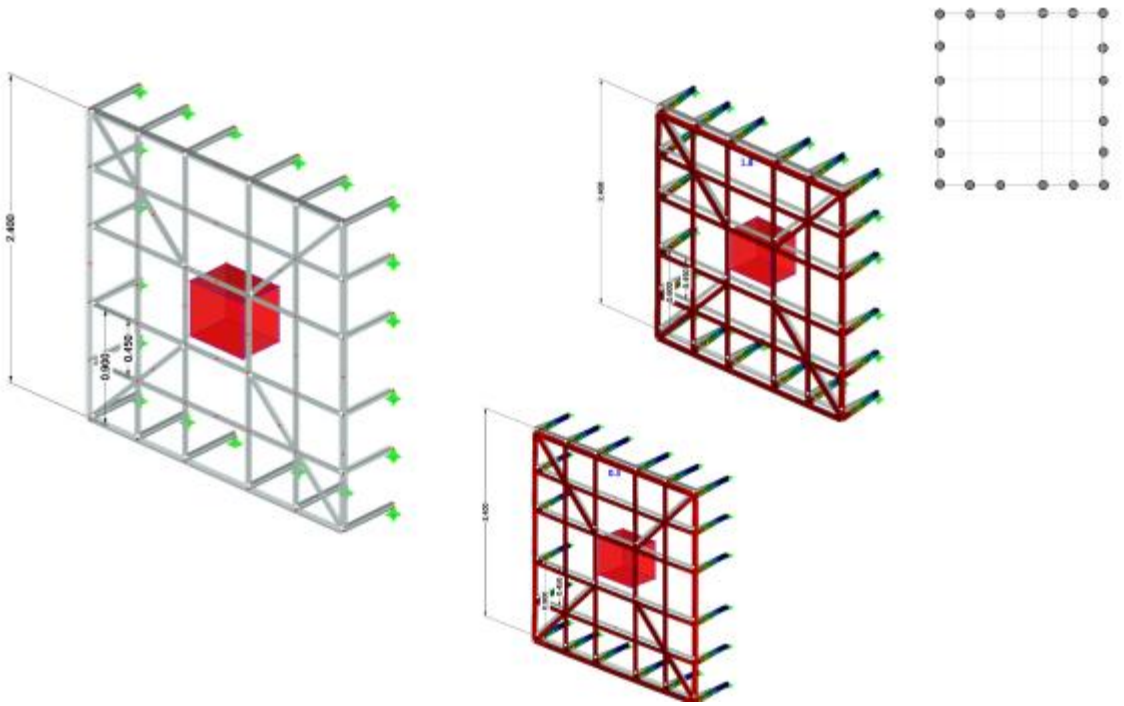

*Figure 76: SLS deflection 1.8mm*

For the 45º inclined configuration the maximum deflection under service load (D+SDL) is 6.5mm which is above our set limit.

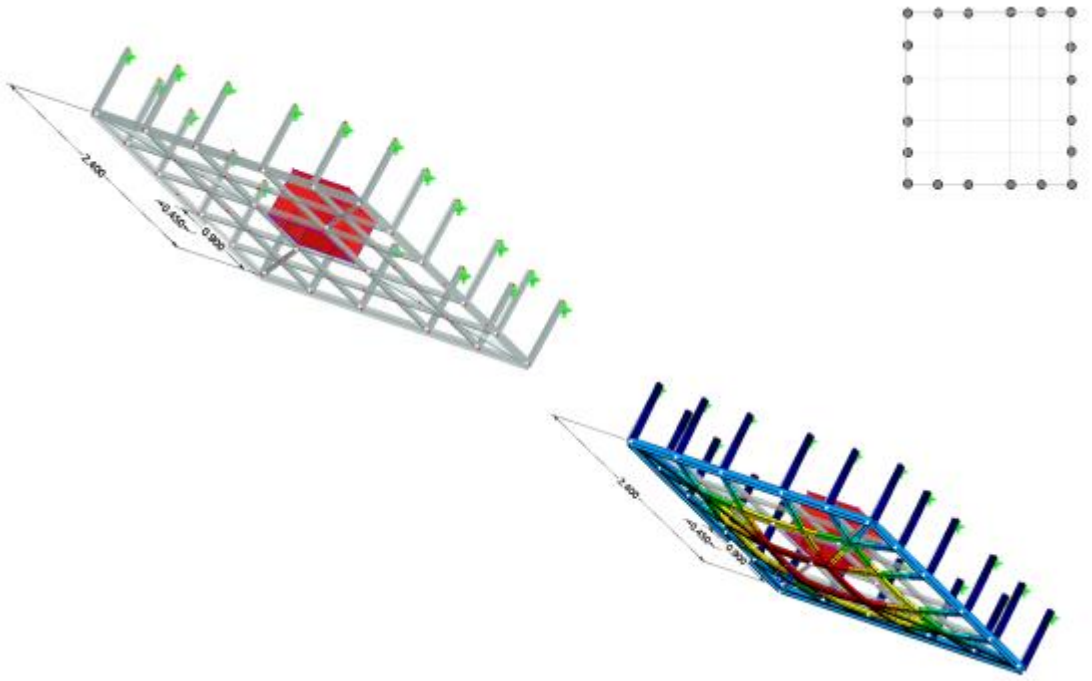

*Figure 77: SLS deflection 6.5mm*

### Option B.1

The following cases show variations of the panel attachments when the back structure is the dome space frame. If the panels are supported by the space frame and are centered to the node, deflections reach up to 2.5mm and only 8 suspenders are needed because as we see below the difference of deflections between 8 and 12 suspenders is negligible.

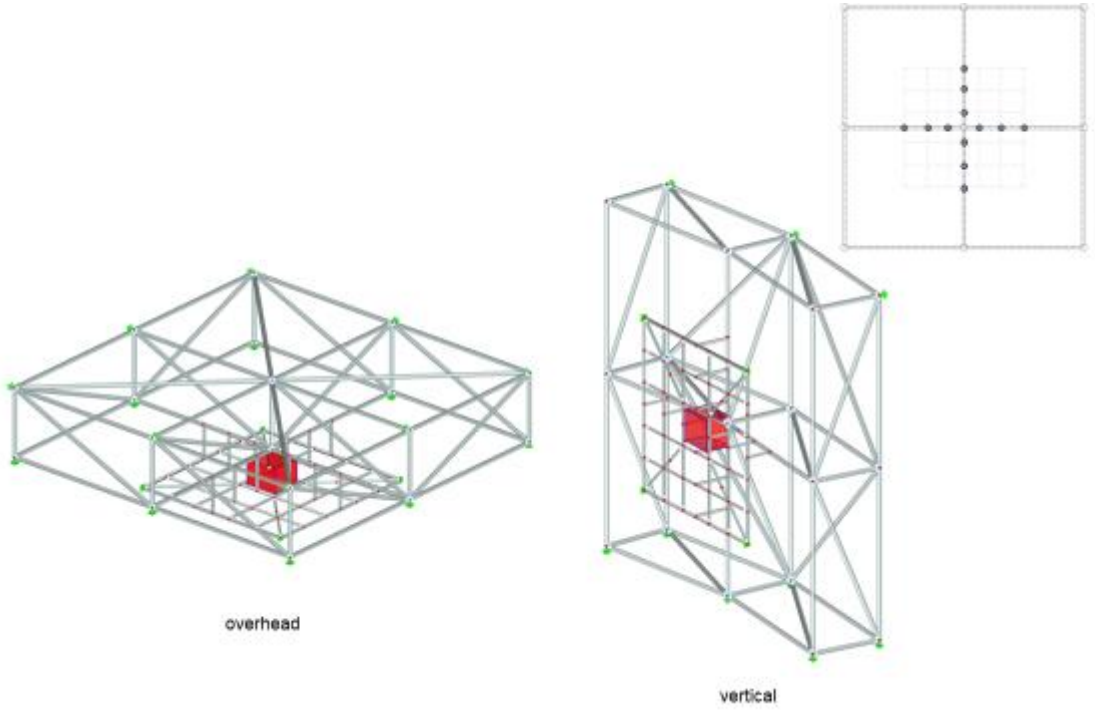


*Figure 78: Panel to space truss configurations*

For the overhead flat configuration with 12 suspenders the maximum deflection under service load (D+SDL) is 1.8mm.

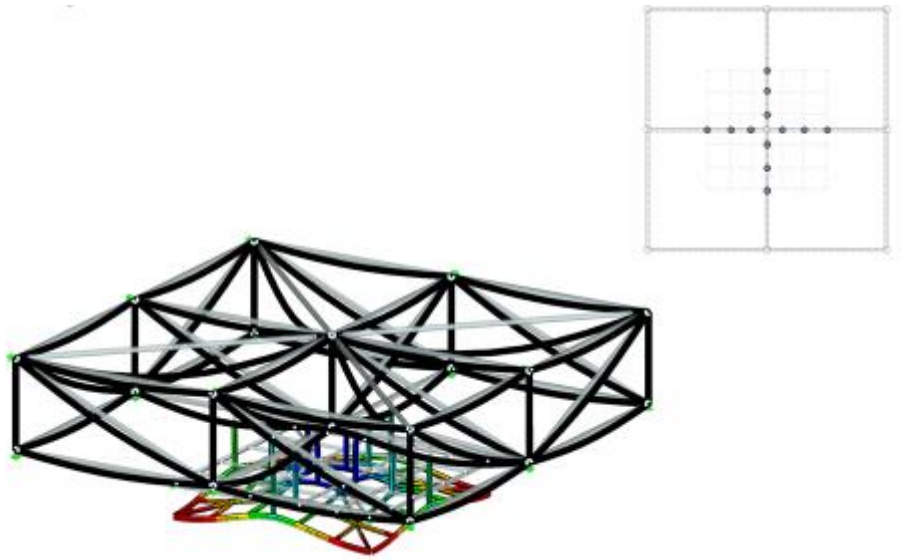

*Figure 79: SLS deflection 1.8mm*

For the vertical cylindrical configuration with 12 suspenders the maximum deflection under service load (D+SDL) is 2.1mm.

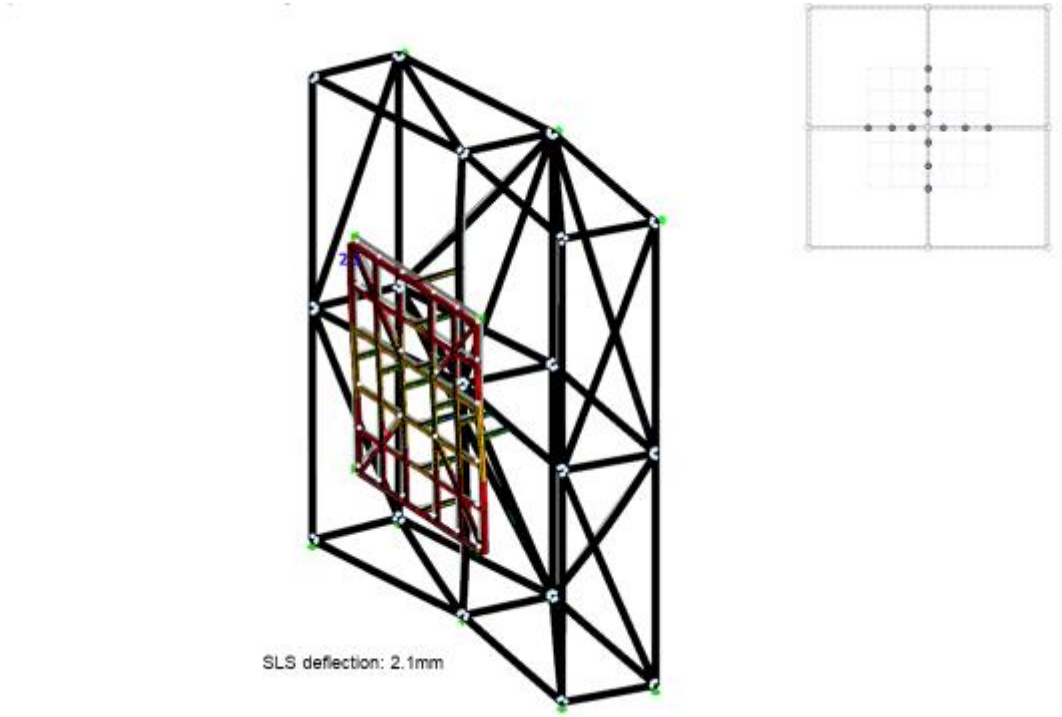


*Figure 80: SLS deflection 2.1mm*

For the overhead spherical configuration with 12 suspenders the maximum deflection under service load (D+SDL) is 2.0mm.

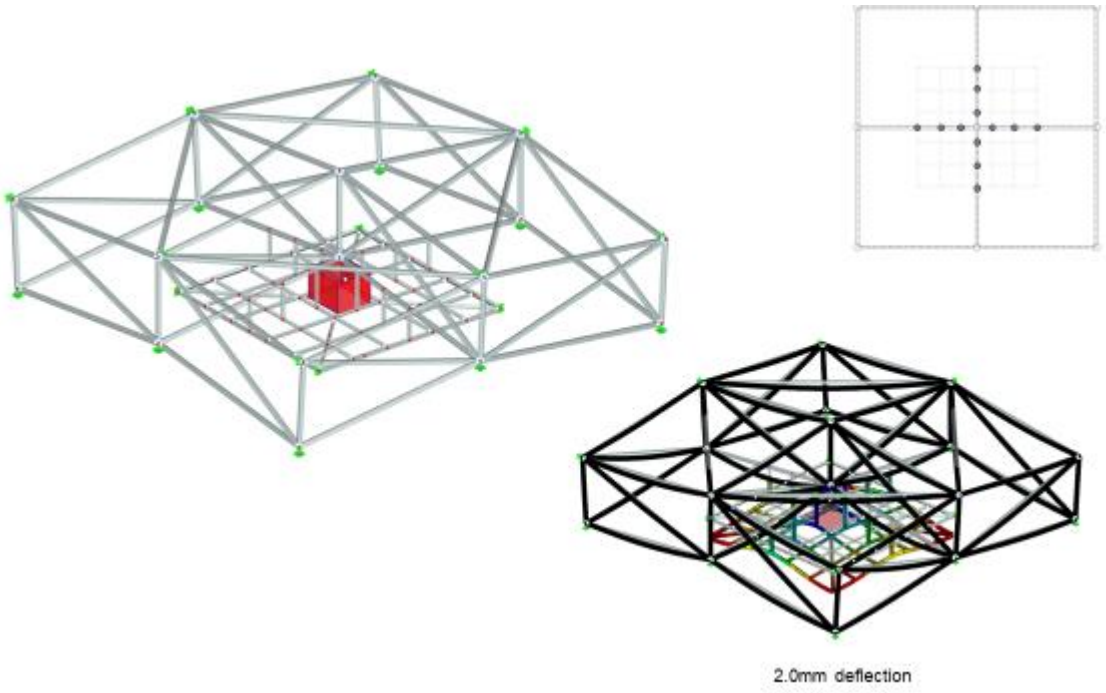


*Figure 81: SLS deflection 2.0mm*

For the overhead spherical configuration with 8 suspenders the maximum deflection under service load (D+SDL) is 2.2mm (only 0.2mm larger than the 12 suspenders).

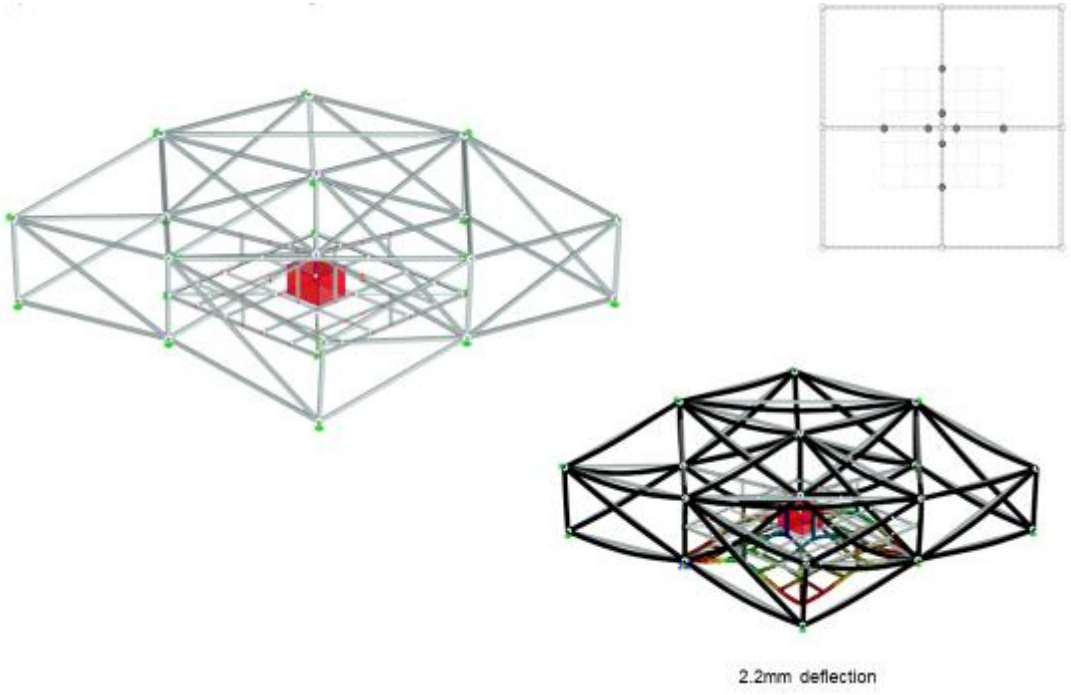


*Figure 82: SLS deflection 2.2mm*

For the overhead 45-degree configuration with 12 suspenders the maximum deflection under service load (D+SDL) is 2.3mm.

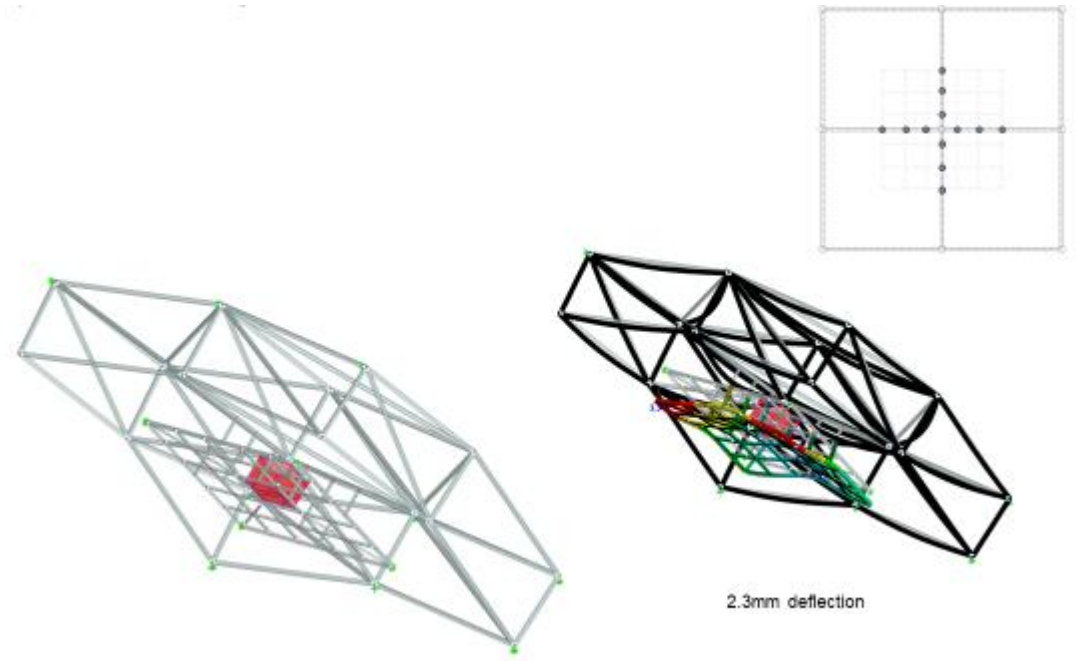


*Figure 83: SLS deflection 2.3mm*

For the 45-degree spherical configuration with 8 suspenders the maximum deflection under service load (D+SDL) is 2.5mm (only 0.2mm larger than the 12 suspenders).

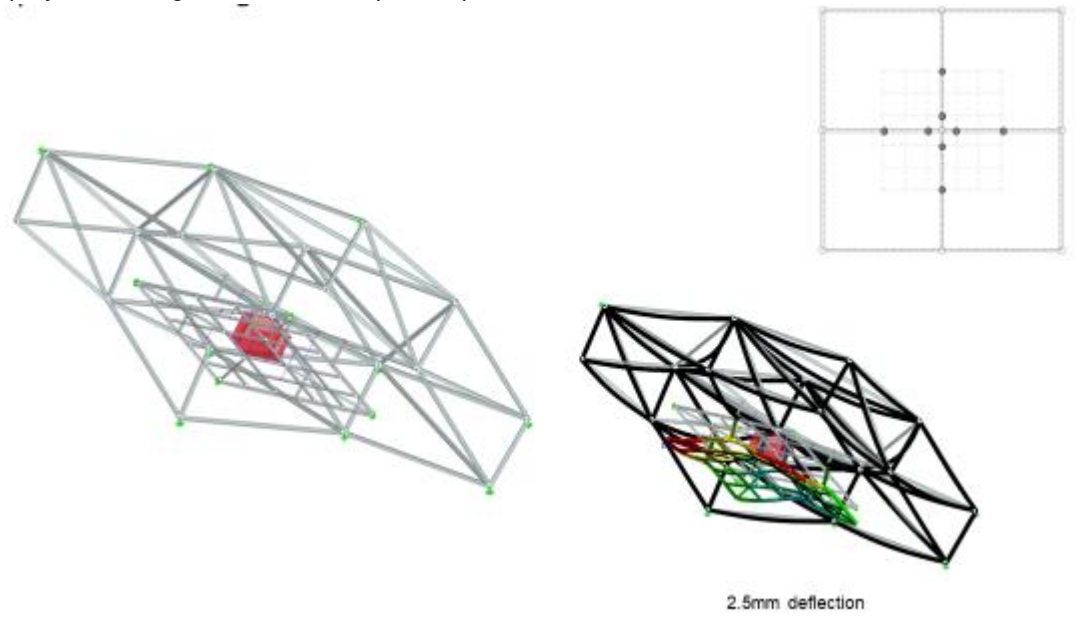


*Figure 84: SLS deflection 2.5mm*

For the vertical spherical configuration with 12 suspenders the maximum deflection under service load (D+SDL) is 1.5mm.

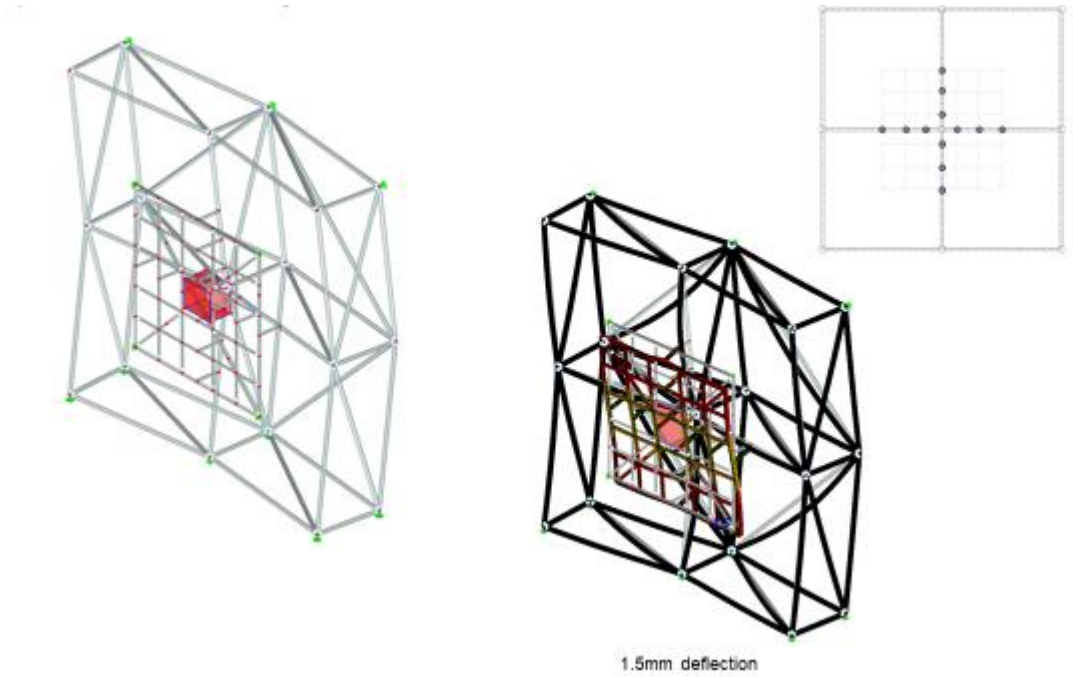


*Figure 85: SLS deflection 1.5mm*

For the vertical spherical configuration with 8 suspenders the maximum deflection under service load (D+SDL) is 1.6mm (only 0.1mm larger than the 12 suspenders).

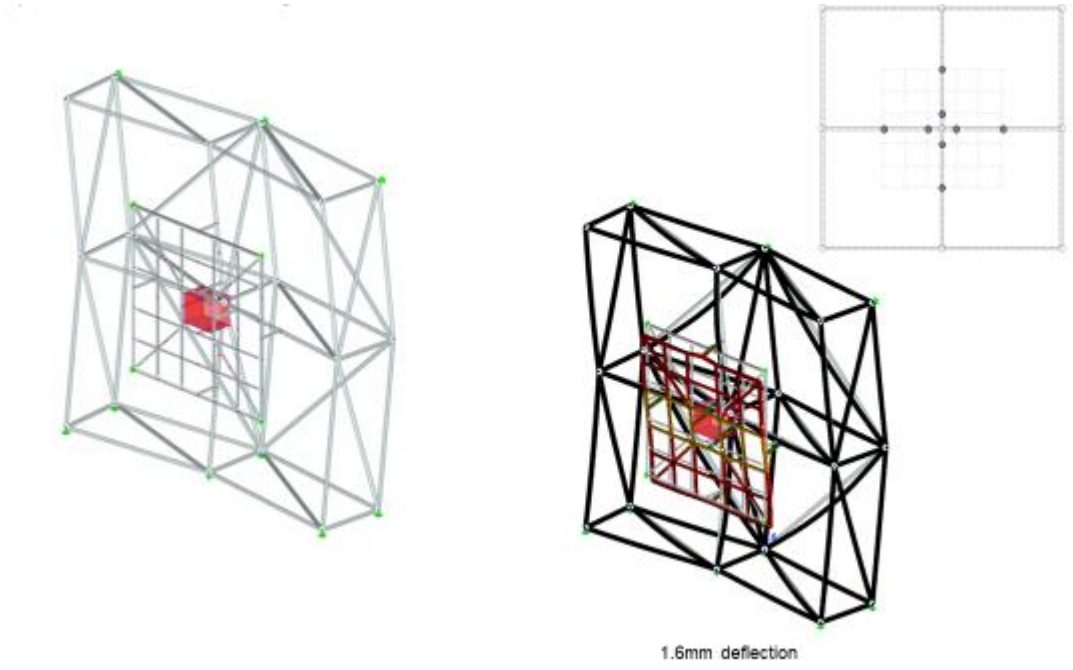


*Figure 86: SLS deflection 1.6mm*

### Option B.2

If the panels are supported perimetrically, as we saw before, the deflections are too big. So, this option cannot be retained and is only shown informatively.

For the overhead spherical configuration with 12 suspenders the maximum deflection under service load (D+SDL) is 11mm.

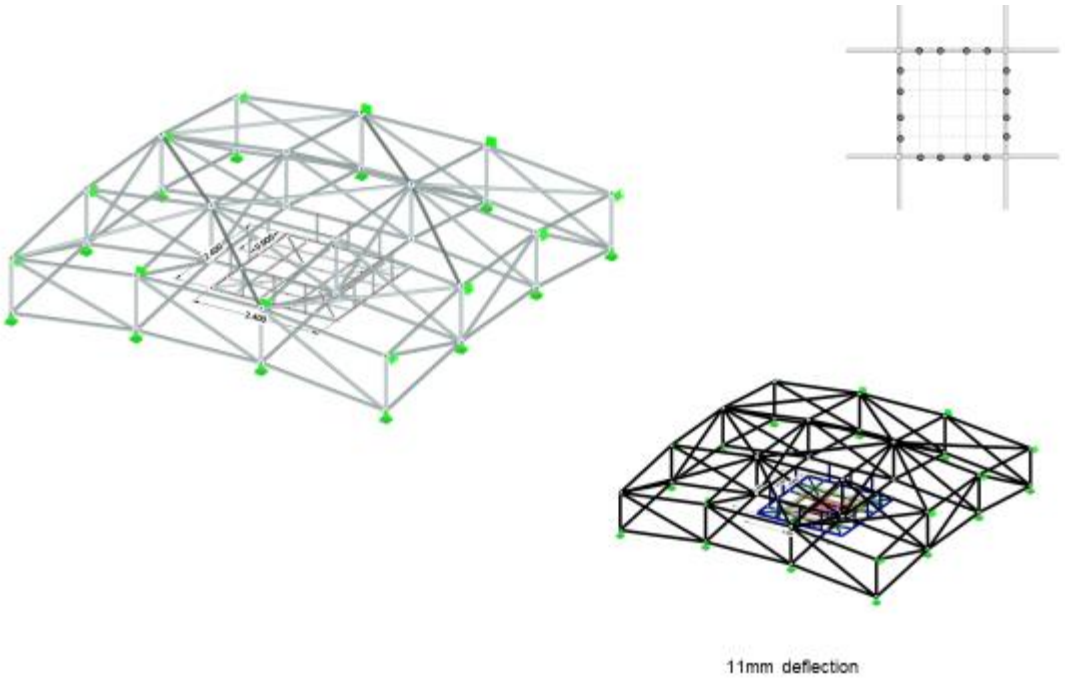


*Figure 87: SLS deflection 11mm*

For the 45-degree spherical configuration with 12 suspenders the maximum deflection under service load (D+SDL) is 7.9mm.

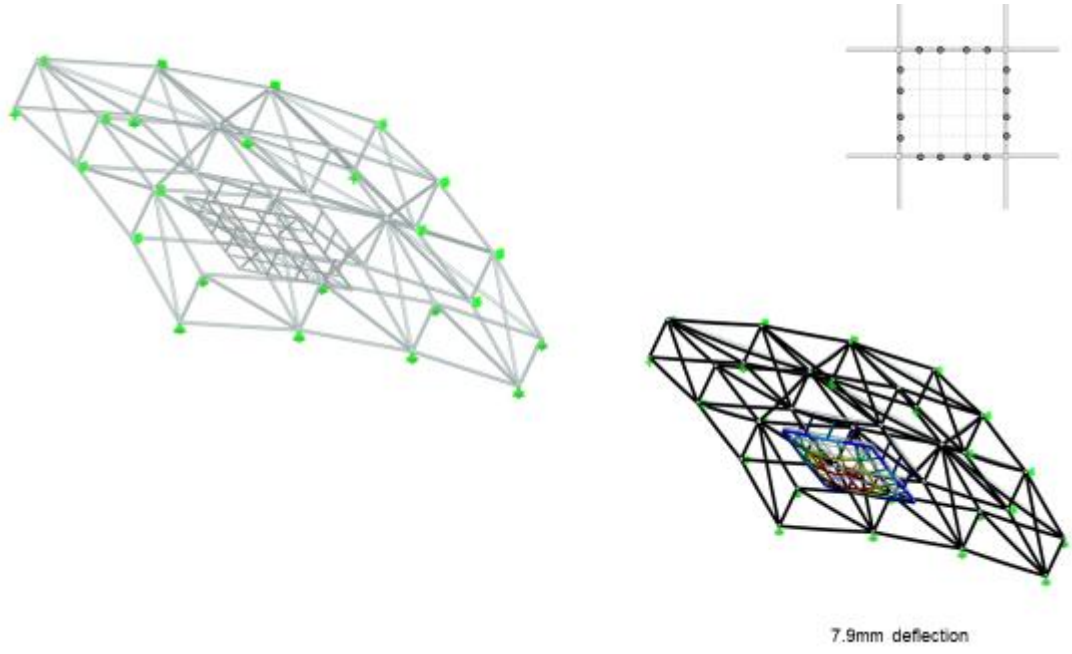


*Figure 88: SLS deflection 7.9mm*

For the vertical cylindrical configuration with 12 suspenders the maximum deflection under service load (D+SDL) is 1.2mm.

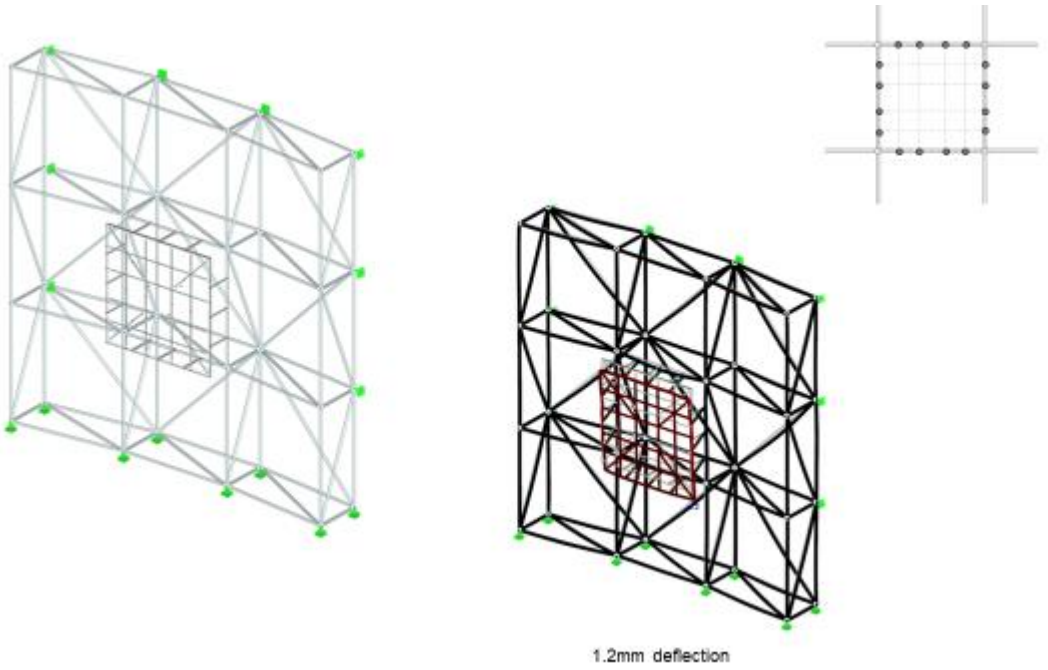


*Figure 89: SLS deflection 1.2mm*

## Speaker option 1.1

The current panel subframe design is meant to accommodate the X12 “L’Acoustics” speaker at the center opening. Nevertheless, slight adjustments in it could be easily made so that it has the required opening dimensions off-center.

Considering the centered scenario, the speaker could be attached to the node. Such a connection can be made with a pre-welded plate and rectangular HSS to the node. The connection would be a cantilever. Even though this connection can take the stresses caused from bending the deflections would need to be further verified, as the node cannot be considered a totally rigid fixed support on the cantilever.

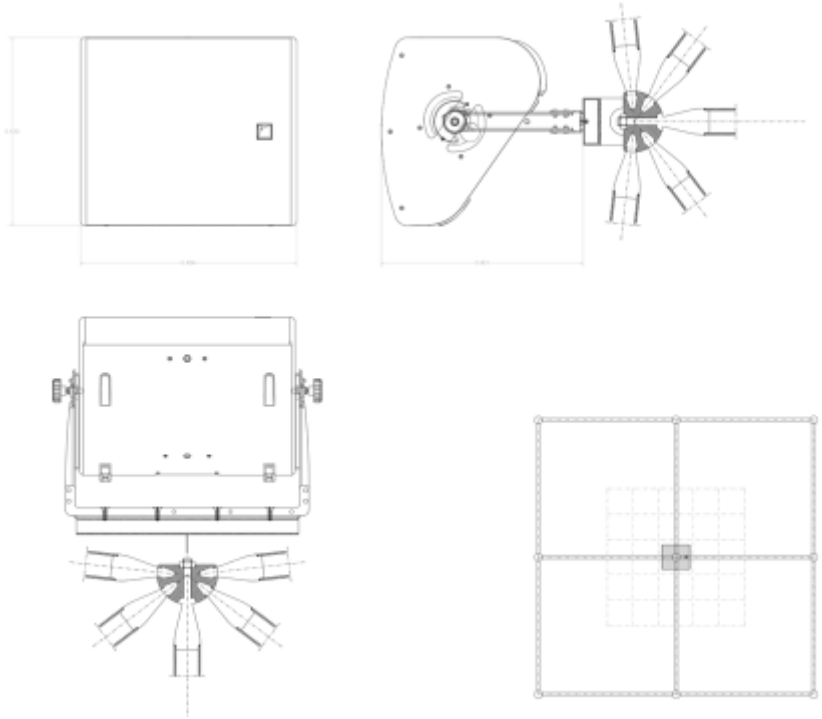

*Figure 90: Speaker to node attachment via plates*

### Speaker option 1.2

The following is another attachment option centered to the node. In this case, the end rod of the member is extended through the node outwards and is connected then to the HSS supporting the speaker. This option has the downside that the cantilevering rod can cause some small bending in the node depending on its length, which is undesirable.

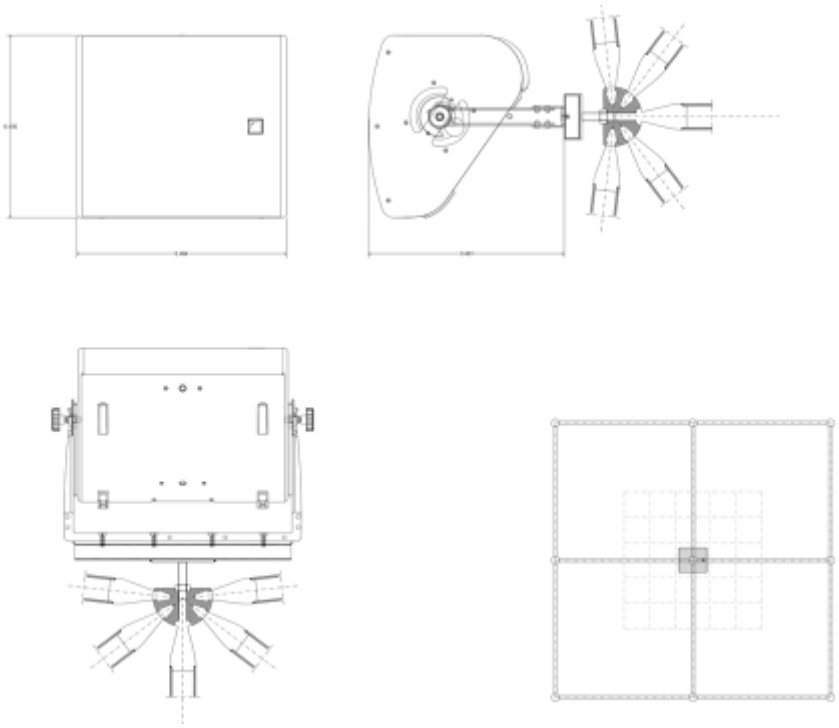

*Figure 91: Speaker to node attachment via extended rod*

### Speaker option 2.1 - additional diagonal

A different case scenario is to have an additional diagonal and support the loudspeaker off-center from the node. The new diagonal however, would introduce a small bending to the truss members. The connection of the speaker to the member would require a clamp with a flat side and additional self-tapping screws. The different HSS members could be pre-welded together.

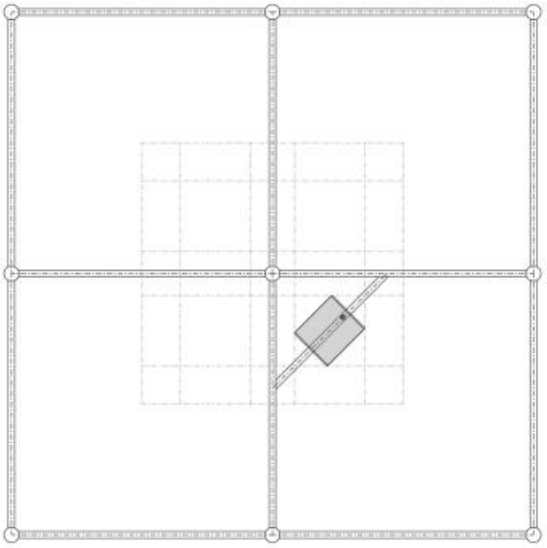

*Figure 92: Speaker attachment to additional diagonal*

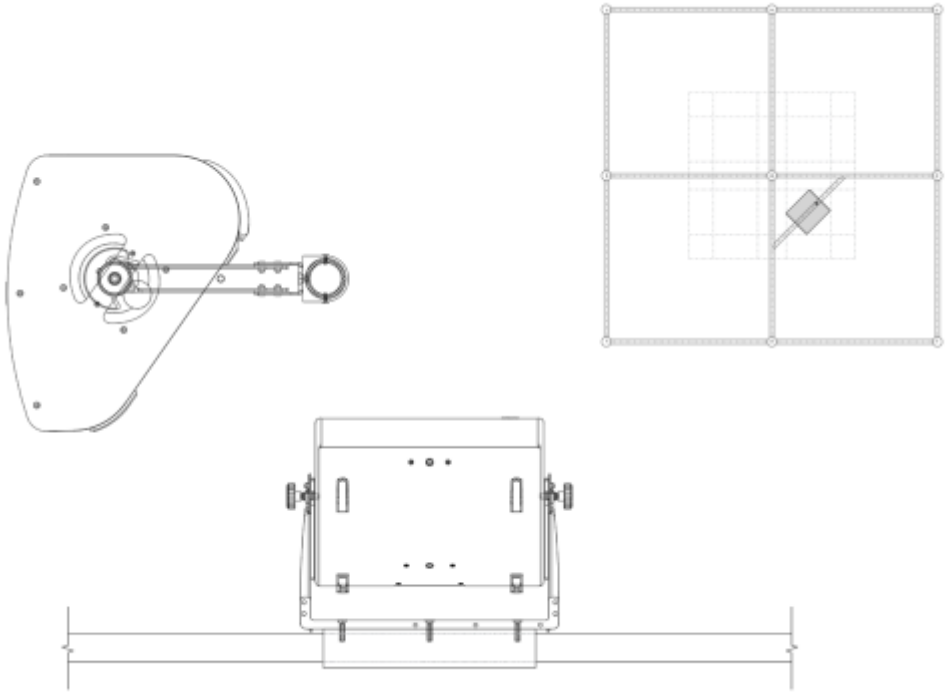

*Figure 93: Details - speaker to additional diagonal attachment*

## Speaker option 2.2

The safest option in terms of the rigidity of the connection is the following one as the maximum lever arm of the speaker bracket is activated in the vertical and inclined configurations. For the overhead configuration no moment is present in the connection detail - all three screws work in tension. For the bracket to connect to the circular member a clamp with a flat surface is tightened around the HSS as shown in the detail below.

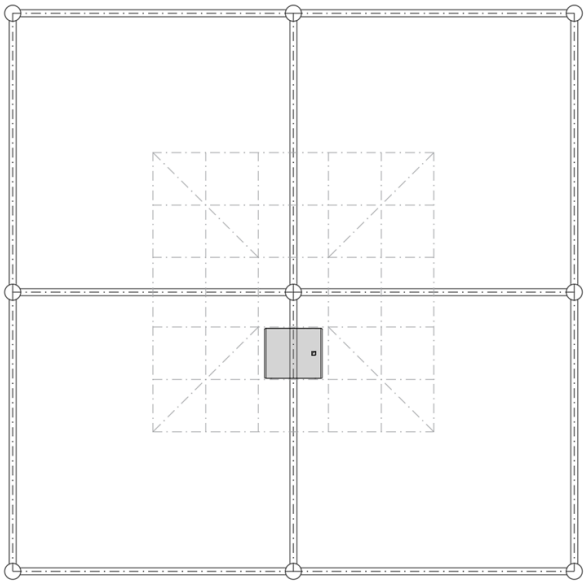

*Figure 94: Speaker to member attachment*

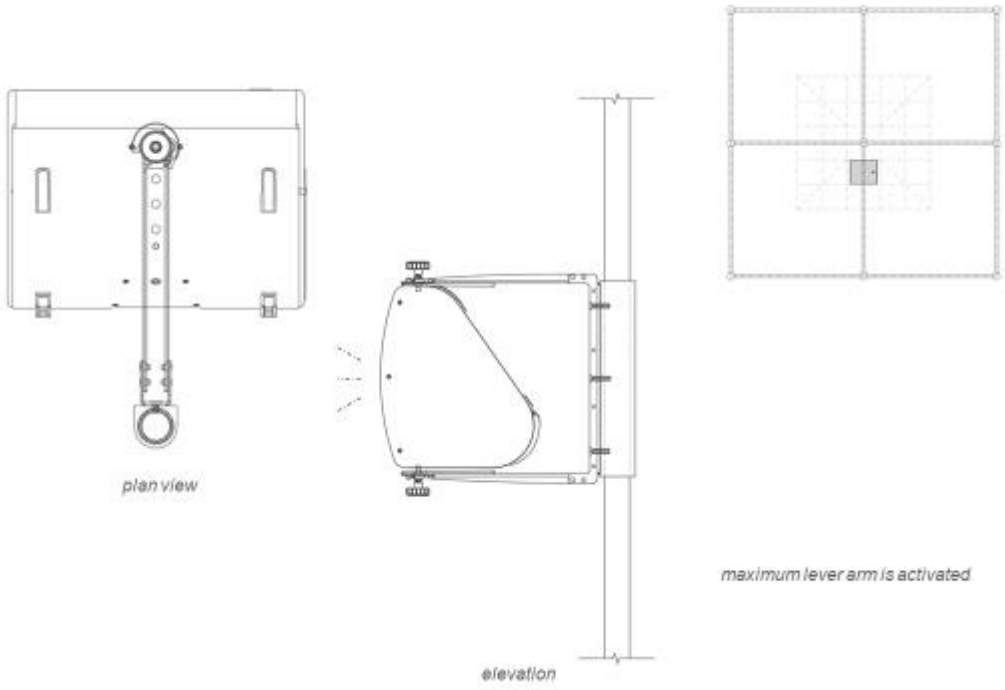


*Figure 95: Details - speaker to member attachment*

## Wall connection details

In this section we look into how the panel frame which is pre-welded or pre-bolted to the suspenders is connected to the existing walls or new spaceframe.

- Cassette attachment:

A typical way in facade systems to design the attachment of cladding to a building wall is with cassettes. This solution doesn't require many fasteners or weldings - it is rather the placement of the panel to the wall and then the locking of possible movements via some self-tapping screws at the ends. Other connection details with more fasteners are hard to realize as there is very little accessibility behind the panel (around 0.5m gap).

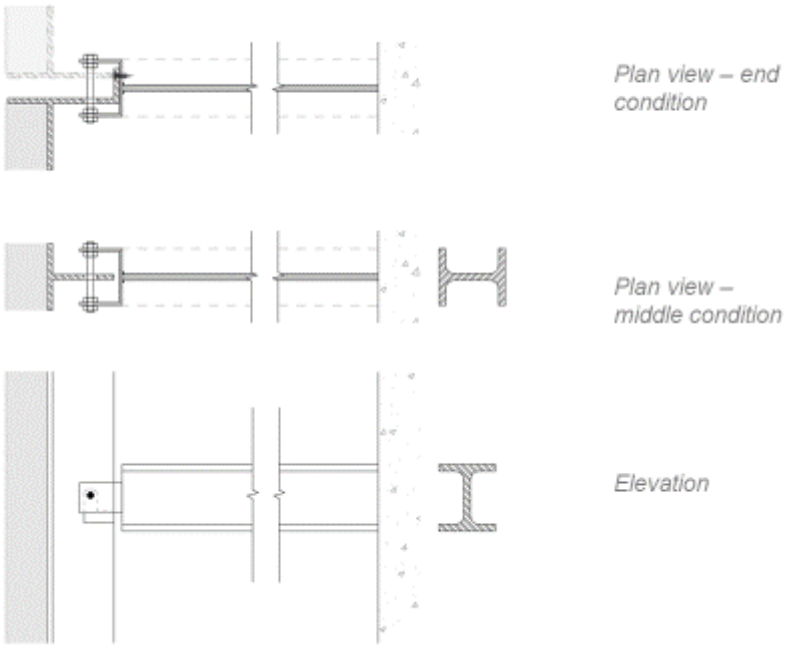


*Figure 96: Vertical configuration*

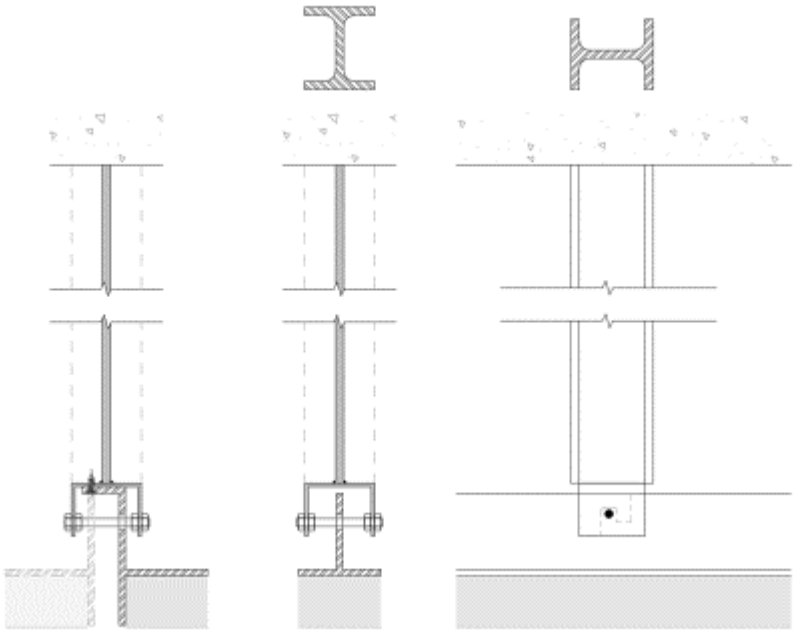

*Figure 97: Overhead & 45d configuration*

- Suspender to space frame connection

If the panel is connected to a spaceframe that connection can be made with the use of two plates pre-welded to the member and some self-tapping screws as below. Self-tapping screws are easier for this case than bolts because there is limited width to the connected sections. Adjustability in the direction of the member axis can be ensured by oversizing the plate distance and using shims if necessary. Accessibility for making this connection is ensured through the back of the spaceframe.

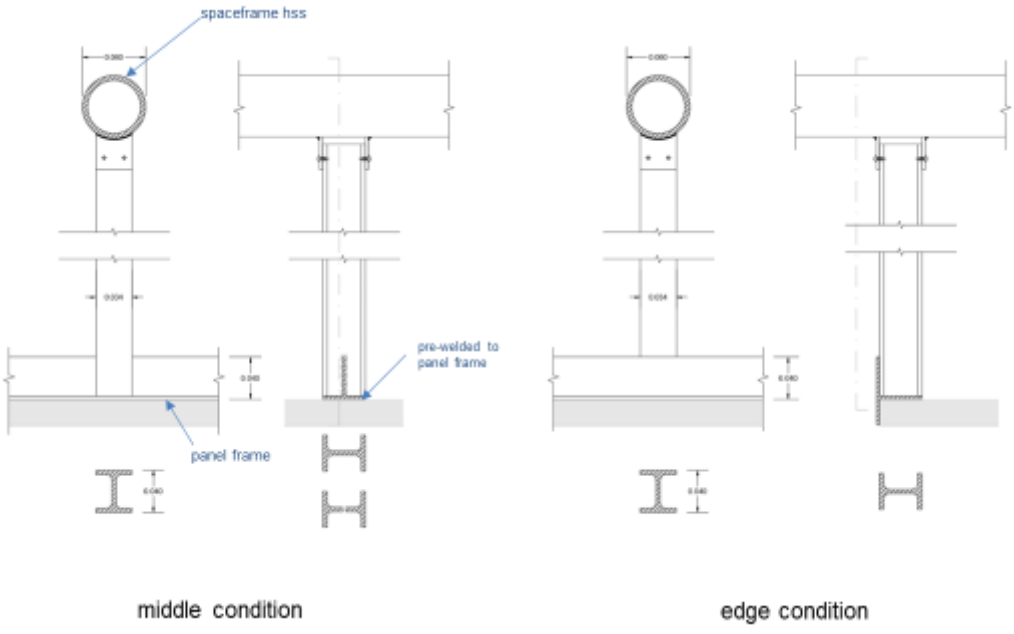


*Figure 98: Overhead configuration*

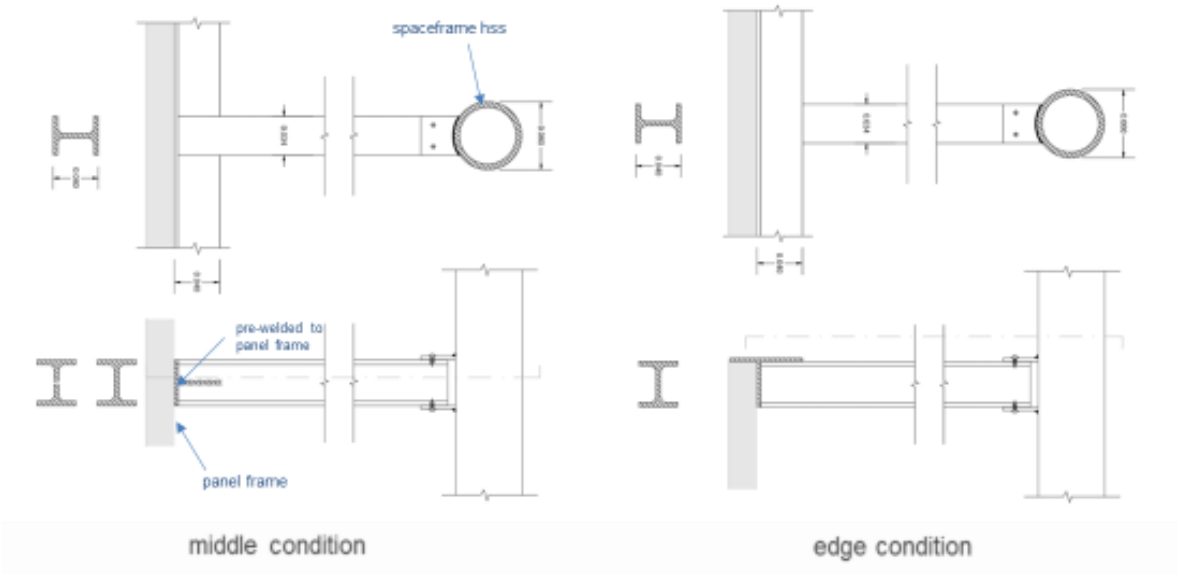


*Figure 99: Vertical configuration attachment*

Suspender connection sizing:

The required edge distances are given in the Eurocode 9 (EN 1999-1-1, Table 8.2) and are:

$$e_1 \geq 1.2d_0\,, e_2 \geq 1.2d_0\,, p_1 \geq 2.2d_0\,, p_2 \geq 2.4d_0$$

For an M5 bolt of class 8.8:

$$e = 6mm,\ \ p_2 = 12mm$$
$$Tensile\ resistance\ =\ 8.18\ kN$$
$$Shear\ resistance\ =\ 5.45\ kN$$

$$M = 0.114\ kNm\ \rightarrow\ additional\ shear =\ M/0.022\ =\ 5.18\ kN$$
$$Max\ shear\ (V_z)\ =\ 0.23\ +\ 5.18\ =\ 5.41\ kN$$
$$Max\ tension\ (N)\ = 0.26\ kN$$

Tension utilization = 0.26/8.18 = 0.03 - ok
Shear utilization = 5.41/5.45 = 0.70 - ok

- Scaffold clip:

An easier way to connect the panels to the spaceframe is by using a standard scaffold clip. This would require the suspenders to be of circular hollow section however. In this case, because it is complicated to connect a circular section to the panel geometry, pre-welding them would be the best option. Because of the eccentricity there is a small torque developed in the horizontal element, but as we are using circular hollow sections the torsional resistance is very high. The clip design is up to the scaffold manufacturer.

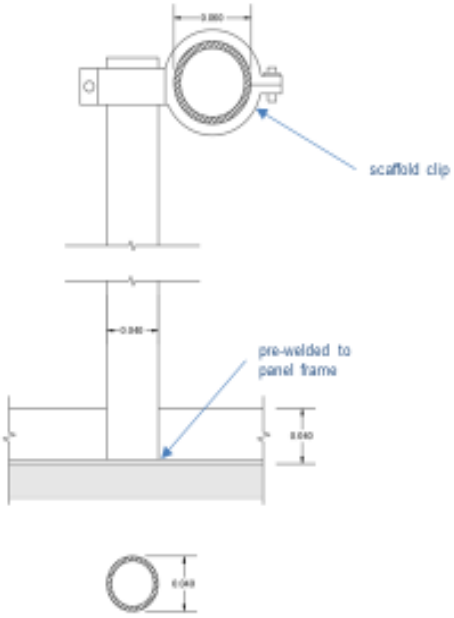


*Figure 100: Scaffold clip connection detail*

- Panel to panel connection

The connection between panels when attached to the spaceframe is at an angle following the curvature of the dome. This angle can be accommodated with the use of shim plates creating two flat end surfaces secured with a bolt, washer and nut.

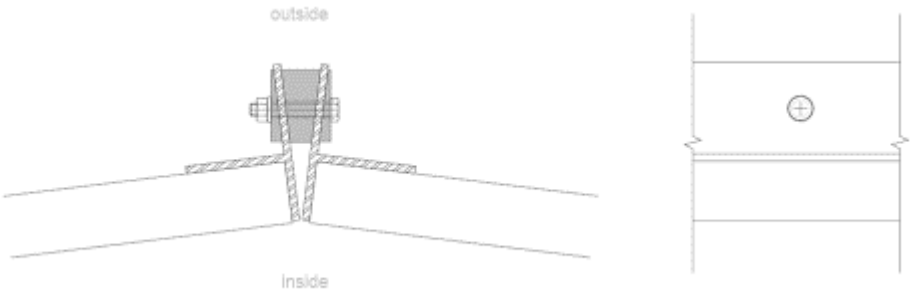


*Figure 101: Panel to panel connection detail*

- Sub-frame panel members connection

The aluminum T-section members comprising the sub-frame panel are connected with some additional plates and screws to each other. The connections are schematically shown below.

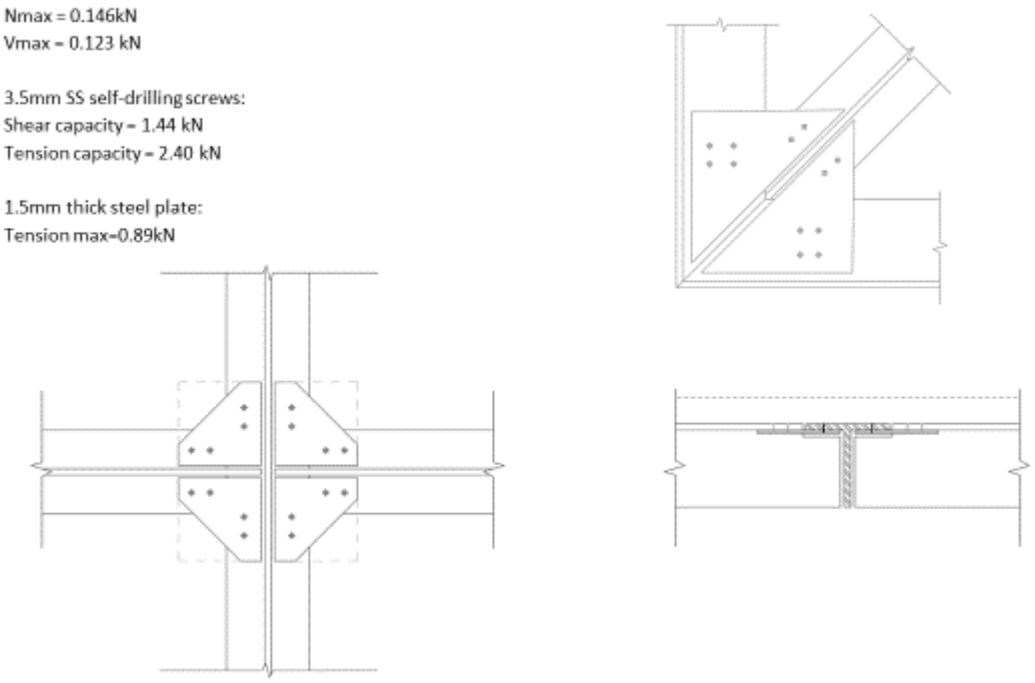


*Figure 102: Panel members connections*

# 7. Dome global analysis

The dome studied is 38m (length) x32m (width) x16m (height), and it consists of a double layer offset of 1m. The dome typology doesn't exactly match any of the existing ones. It is similar to the lamella type and the Schwedler.

## 7.1 Static Analysis

The members' section is a circular HSS (Hollow Structural Section) of 60mm diameter, 4.1mm thickness made of aluminum 6060 T6:

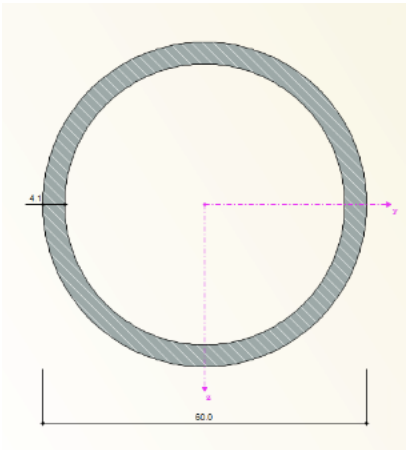


*Figure 103: HSS member cross-section*

Given that the exact location of the dome is not determined as the dome is meant to be built anywhere (inside or outside), some general loading assumptions have been made concerning wind pressure and the acoustic panels dead weight:

- Wind pressure (x,y directions): 0.10 kPa
- Super Dead Load: 0.2 kPa

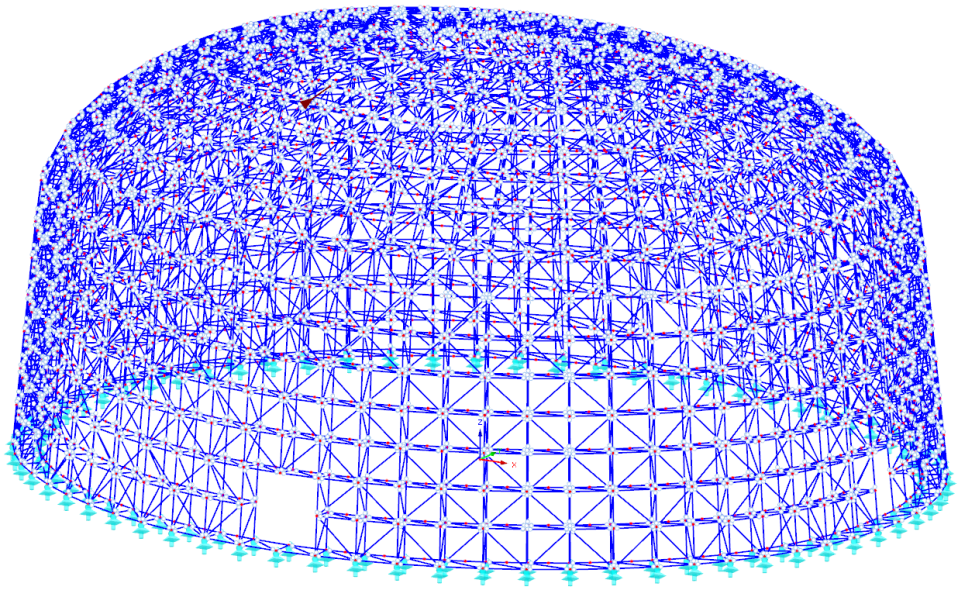

*Figure 104: Perspective view of dome*

The internal forces observed under the worst-case combination for the Ultimate Limit State (1.35G+1.5Wy) are 5.83kN of tension and 15.53kN of compression.

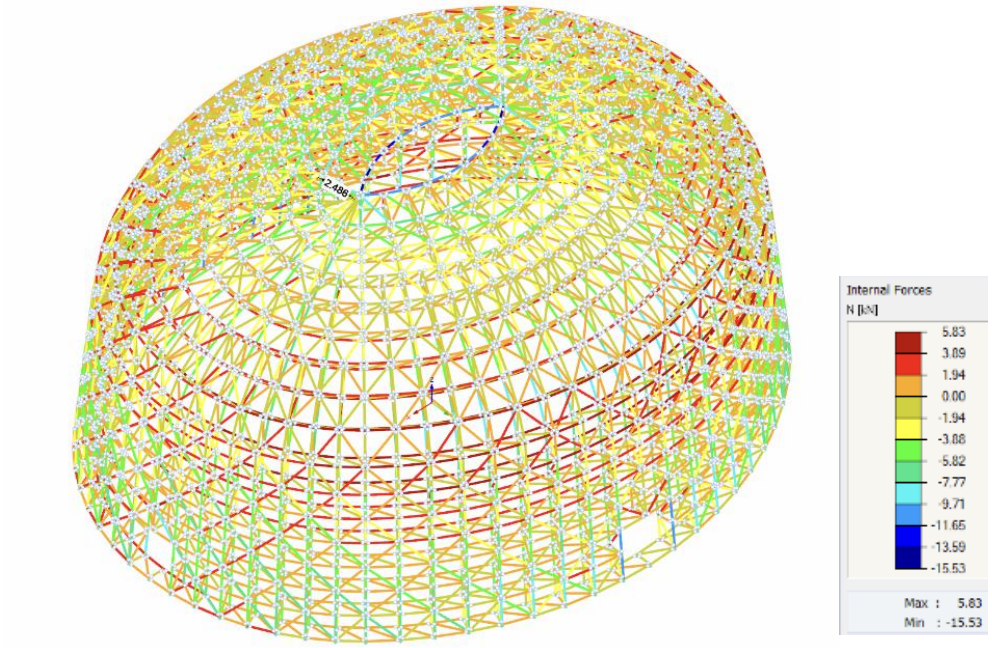


*Figure 105: Internal forces under ULS 1.35G+1.5Wy*

Under self-weight the structure sags by 3mm as shown in the figure.

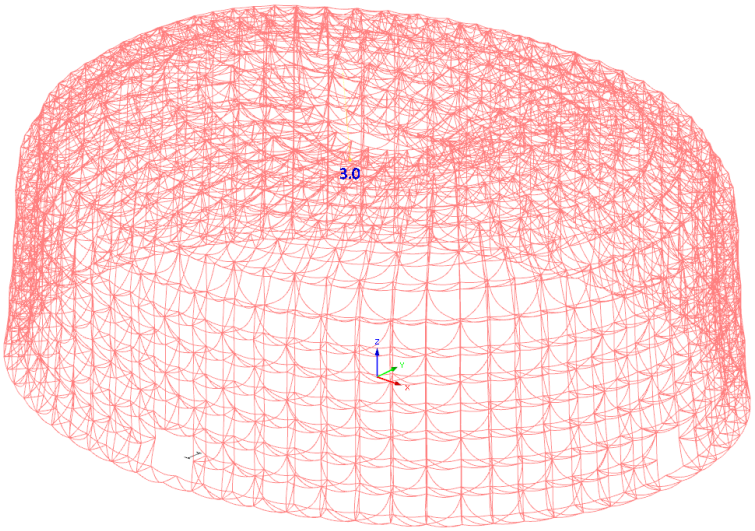


*Figure 106: Deflection 3mm under self-weight*

Under the additional weight of the insulation panels the total deflection goes to 8.4mm.

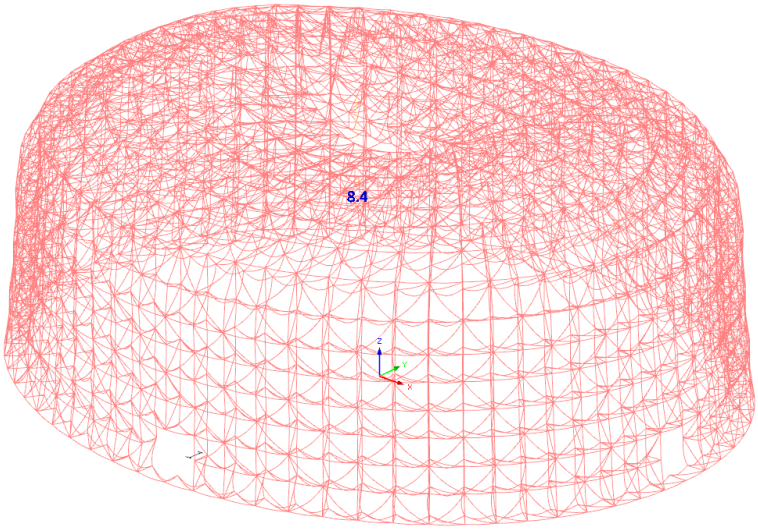


*Figure 107: Deflection 8.4mm under D+SDL*

In the case of wind in the x (long) direction, there is an 8.6mm deflection.

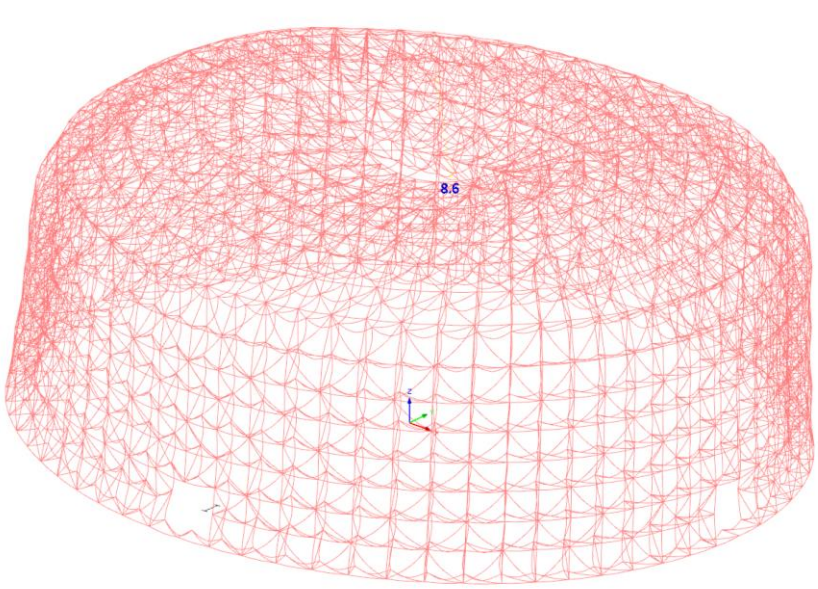


*Figure 108: Deflection 8.6mm under D+SDL+Wx*

If the wind is acting in the y (short) direction the deflections are greater than before, 9.4mm, as the structure is less rigid in the y axis. This deflection corresponds to L/3400 so it is considered negligible.

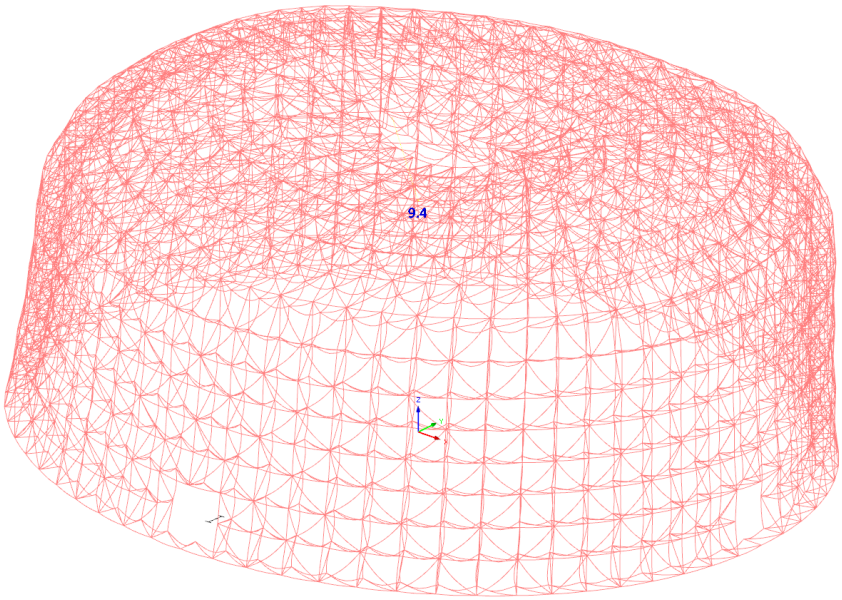


*Figure 109: Deflection 9.4mm under D+SDL+Wy*

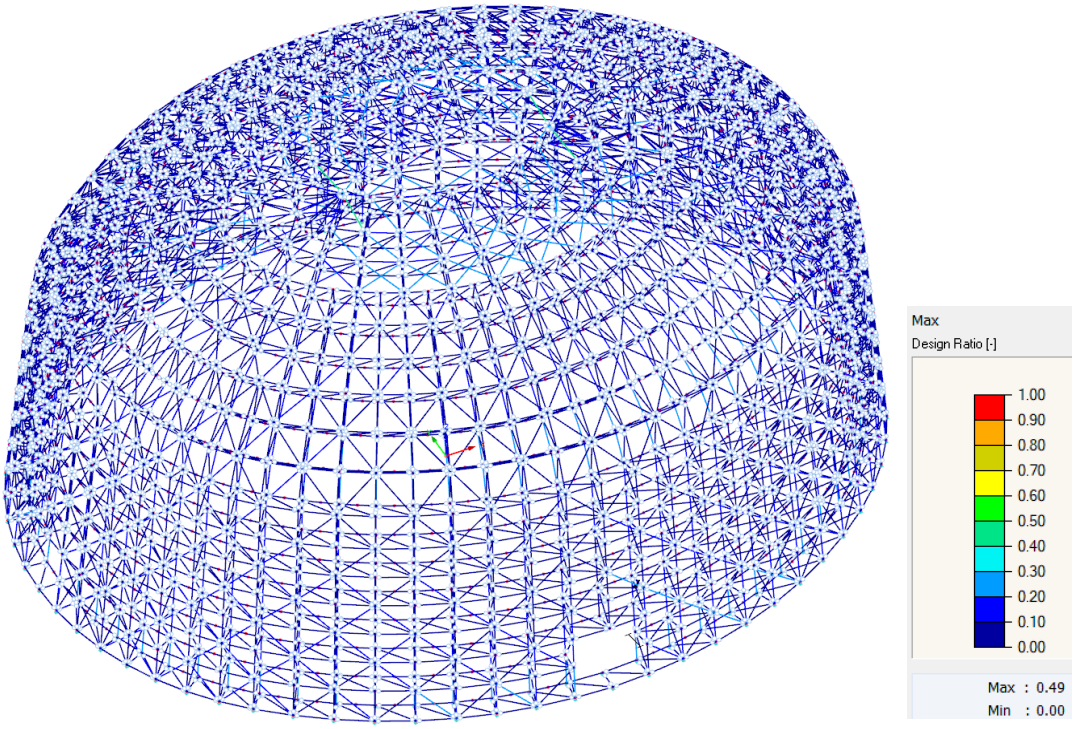


*Figure 110: Member utilization ratios*

Member to node connection weld check

The welding happens around the entire perimeter of the member and is designed according to EN 1999 chapter 8.6. The heat-affected zone (HAZ) is taken into account since we have heat-treatable alloys in temper T6.

$$\sigma_{\perp Ed} = F/aL = 15500N/(a * 189.44mm)$$
$$\sigma_{\perp Ed} \leq \frac{f_{u,haz}}{\gamma_{Mw}} = \frac{100}{1.25} = 80\ MPa$$
$$a = 1.02\ mm \rightarrow a = t = 4mm$$

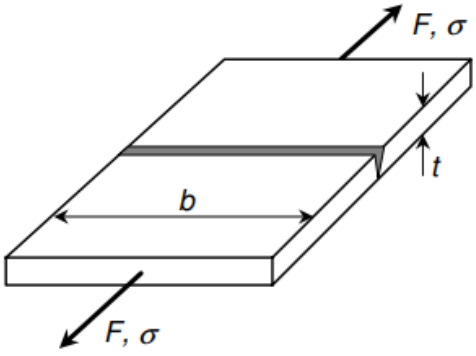


*Figure 111: Weld check sketch from EC9*

The throat thickness required is 1.02mm, however full penetration is required since these are load-bearing members. So, the weld throat thickness would be 4mm.

## 7.2 Stability analysis

For this brief stability analysis, we are going to determine the critical load factor for local instability.

The effective length of a member is $L_{cr}$ = 2.255m obtained from the model.

$$Euler\ buckling\ load\ =\ EI\pi^2/{L_{cr}}^2\ =\ 70000000 * 28 * 10^{-8}\ \pi^2/2.255^2 = 38\ kN$$
$$N_{Ed} = 9.8\ kN$$

Material: 6060 T6 aluminum
Buckling class: A

$$a = 0.2 \quad (imperfection\ factor)$$
$$\overline{\lambda_0} = 0.1 \quad (limit\ of\ the\ horizontal\ plateau)$$

$$\bar{\lambda} = \sqrt{\frac{A_{eff} f_0}{N_{cr}}} = \sqrt{\frac{7.15cm^2 * 160MPa}{38kN}} = 1.74$$

$$\varphi = 0.5(1 + \alpha(\bar{\lambda} - \overline{\lambda_0}) + \bar{\lambda}^2) = 2.18$$

$$\chi = \frac{1}{\varphi + \sqrt{\varphi^2 - \lambda^2}} = 0.286\ \leq 1$$

$$N_{b,Rd} = \kappa\ \chi\ A_{eff}\ f_0/\gamma_{M1} = 29.7\ kN$$

$$Critical\ load\ factor\ =\ 29.7/9.8 = 3$$

A similar result is obtained in RFEM. The small 0.53 difference is possibly caused due to global stiffness effects, and other imperfections which are not accounted for in the hand calculation.

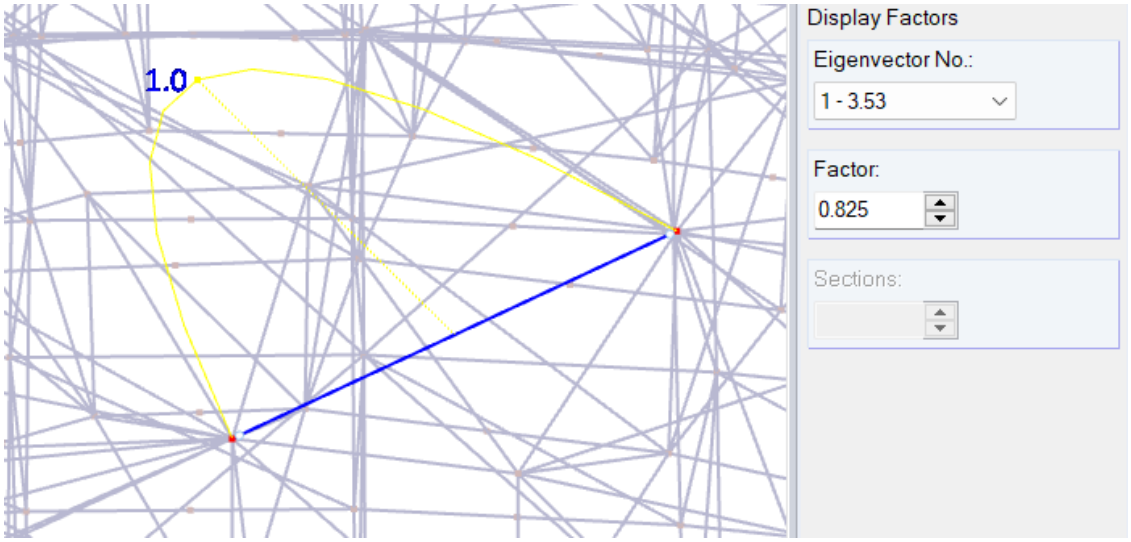


*Figure 112: RFEM stability analysis results*

## 7.3 Preliminary dynamic frequency check

For the 1st mode of frequency, the effective mass factor (eff. mass/total mass) obtained is close to 0% (f1=6.77 Hz), therefore we pass to the 2nd mode which has a 70% factor and represents sway in the y direction. The 2nd mode's frequency is 7.06Hz.

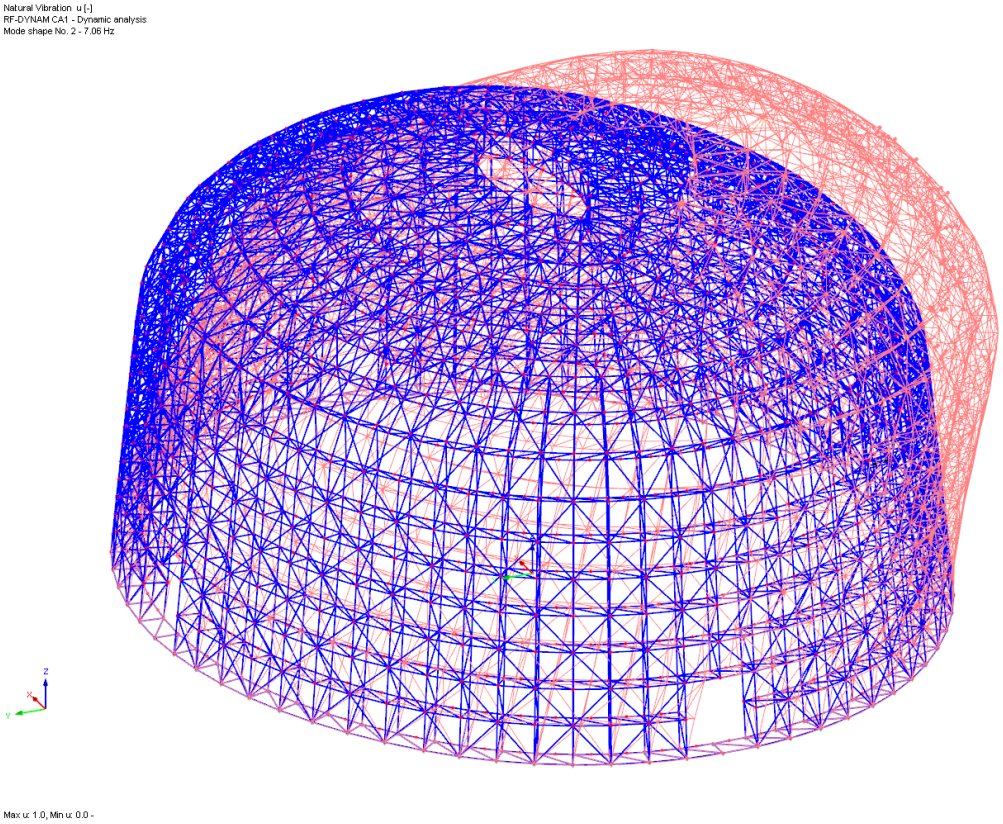


*Figure 113: 2nd mode shape - sway in y direction*

Overall, considering the first 30 modes gives us over 0.83 as effective mass factor, and the natural frequencies corresponding are well below the lowest frequencies of the loudspeakers (>40Hz), and far higher than the wind (~1.5hz) or human vibrations. Therefore, there is no risk of resonance.

# 8. Nodal analysis

From the global model analysis, we get that our maximum compression is 15.5kN and the maximum tension is 5.83kN. We note that the highest compression is found around the top ring (as is typical for dome structures) and the base vertical member acting as columns.

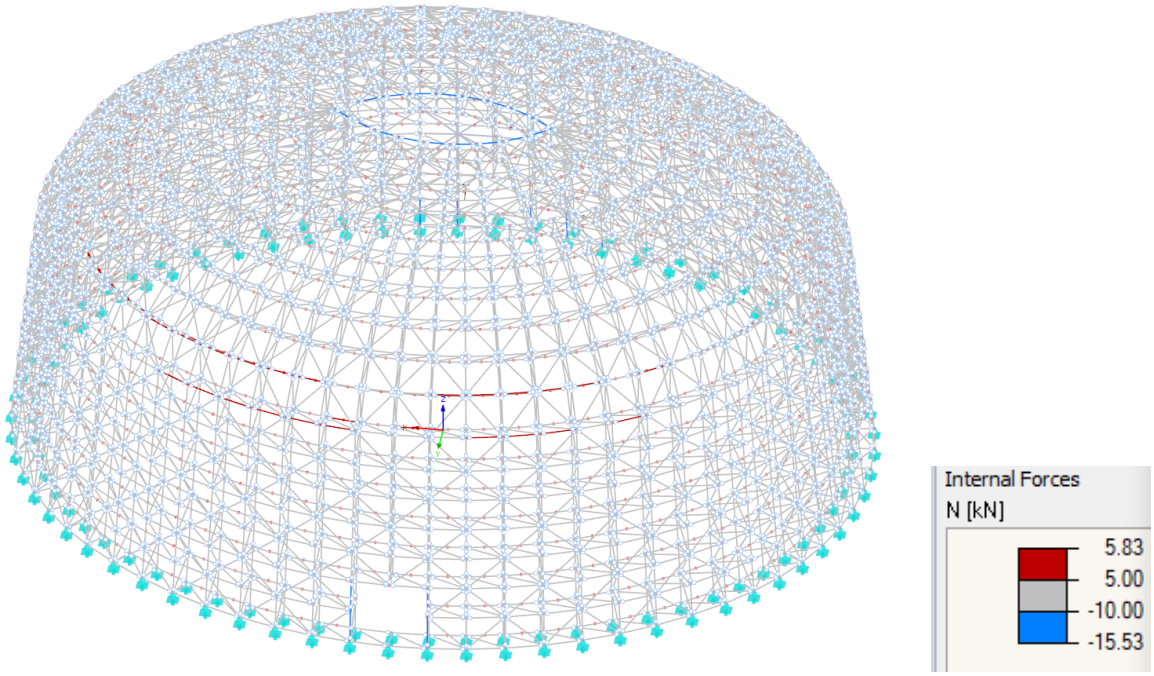


*Figure 114: Max and min axial internal forces*

As expected, we see the highest values of tension on the horizontal ring elements, which are activated as the dome tries to open up towards the base. The highest values of compression are observed at the top ring and at the base, in particular where there are door openings.

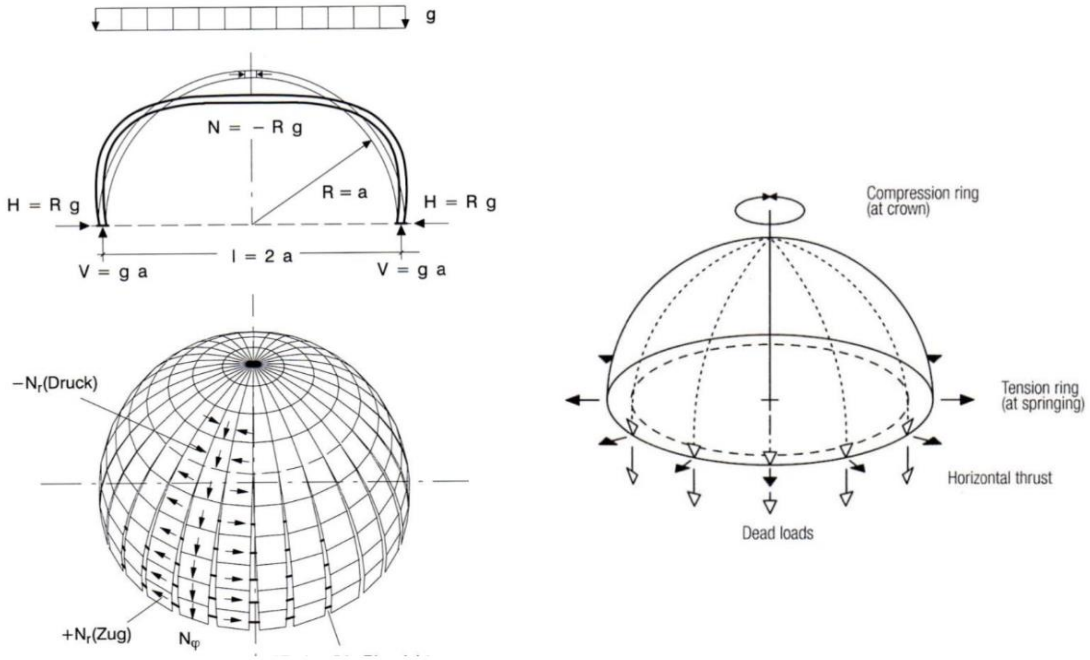


*Figure 115: Load paths for domes*

## 8.1. Modeling assumptions

The node is composed of three separate parts. They share common points (nodes) in the center area but are offset from each other at the outer perimeter by 0.5mm distance. The node was modeled this way as near the center, the three parts are held together (compressed) by the pretensioned bolts, so they are in full contact. Near the edges, the effect of the bolt pretension is less significant therefore if a member is in tension, it is likely that the node may open up slightly and the different parts get detached from each other. Ideally the interfaces should be modeled as a thin contact solid that can transfer only compression (no tension) and has the appropriate material friction. In the available software used for this study (RFEM) non planar contact surfaces are not possible to be modeled, which is the reason why the previous modeling technique was followed.

Surface supports are located around the contact area of the middle rod. In reality though, the support conditions of the node are more complex than that. The node is not only supported by the middle rod, it is supported by all the members connecting to it, and the direction of the supports depends on the inclination of the node in the dome and the connecting angle of each member. It is essentially an equilibrium where each member has a role. The middle support condition will suffice for the purposes of this analysis as it is necessary to have some supports in order for the model to run. In full equilibrium the support reactions should be zero.

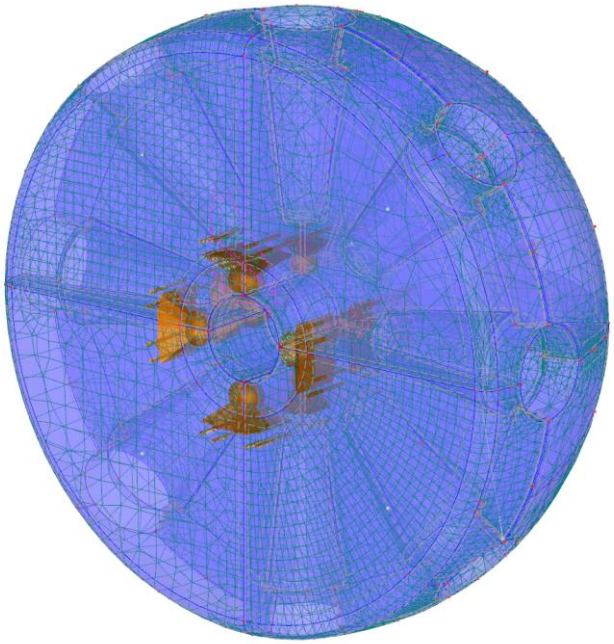

*Figure 116: Perspective view of model with boundary conditions*

## 8.2. First case study - base of dome

As a first step, a node near the base of the dome was chosen to be studied as in that zone we see some of the highest compression values. It is chosen to start by this in order to understand the behavior of the general stress patterns in compression.

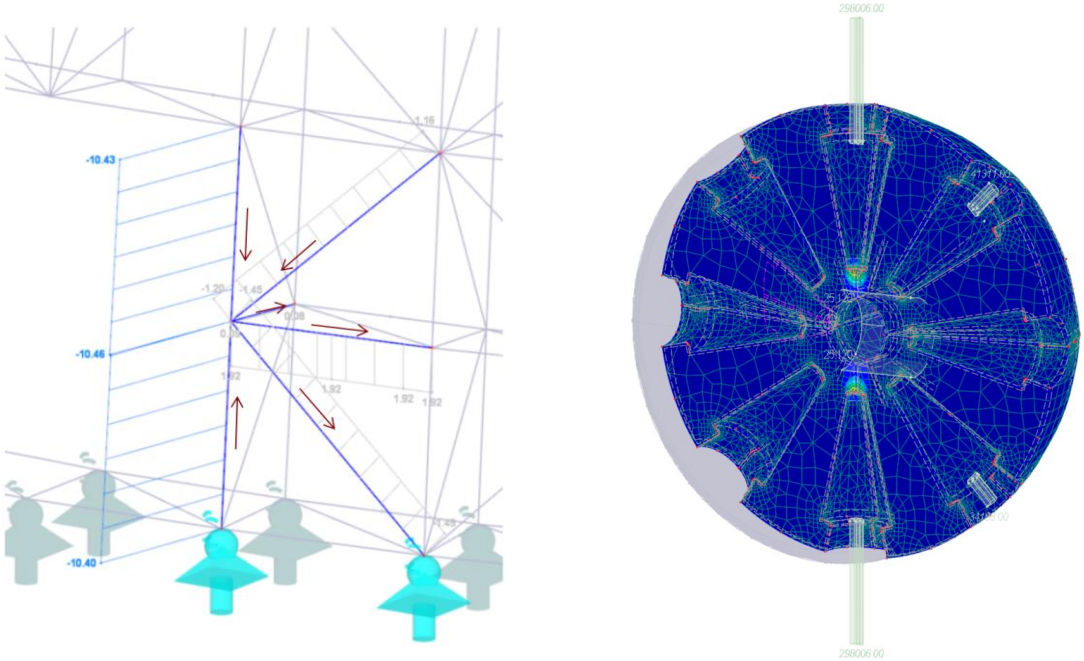


*Figure 117: High compression effect*

As we can see the yield stress is surpassed here. We can observe from this loading case that the node stress patterns are independent per member slot. Therefore, next we will test individual slots (front and back layer) for the worst-case loading scenarios. It is noted however that in reality, interaction may occur in the node even though the 3D model does not show any. This is why lab testing is necessary in addition to this analysis.

## 8.3. Maximum compression case study

The maximum compression from the global model corresponds to 5.83 kN and is found in the top ring of the dome

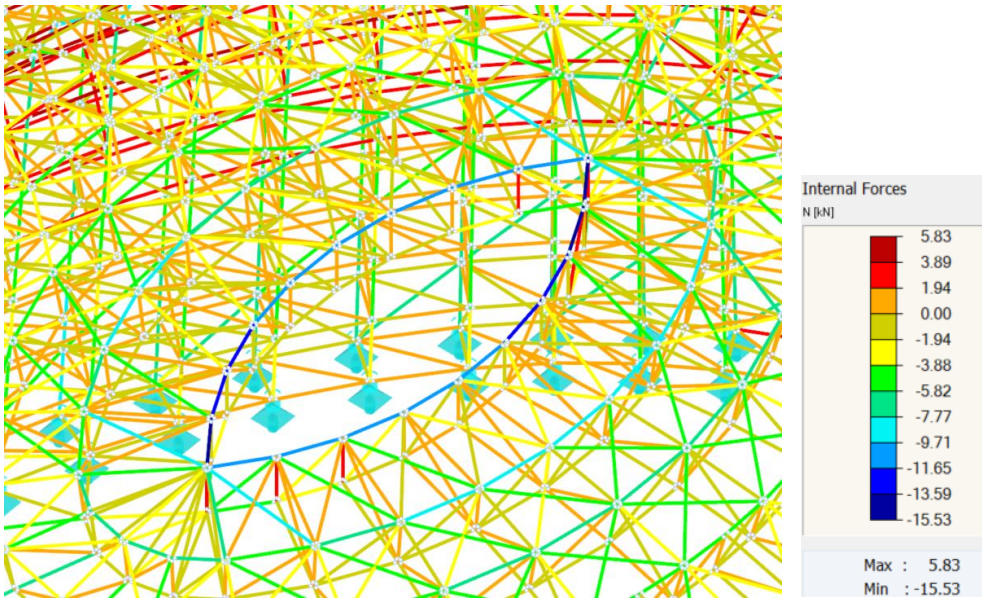


*Figure 118: Top compression ring of dome*

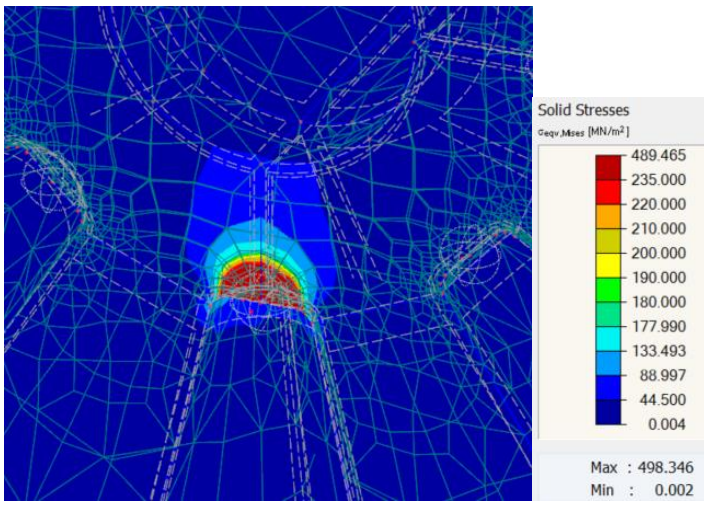


*Figure 119: Von Mises stress*

It is evident here that the stress overpasses the steel capacity assumed (S235). If we therefore increase the contact area to double the current one, we have the following stresses which remain well below 235MPa.

The initial total diameter of the tip of the member was 6.69mm corresponding to 35.1mm$^2$ area. This initial assumption included the rounded corners as well. We see that even with this larger area assumed, the node is overstressed ($\frac{15.5\ kN}{35.1\ mm^2} = 442\ MPa > 235\ MPa$). In reality though, full contact on the rounded corners cannot be achieved. To refine this calculation and determine the exact contact area around the edge we are going to use the Hertzian equations.

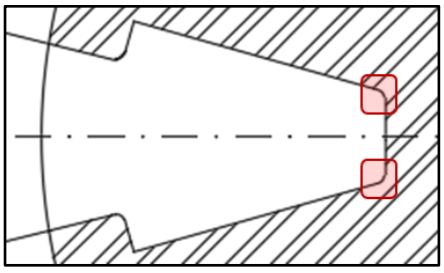

*Figure 120: Rounded edge*

### Rounded contact area at cone edge

The end of the cone has a flat circular surface and a quarter-torus surface. For the rounded part, the exact contact area needs to be determined. The Hertzian equations for contacting spheres and cylinders may be used, as our shape is in reality between these two.

$$R_1 = 1\ mm\ (member)$$
$$R_2 = 1.2\ mm\ (node\ cavity)$$
$$F = 15.5\ kN$$

Hertzian spherical contact in cavity:

Contact width:

$$\alpha = \sqrt[3]{\frac{3FR_e}{4E_e}}$$

$$\frac{1}{E_e} = \frac{1-{v_1}^2}{E_1} + \frac{1-{v_2}^2}{E_2} = 1.73 * 10^{-5}$$

$$\frac{1}{R_e} = \frac{1}{R_2} + \frac{1}{R_1} = 1.83$$

$$a = 0.48\ mm$$

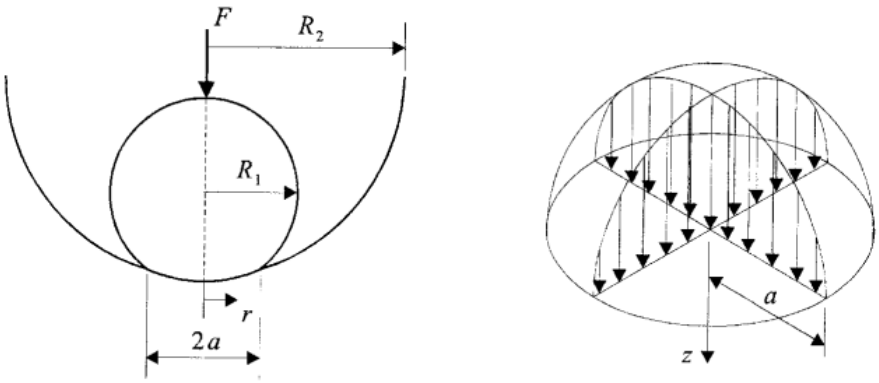


*Figure 121: Spherical contact in cavity*

Hertzian cylindrical contact:

$$\alpha = \sqrt[3]{\frac{4FR_e}{\pi E_e}} = 0.43\ mm$$

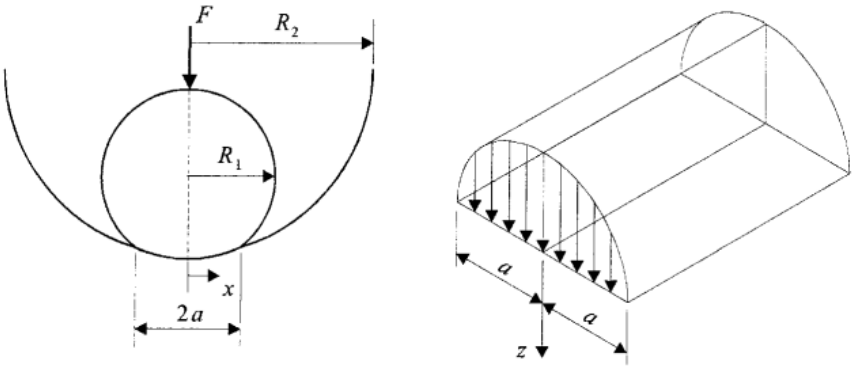


*Figure 122: Cylindrical contact in cavity*

For what follows, we are going to consider a width of 0.45 mm as it is between the spherical and cylindrical contact widths and the actual geometry corresponds more to a torus.

$$a = 0.45\ mm$$
$$A = 7.32\ mm^2\ area\ of\ sphere\ contact\ \ (42\%\ of\ initial\ flat\ area)$$
$$initial\ flat\ area\ =\ 17.5\ mm^2$$
$$initial\ total\ area\ =\ 24.8\ mm^2$$

From the previous analysis where we had considered a full contact area (35.1 mm$^2$) we can see that we need to bring down the stresses to half, so we are going to increase the flat area radius to 4.48mm while keeping the rounded 1 mm.

$$R_{new\ flat} = 4.48\ mm$$
$$New\ total\ area = 70.5\ mm^2$$
$$New\ applied\ pressure\ = P/A = 220\ MPa$$

It is verified in RFEM that the VM stresses are indeed around 220 MPa.

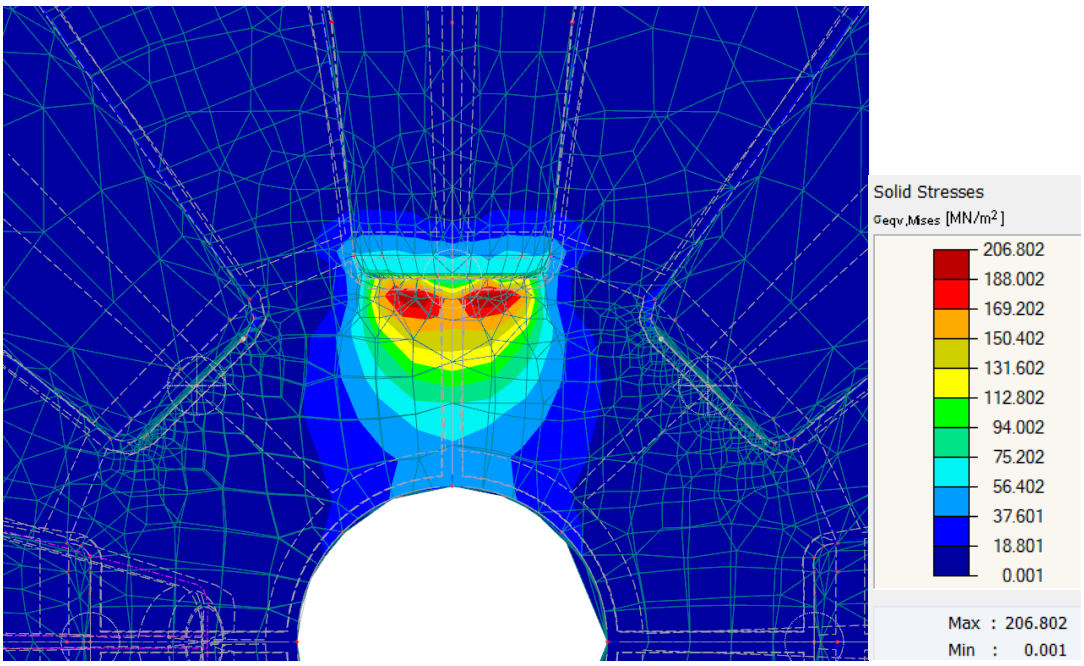


*Figure 123: New stresses on increased surface*

## 8.4. Stress distribution patterns

For the maximum compression of 15.5 kN, we are going to look into more detail the stress distribution pattern.

It is interesting to note the similarities between Boussinesq's theory and the node. The theory can be generally applied to our node as his assumptions match our own:

- Soil is elastic, homogenous, isotropic
- Soil is weightless
- Soil is not subjected to any other stress before the load application
- Continuity of stress
- Change of the soil volume due to loading is neglected
- Symmetrical stress distribution with respect to z axis

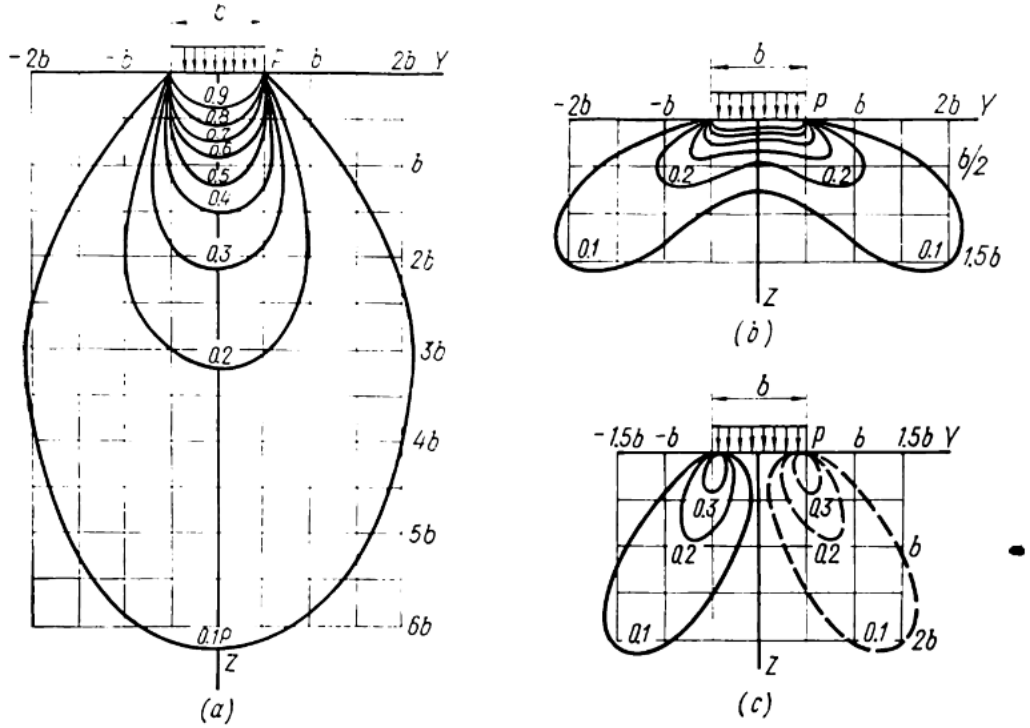


**Fig. 49. Lines of equal stresses in a linearly deformable massif for the planar problem**

(*a*) isobars $\sigma_z$; (*b*) lateral pressure $\sigma_y$; (*c*) shears $\tau_{zx}$

*Figure 124: Boussinesq's distribution under square load*

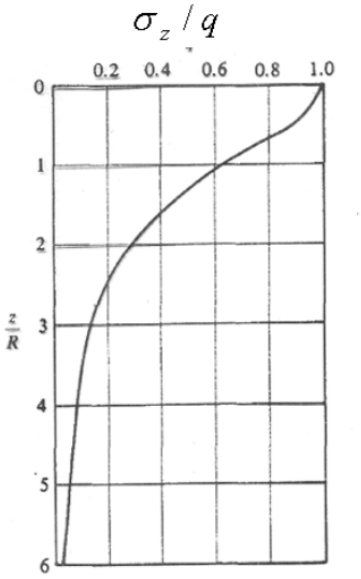


Variation of $\sigma_z/q$ with z/R

| z/R | $\sigma_z/q$ |
|---|---|
| 0 | 1 |
| 0.02 | 0.9999 |
| 0.05 | 0.9998 |
| 0.10 | 0.9990 |
| 0.2 | 0.9925 |
| 0.4 | 0.9488 |
| 0.5 | 0.9106 |
| 0.8 | 0.7562 |
| 1.0 | 0.6465 |
| 1.5 | 0.4240 |
| 2.0 | 0.2845 |
| 2.5 | 0.1996 |
| 3.0 | 0.1436 |
| 4.0 | 0.0869 |
| 5.0 | 0.0571 |

**Intensity of stress under the center of a uniformly loaded flexible area**

*Figure 125: Boussinesq's distribution under circular loaded surface*

We note that at the center axis under the load, the z-direction stresses are at their maximum as a function of depth. The shear stresses along that axis are zero, and are at their maximum under the edges.

Comparing the two diagrams for $\sigma_z$ in the x-z plane, we see that in fact 2*D corresponds to 90% dissipation, 1*D corresponds to about 60%, and 10% is less than one radius.

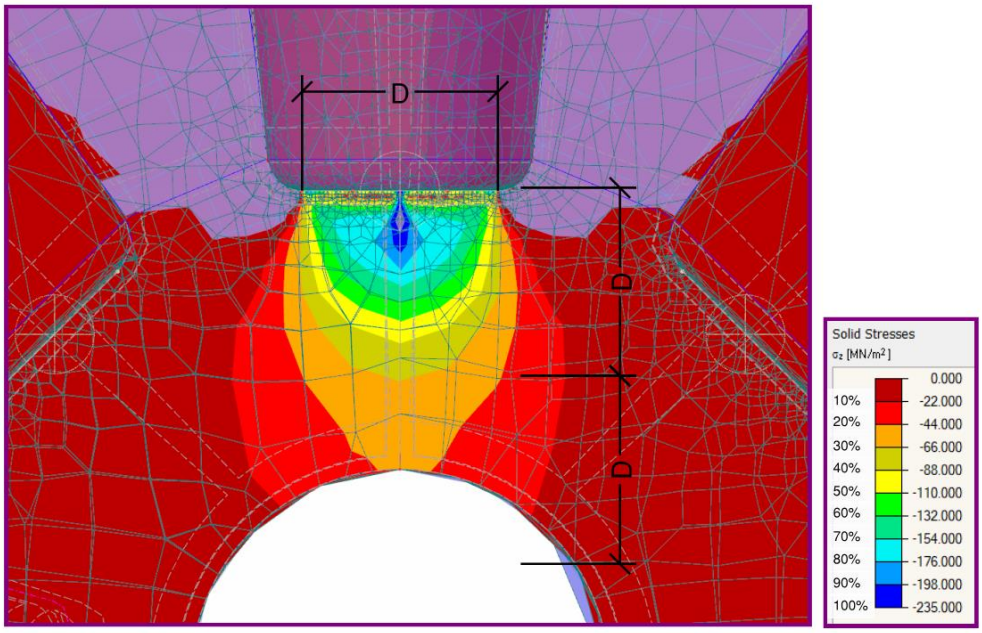


*Figure 126: $\sigma_z$ stress distribution x-z plane*

For $\sigma_z$ in the y-z plane, we note a slightly different distribution. 1D corresponds to 40% of the applied pressure. This difference is probably caused by modeling inaccuracies.

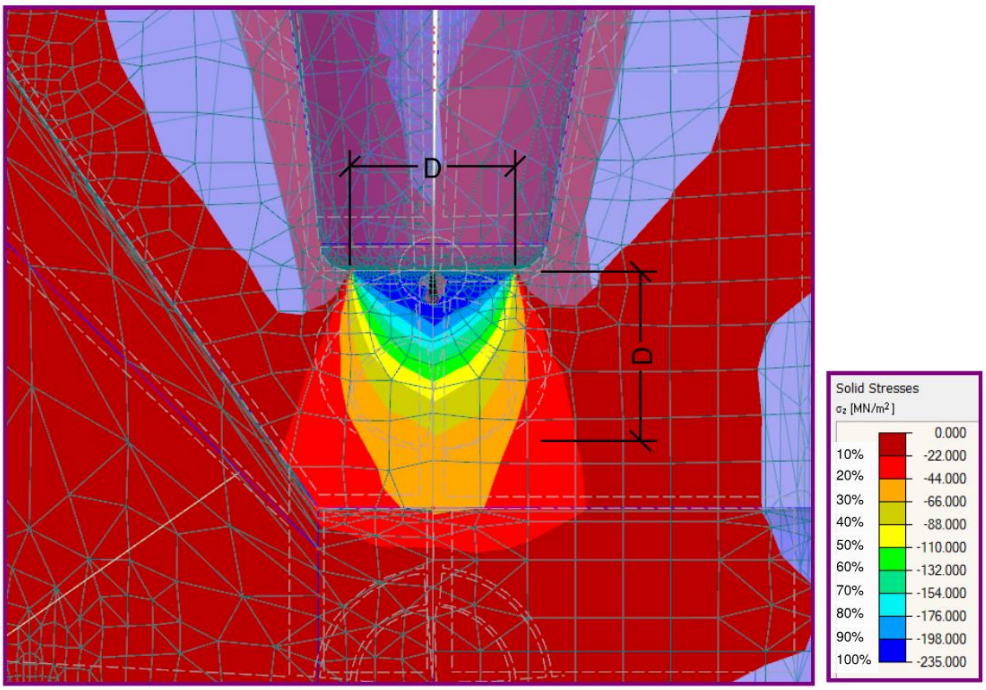


*Figure 127: $\sigma_z$ stress distribution y-z plane*

For the case of shear stress $\tau_{xz}$ we see similar distribution patterns as in Boussinesq's diagram. At a little less than 1D, stresses are at 20%*q and at about half D they are 30%*q.

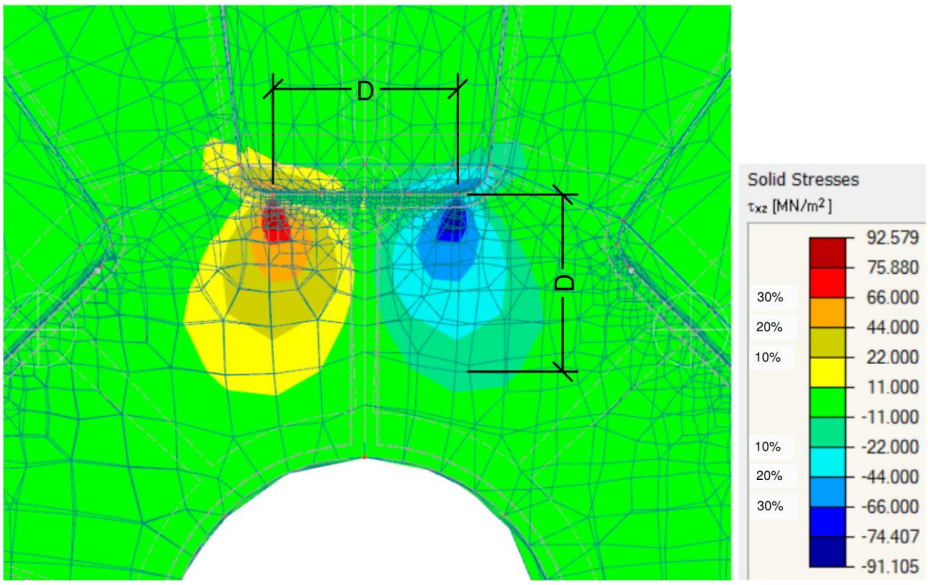


*Figure 128: $\tau_{xz}$ stress distribution*

## 8.5. Maximum tension

We are now going to evaluate the stresses coming from a tensile force in the connecting member. The contact area around the cone base is actually compressed as the member pulls outward.

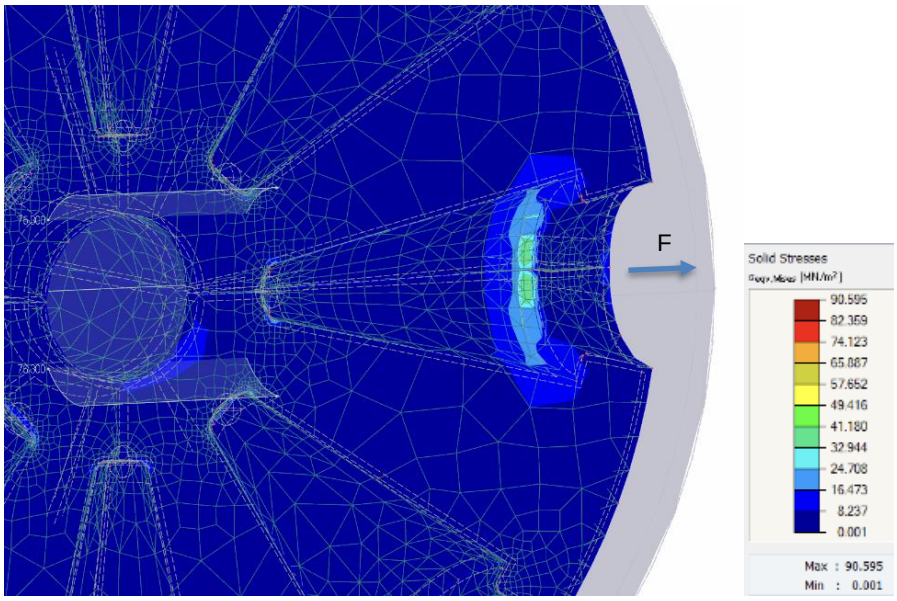


*Figure 129: Von Mises* stresses

It is noted that the real maximum stress due to compression on the contact area is:

$$F/A = 5.83\ kN/166\ mm^2 = 35\ MPa$$

The 90MPa on the scale corresponds to tiny numerical peaks in irrelevant parts of the node. It is also important to note that in the RFEM model this load is actually modeled as a line load instead of a uniform pressure because of some modeling constraints. This is a probable reason for the peaks we are seeing, as the load is not actually distributed in the larger area.

Our given pressure, 35 MPa, is well below the yield capacity therefore there is no concern about plastifying under tension in the node. Optimizing the node in tension would perhaps entail reducing the contact surface but as it is already just a few millimeters wide, it is not truly necessary and wouldn't save much material.

When in tension the node on its solid interface tends to open up. The corresponding deformation for the 5.9kN tension is 0.0031mm, which is negligible.

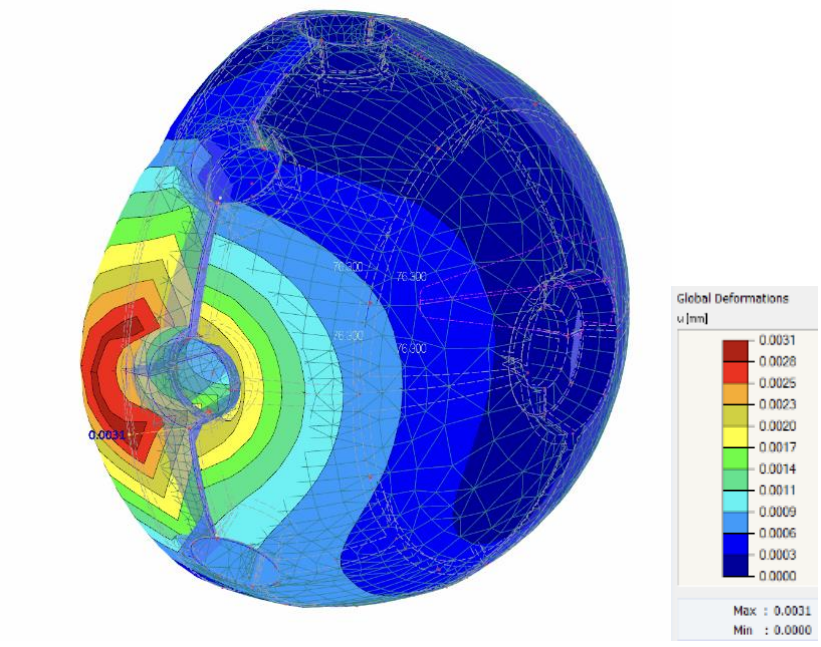


*Figure 130: Deformation under tension*

## 8.6. Case of interior node

In this case an interior node is studied with the effect of shear from the cladding panel weight. The axial forces in the connecting members are shown below.

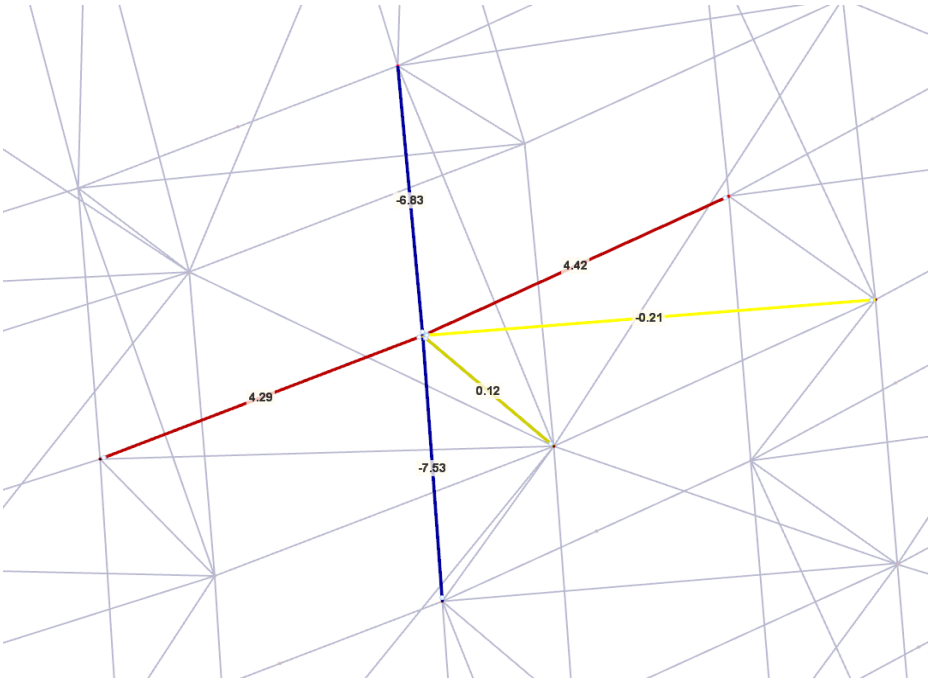


*Figure 131: Interion layer node*

As we see in the node model, the maximum stress is 196 MPa. Higher values are due to local numerical peaks of the model that we can ignore unless verified via physical testing to scale.

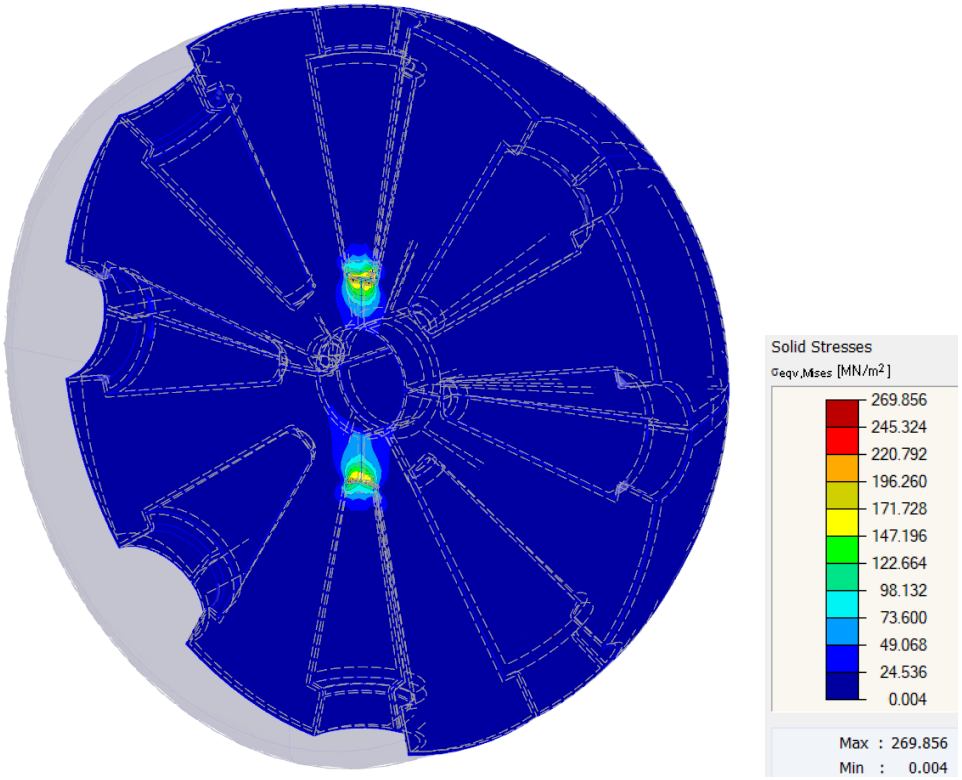


*Figure 132: Von Mises* stresses

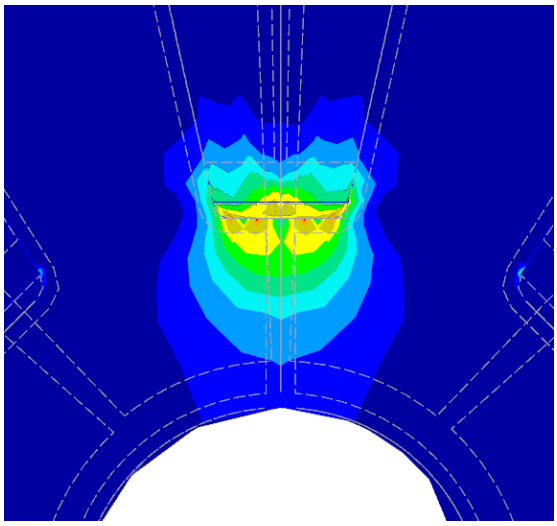

*Figure 133: Point local peaks*

## 8.7. Case with moment load

In this scenario the bending moment from the global model has been studied. This is for the case where we remove all the releases from the dome model and replace them with moment connections, as in reality the node blocks rotation to some degree.

The stresses caused by bending are given by the formula:

$$\sigma = M/S$$

where S is the section modulus and M the bending moment.

However, the node is a solid with non-uniform complex sections and it is difficult and imprecise to determine and hand calculate the equivalent cross section, so we are not going to use the previous formula. We are rather going to read the VM stresses directly from the model. The maximum moment is 0.02 kNm (taken from the global model with no releases) so we are applying 1kN force at 0.02m lever arm.

We note here that the 0.02kNm is almost negligible. It is reasonable to say that when a truss is designed to work with releases at the member's ends, no significant moment would be developed if the releases are replaced with fixed moment connections.

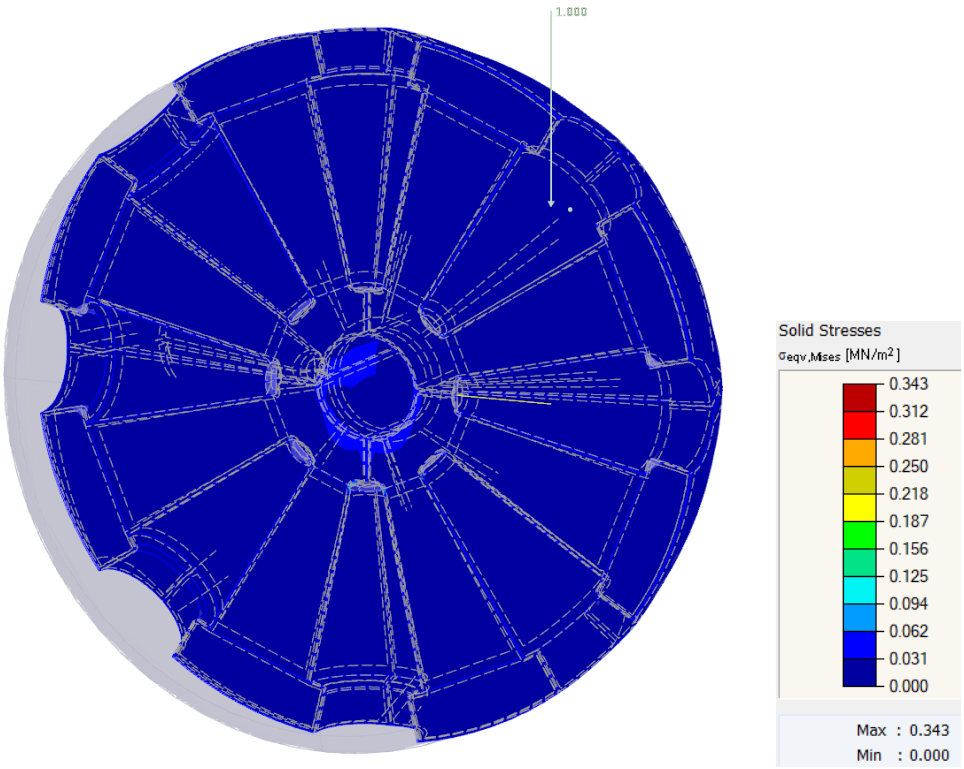


*Figure 134: VM stresses due to 0.02kNm moment*

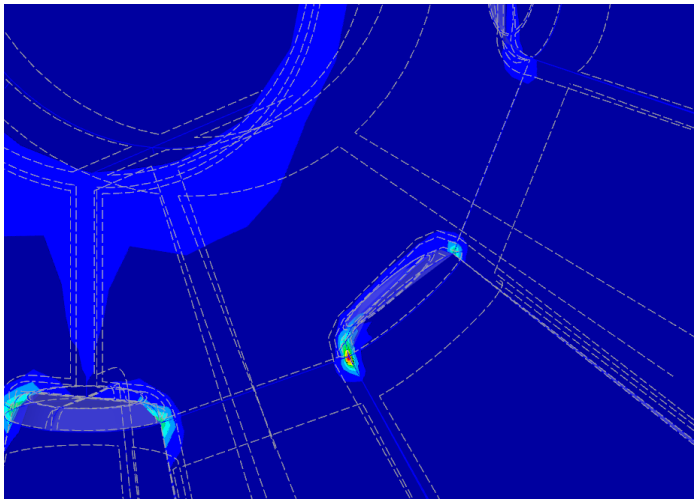

*Figure 135: Local stress peaks*

We can see that even including the peaks the maximum stress caused by bending is 0.3MPa which is a negligible addition to our previous values.

# 9. Member verification

Member end cone failure under compression:

The material properties for the members are the following:

Aluminium 6060 T6:

fo=160 MPa
fu=215 MPa
$\gamma_{M1}$=1.10, $\gamma_{M2}$=1.25

We are going to test the member cone under the maximum compression considering the increased end section found previously while checking the steel node in compression.

A = 70.5mm$^2$ (area required by steel node check)

The strength of the aluminum section in compression is:

$N_{c,Rd} = A_g f_o/\gamma_{M1}$ = 10.25 kN < $N_{Ed}$ = 15.5 kN

We see that the axial compressive strength is lower than the load applied, therefore the section needs to be further increased.

The required area to withstand $N_{Ed}$ = 15.5 kN of compression would be:

Ag=106.6 mm$^2$
A_flat = Ag - 7.32 mm$^2$ = 99.2 mm$^2$ ⇒ R=5.62mm minimum
D_total = 5.62*2+0.45*2 =12.1 mm

The corresponding applied pressure is then 15.5kN/Ag = 145.5MPa.

In RFEM we verify that the equivalent Von Mises stresses remain below 160/1.1=145.5MPa.

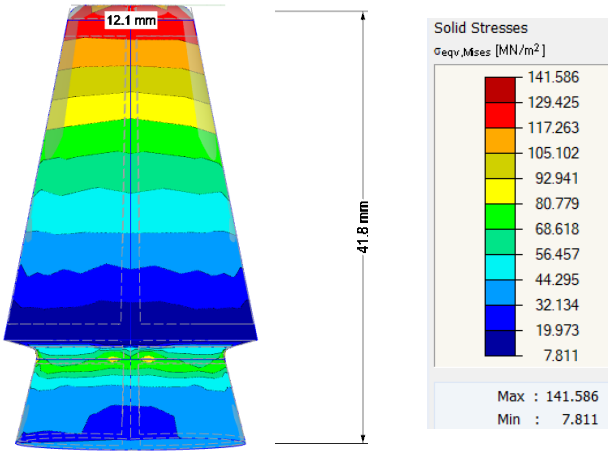


*Figure 136: VM stresses under 15.5kN compression*

We see below in elevation the initial and final shapes of the aluminum cones. In the second modified option, the height has been decreased to 41.8mm as that has no effect on the maximum stresses. Further decrease is possible but the aluminum saved would be replaced with steel from the node which is undesirable since it is heavier.

For the rod passing through the node, if the maximum compression force is applied to it, its cross section is more than 12.1mm (it is 2cm), so yielding is not a risk.

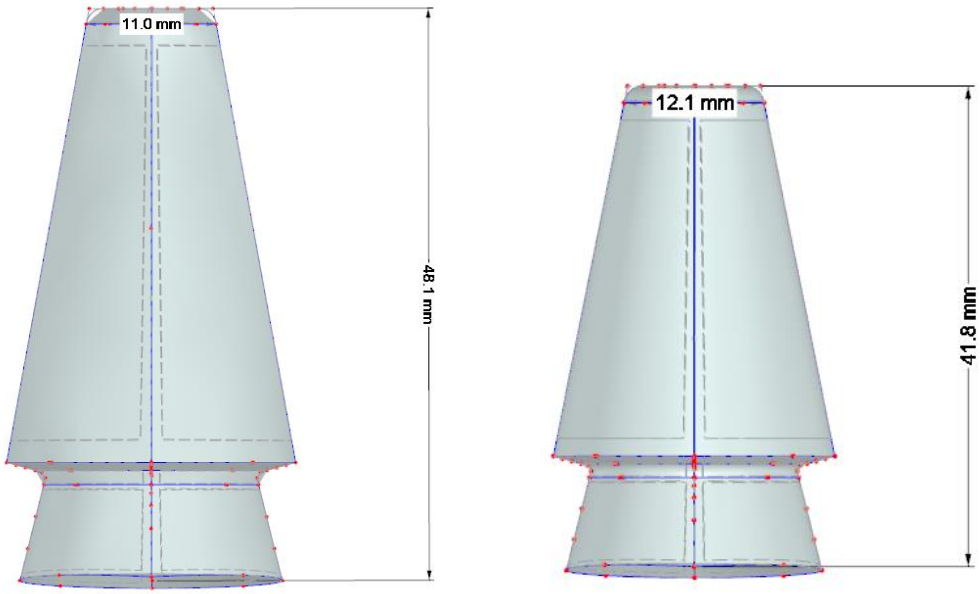


*Figure 137: Initial and modified cone shape*

Under compression the area at the base of the cone is under risk of expanding so the node must have a tolerance to allow that deformation.

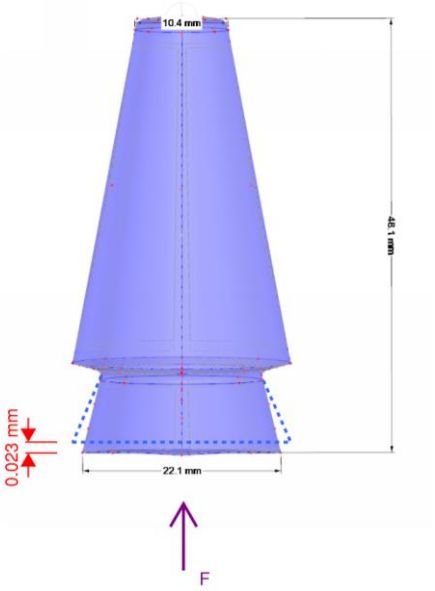


*Figure 138: Expansion*

$$\varepsilon = \Delta l/L \Rightarrow \sigma/E = \Delta l/L \Rightarrow F/AE = \Delta l/L \Rightarrow$$

$$\Delta l = 15.5 * 48.1/(70000 * 464) = 0.023mm$$

$$v = \varepsilon_x/\varepsilon_y \Rightarrow \Delta l_h = v\, L_h\, \Delta l_v/L_v = 0.3 * 24.3mm * \Delta l/48mm$$

$$\Delta l_h = 0.0035mm$$

So, considering the initial length, the oversized sleeve needs to be greater than:

$$\sqrt{{\Delta l_h}^2 + {\Delta l_v}^2} = 0.023mm$$

The minimum gap requirement based on 3D printing tolerances and margin required for adjustability is 0.2mm, so this satisfies the previous check.

We are now going to test the cone in tension of 5.8kN.

We apply a surface load at the area of contact between node and member near the base of the cone. The resulting stresses are 69.3MPa which is well below the yield limit.

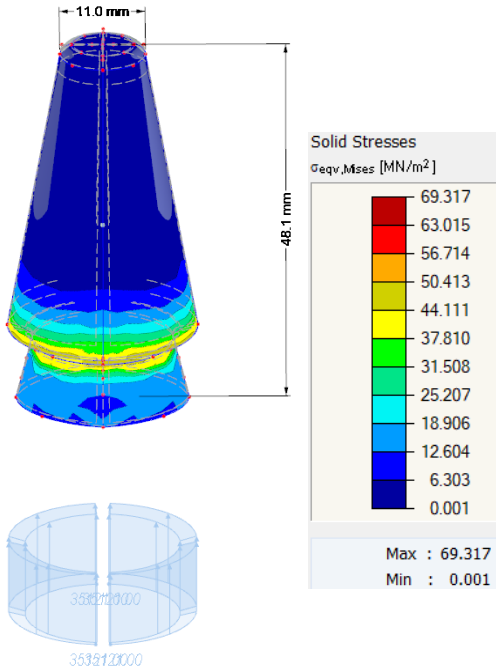


*Figure 139: VM stresses for tension*

Tension check at the throat of the cone:

If we do a hand check for the thinned section of the cone in tension, we see that the current diameter of 18mm is sufficient.

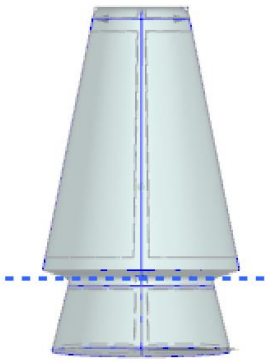

*Figure 140: Cross-section in tension*

$$D = 18mm$$
$$A = 254.5\ mm^2$$
$$p = 5.83\ kN\ /A = 22911\ KPa\ <\ 160MPa$$
$$utilization =\ 0.16$$
$$A_{min}\ =\ 25\ mm^2\ \rightarrow\ D_{min}\ =\ 6\ mm$$

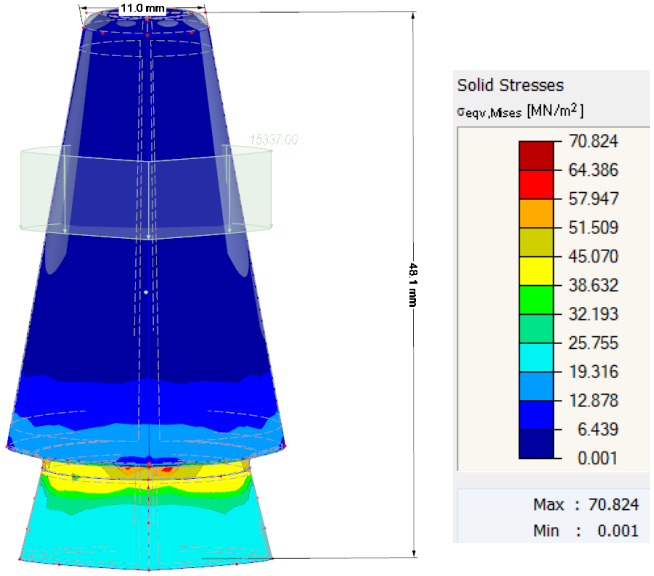


*Figure 141: VM stresses for cone in tension*

We note that although it is possible to reduce the throat section, it is not necessarily a good design decision as that would entail an increase of node material instead.

For the aluminum rod passing through the node, we can safely say that it is not under risk of yielding in tension given its diameter is over 6mm.

## 10. Optimization

The initial weight of the node was over 6kg, which is very heavy for the dome construction and excessive in terms of use of materials.

The zone in between cones is not utilized in either tension or compression, so one option is to increase the porosity in 3D printing for that area. This however is very difficult to simulate in the FE software so it would have to be verified by some 1:1 scaled testing.

In the tension/compression simulations below we see which areas of the node are stressed each time.

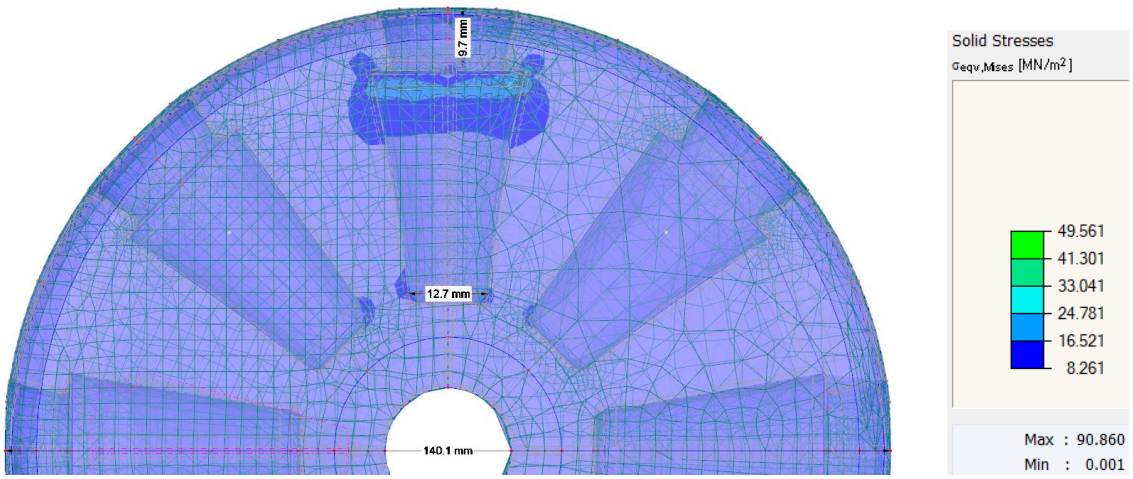


*Figure 142: Initial geometry under tension - VM stresses*

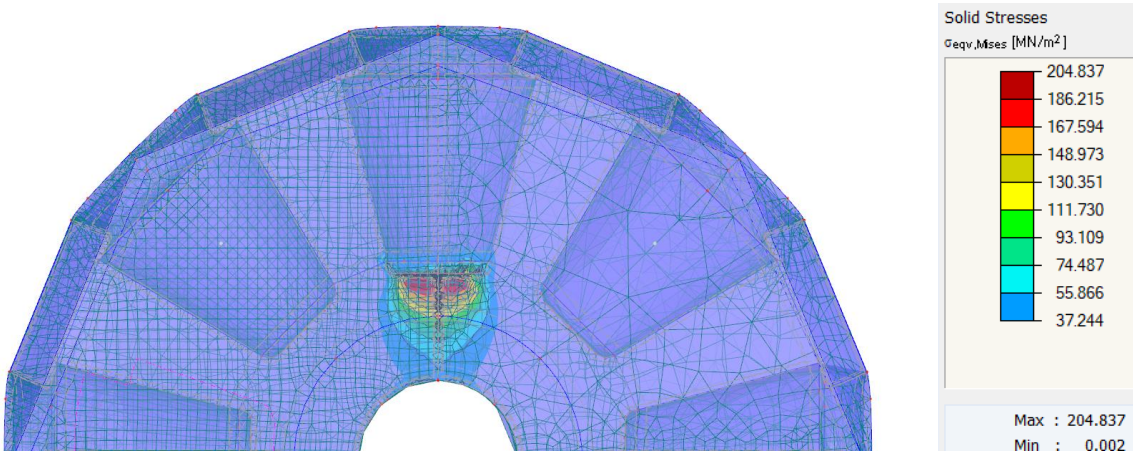


*Figure 143: Geometry under maximum compression*

The compression load only activates the area around the center of the node. We note that already the zone is utilized from 90% to about 20% so reducing it further would create higher stresses and possibly local peaks. So this central zone is considered to be well designed already.

As we saw in the previous result diagrams the area between cones is not really utilized. The current cone length can also be reduced to decrease this unused zone by making the cones shorter as well as the total node diameter.

Reducing the diameter from 140.1mm to 120.1mm by minimizing the area around the sides of the cone does not seem to have an impact on the maximum stresses due to tension loading.

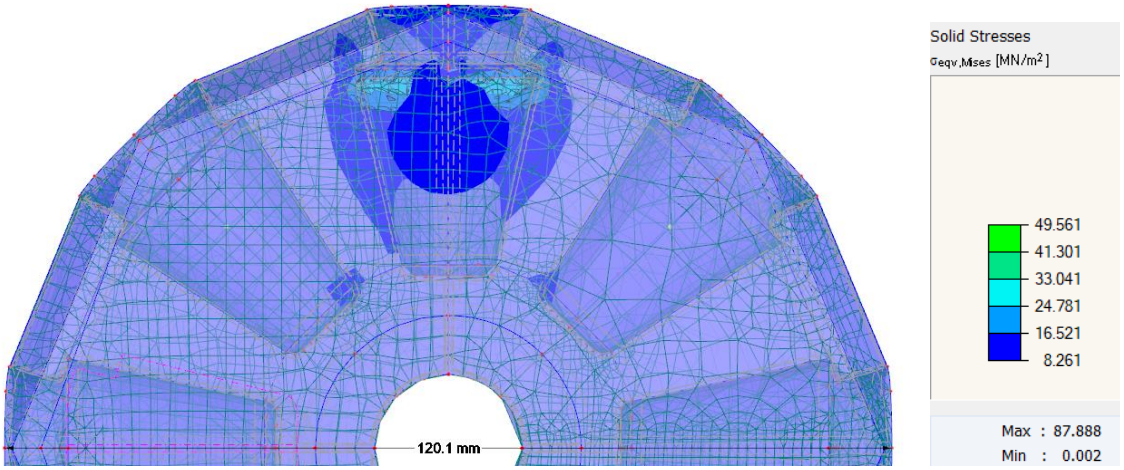


*Figure 144: 120.1mm diameter node in tension*

In the following loading scenario, a 108.1mm diameter node has been tested with the maximum tension in the middle member and 50% of that to the two neighboring ones.

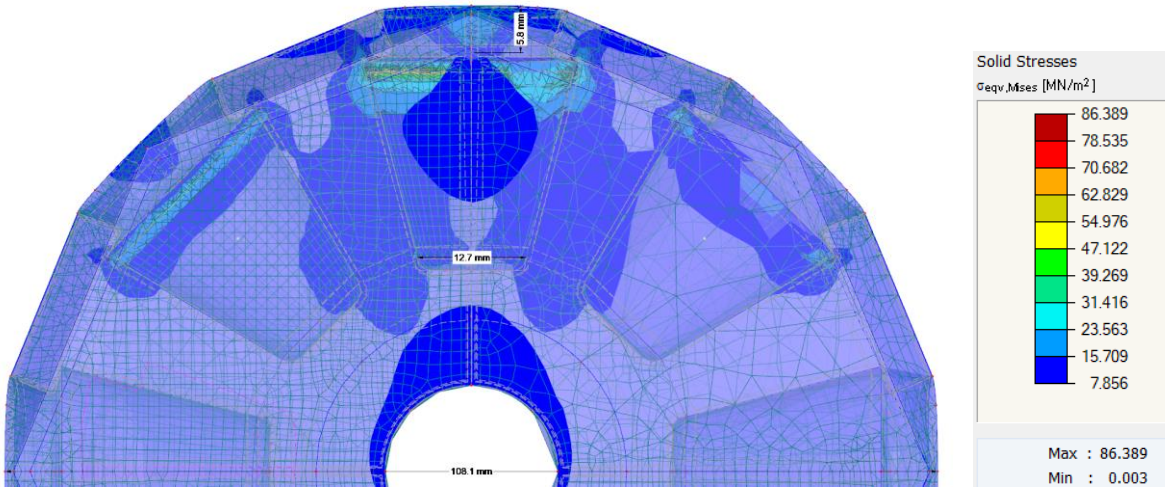


*Figure 145: 108.1mm node geometry in tension*

It appears by reducing the diameter from 140mm to 108mm there is still no difference in the resulting maximum stresses. The weight of the node in this case is 2.5kg.

Further optimization is still possible in theory. The numerical model's limitations however, have been reached at this point. Reducing the diameter further distorts the existing solid geometry and the model fails to run. After the 1:1 lab physical testing takes place for the 108mm diameter node, and on the condition that the results are satisfactory, some more tests can be conducted with an even smaller diameter to fully optimize this design to its capacity.

Angle adjustability:

In terms of the angle adjustability, the initial design (140mm diameter) allowed a minimum 29-degree angle between members with a minimum distance between them equal to 3mm. See figure below.

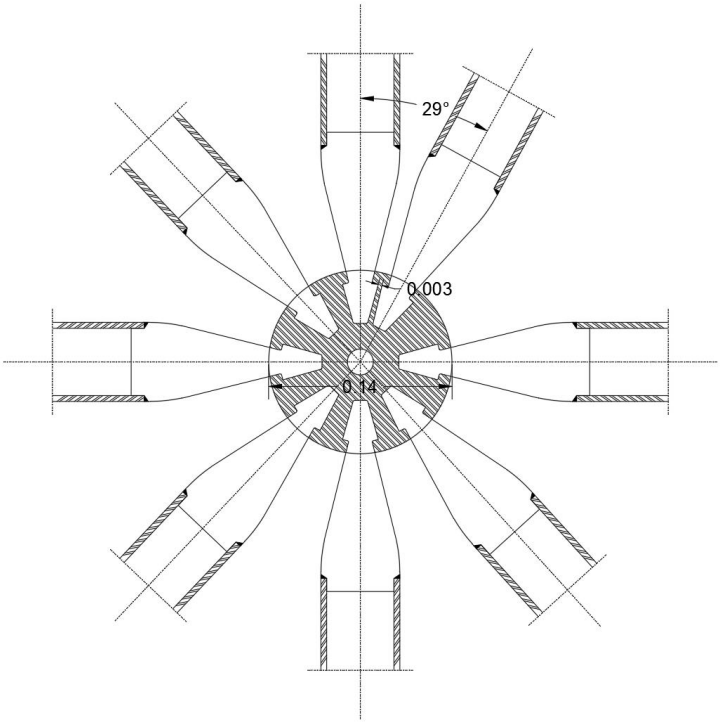


*Figure 146: Initial minimum angle between members*

For the optimized node the minimum possible angle is increased to 35º in order to have the same 3mm material thickness in between. This is due to the reduction of diameter without thinning the throat of the member cones.

In the two following cases the maximum tension and compression load has been applied to the middle member and 50% of that has been applied to the two neighboring ones. The in between angles are 35-degrees.

Under compression, we see that there is interaction of the stress bulbs in the central zone which has stress values of about 20% the capacity in that area. In total, the maximum stresses are same as before (205 MPa).

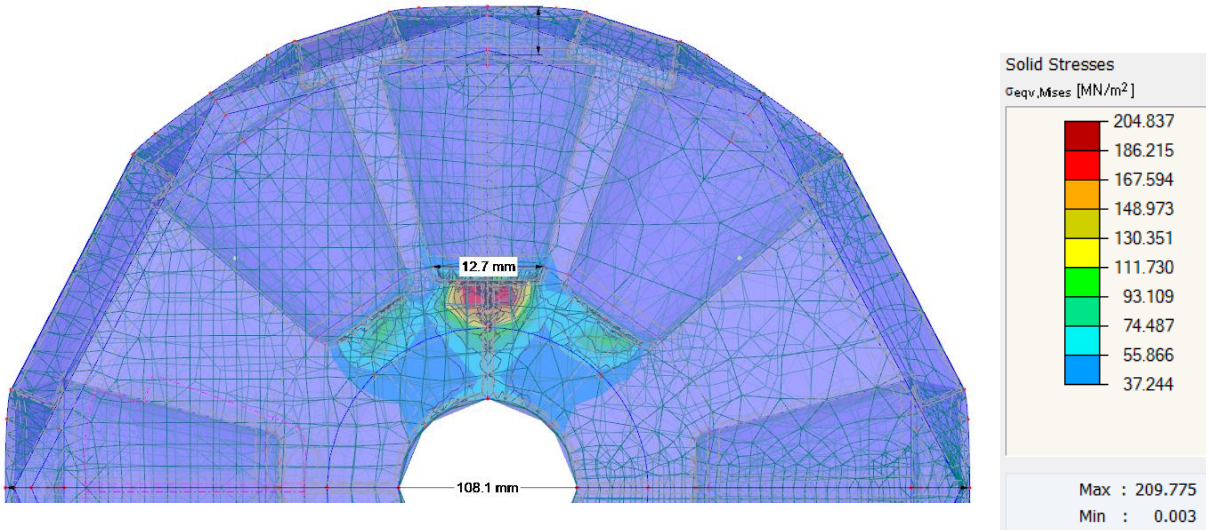


*Figure 147: 35d angle variation under compression loads*

Under tension, there is some interaction in the zone between cones, but the maximum VM stress remains below the limit yield limit.

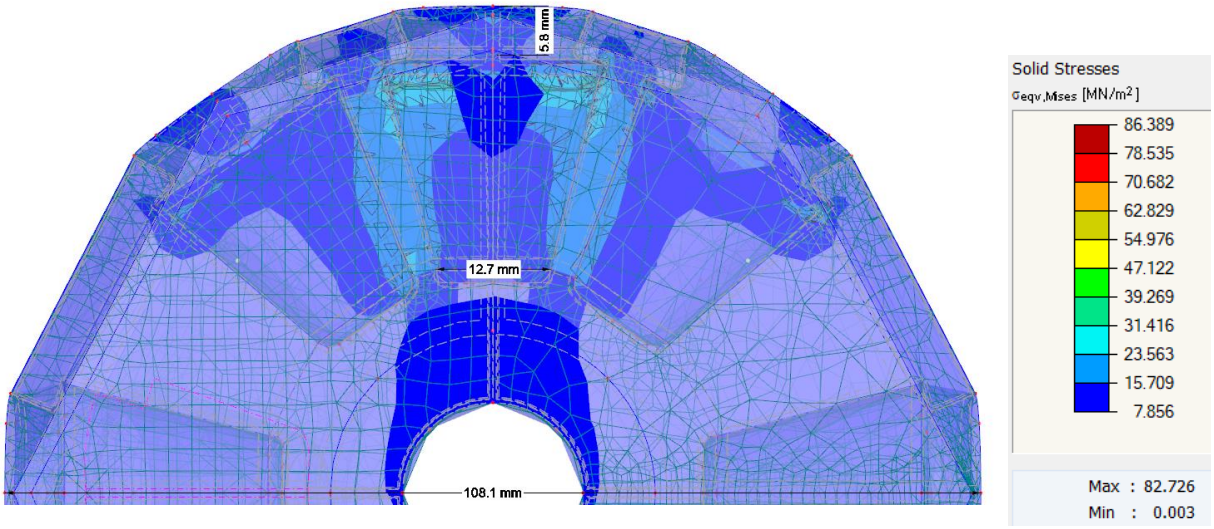


*Figure 148: 35º angle variation under tensile loads*

The maximum tension applied from a member that would cause yielding of the node is approximately 39kN without considering a partial factor.

$$F = f_y * A = 39\ kN$$

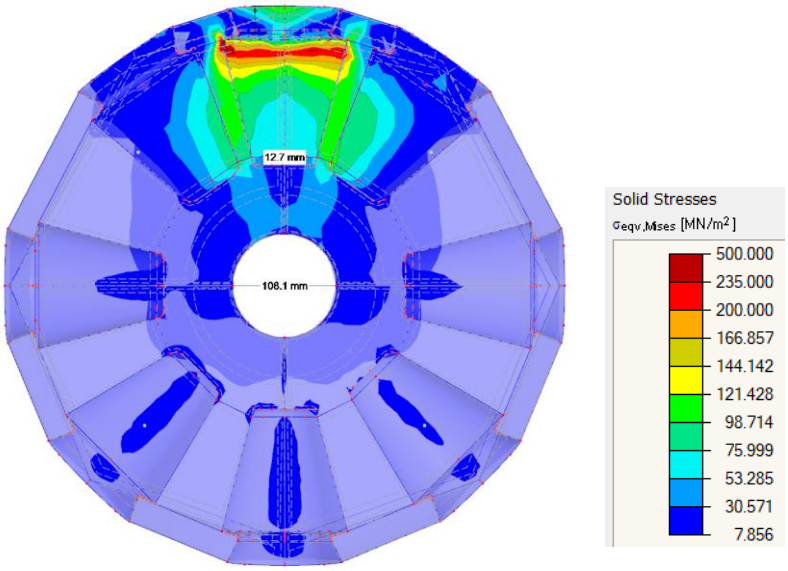


*Figure 149: Stresses under 39kN tensile load*

The previous result is verified in RFEM, and indeed the maximum stresses remain below 235MPa, with a few peaks reaching 500MPa where the separate solid elements connect in the model.

# 11. Environmental self-assessment

In this section, we are going to look into the placement of the thesis project in terms of the "green budget" criteria. The green budget (Ministry of the Economy, Finance and Industrial and Digital Sovereignty, 2023) is a method used by the state to classify its expenditure, according to their impact (favorable, neutral, or unfavorable) on six criteria:

1. the fight against climate change,
2. adaptation to climate change and prevention of natural risks,
3. management of water resources,
4. the transition to the circular economy, waste management and prevention of technological risks,
5. the fight against pollution,
6. the preservation of biodiversity and the protection of natural, agricultural and forestry areas.

Our dome is composed of aluminum members and steel nodes. In terms of the choice and use of materials the project has some important advantages. It is well known that 75% of all aluminum ever produced (starting decades ago) is still in use today. Therefore, it plays part in the circular economy while reducing waste and ensuring the used parts don't go into landfill but are fully recycled. Recycled aluminum has about 90% less carbon footprint than new aluminum, resulting in less air and water pollution. Also, aluminum's high strength-to-weight ratio makes it especially useful as a structural material, weighing up to 65% less than steel. This is especially important when it comes to transporting the members to the construction site. A lighter load on the trucks means less energy used on the transportation and therefore less pollution. While other materials such as wood, may be more sustainable, they would not be suited for this kind of design and would pose restraints on different parameters of the structure.

The nodes on the other hand, are required to be in steel which is also 100% recyclable. One of the possible options that are being considered for the nodes is to 3D print them in steel. Recycling steel scraps into Additive Manufacturing (AM) grade powder is something many companies have been looking into. The choice to use AM for the making of the nodes also means there would be no wasted material in the manufacturing process. Both aluminum members and steel nodes will be fully recyclable after their life cycle in this project is complete.

Considering all the above, we can safely say that the contribution of the Limes360 project to the "green budget" criteria is generally favorable.

# 12. Conclusions

Limes360 is an ambitious project aimed at creating an innovative digital theater space with a modular spatial truss structure. The design of the 3D truss nodes and their structural analysis are essential elements of this project. Different dome geometries have been explored to determine the most efficient in terms of structural performance and lightweight design. Finite element analysis of the nodes has allowed for optimizing their shape to minimize the weight while keeping local stresses below the elastic limit.

Regarding nodal analysis, we can say that even though the initial design of the node was satisfactory in terms of geometry and angle adjustment, some changes were necessary to make it work within this spatial truss. The general idea for the node was to have a simple system with few parts or fasteners that could be assembled quickly.

The required changes involve the dimensions of the cone tip slots where the elements connect and a reduction in the node's diameter to bring down the total weight to a reasonable level.

Before moving on to the construction phase, 1:1 laboratory testing would be necessary to verify this analysis. Indeed, such a product is innovative, has never been used before, and possesses complex characteristics. The tests would ensure that the behavior and limits are as predicted above.

Limes360 represents a fascinating example of the convergence of architecture, engineering, and technology to create a one-of-a-kind performance space.

## References


1. EN 1991-1-1, 2002. *Eurocode 1 : Actions on structures. General actions. Densities, self-weight, imposed loads for buildings*
2. EN 1993-1, 2005. *Eurocode 3: Design of steel structures*
3. EN 1999-1, 2007. *Eurocode 9: Design of aluminium structures*
4. Herbert KLIMKE, Jaime SANCHEZ, 2020. *Design, analysis, and construction of space structures: The Mero Legacy.* Available at: https://www.researchgate.net/publication/340488188_The_Mero_Legacy
5. Tien T. LAN, 1999. *Space Frame Structures, Structural Engineering Handbook*. Ed. Chen Wai-Fah, Boca Raton: CRC Press LLC. Beijing
6. M. F. A. ELFAWAL, 2014. *The technical and feasibility selection of space truss construction systems*. WIT Transactions on The Built Environment, Vol 136, 2014 WIT Press. www.witpress.com, ISSN 1743-3509
7. Cleirton André SILVA DE FREITAS, Luciano MENDES BEZERRA, Ramon SALENO YURE COSTA SILVA, 2011. *Numerical and Experimental Study of Steel Space Truss with Stamped Connection*. Vol. 5, No. 6 (Serial No. 43), p. 494-504, Journal of Civil Engineering and Architecture, ISSN 1934-7359, USA
8. Welington V. SILVA, Ramon SILVA, Luciano M. BEZERRA, Cleirton A. S. FREITAS and Jorge BONILLA, 2020. *Experimental Analysis of Space Trusses Using Spacers of Concrete with Steel Fiber and Sisal Fiber.* Materials 13(10):2305
9. John CHILTON, 2000. *Space Grid Structures.* Architectural Press. ISBN 0 7506 3275 5. England Available at: https://library.uoh.edu.iq/admin/ebooks/34182-space_grid_structures.pdf
10. Wilfried LAUFS, 2021. *Tragende 3D-Druck-Verbindungsknoten für Metallanschlussstäbe*, Stahlbau
11. Erwin HEINLE, Jörg SCHLAICH, 1996. *Kuppeln aller Zeiten - Kuppeln aller Kulturen.* ISBN-10 3421030626
12. E. J. HEARN, 1997. *Mechanics of Materials 2: An Introduction to the Mechanics of Elastic and Plastic Deformation of Solids and Structural Materials*. Third Edition. University of Warwick, United Kingdom
13. M. J. FAGAN, J. MCCONNACHIE, 2001. *A review and detailed examination of non-layered conformal contact by finite element analysis.* Journal of Strain Analysis Vol 36 No 2. United Kingdom
14. ESDEP - European Steel Design Education Program. *Lecture 14.5: Space Structure Systems*. University of Ljubljana. Available at: http://fgg-web.fgg.uni-lj.si/~/pmoze/esdep/master/wg14/l0500.htm
15. Virginia Polytechnic Institute and State University, 2011. *Issues Related to the Design of Spatial Structures: Effective Buckling lengths.* Available at: https://www.setareh.arch.vt.edu/safas/008_design_05_IRDSS_3_EffectiveBucklingLength.html
16. Markforged. *Three benefits of 3D printing metal parts.* https://markforged.com/fr/resources/learn/design-for-additive-manufacturing-metals/metal-additive-manufacturing-introduction/benefits-of-3d-printing-metal-parts
17. PROTOLABS. *Direct Metal Laser Sintering*. https://www.protolabs.com/services/3d-printing/direct-metal-laser-sintering/
18. GEOMETRICA. *Domes & Triodetic node.* https://www.geometrica.com/

# APPENDIX

## 1. Dynamic analysis – 30 first modes

| E-vector | Natural Frequency | Natural Period | Modal Mass | Effective Modal Mass Factor | | |
|---|---|---|---|---|---|---|
| No. | f [Hz] | T [s] | $M_i$ [kg] | $f_{meX}$ [-] | $f_{meY}$ [-] | $f_{meZ}$ [-] |
| 1 | 6.768 | 0.148 | 494.39 | 0.000 | 0.000 | 0.000 |
| 2 | 7.063 | 0.142 | 9955.25 | 0.000 | 0.706 | 0.000 |
| 3 | 7.861 | 0.127 | 419.23 | 0.000 | 0.000 | 0.000 |
| 4 | 8.049 | 0.124 | 8809.08 | 0.738 | 0.000 | 0.000 |
| 5 | 8.066 | 0.124 | 350.63 | 0.002 | 0.000 | 0.000 |
| 6 | 10.640 | 0.094 | 227.26 | 0.000 | 0.000 | 0.000 |
| 7 | 10.925 | 0.092 | 1527.39 | 0.000 | 0.000 | 0.179 |
| 8 | 12.332 | 0.081 | 2574.94 | 0.000 | 0.079 | 0.000 |
| 9 | 13.373 | 0.075 | 2700.89 | 0.045 | 0.000 | 0.000 |
| 10 | 13.882 | 0.072 | 11045.26 | 0.000 | 0.000 | 0.000 |
| 11 | 15.211 | 0.066 | 4756.07 | 0.000 | 0.000 | 0.001 |
| 12 | 15.534 | 0.064 | 2695.32 | 0.000 | 0.000 | 0.004 |
| 13 | 16.252 | 0.062 | 4591.44 | 0.000 | 0.000 | 0.043 |
| 14 | 17.171 | 0.058 | 3880.96 | 0.000 | 0.003 | 0.000 |
| 15 | 17.454 | 0.057 | 4622.52 | 0.006 | 0.000 | 0.000 |
| 16 | 17.729 | 0.056 | 5454.89 | 0.000 | 0.000 | 0.001 |
| 17 | 18.510 | 0.054 | 1013.03 | 0.000 | 0.000 | 0.000 |
| 18 | 18.833 | 0.053 | 7542.22 | 0.000 | 0.000 | 0.000 |
| 19 | 19.218 | 0.052 | 3693.84 | 0.000 | 0.000 | 0.001 |
| 20 | 19.533 | 0.051 | 3988.98 | 0.000 | 0.000 | 0.000 |
| 21 | 19.766 | 0.051 | 147.34 | 0.000 | 0.000 | 0.000 |
| 22 | 19.992 | 0.050 | 144.26 | 0.000 | 0.000 | 0.000 |
| 23 | 20.367 | 0.049 | 140.01 | 0.000 | 0.000 | 0.000 |
| 24 | 20.989 | 0.048 | 132.12 | 0.000 | 0.000 | 0.000 |
| 25 | 21.125 | 0.047 | 2148.94 | 0.000 | 0.000 | 0.000 |
| 26 | 21.373 | 0.047 | 1648.28 | 0.000 | 0.000 | 0.098 |
| 27 | 21.648 | 0.046 | 1073.77 | 0.000 | 0.046 | 0.000 |
| 28 | 21.996 | 0.045 | 121.61 | 0.000 | 0.000 | 0.000 |
| 29 | 22.416 | 0.045 | 3354.40 | 0.002 | 0.000 | 0.000 |
| 30 | 22.504 | 0.044 | 2904.56 | 0.000 | 0.000 | 0.000 |
| | | | | 0.793 | 0.835 | 0.327 |

MODE 1 natural vibration

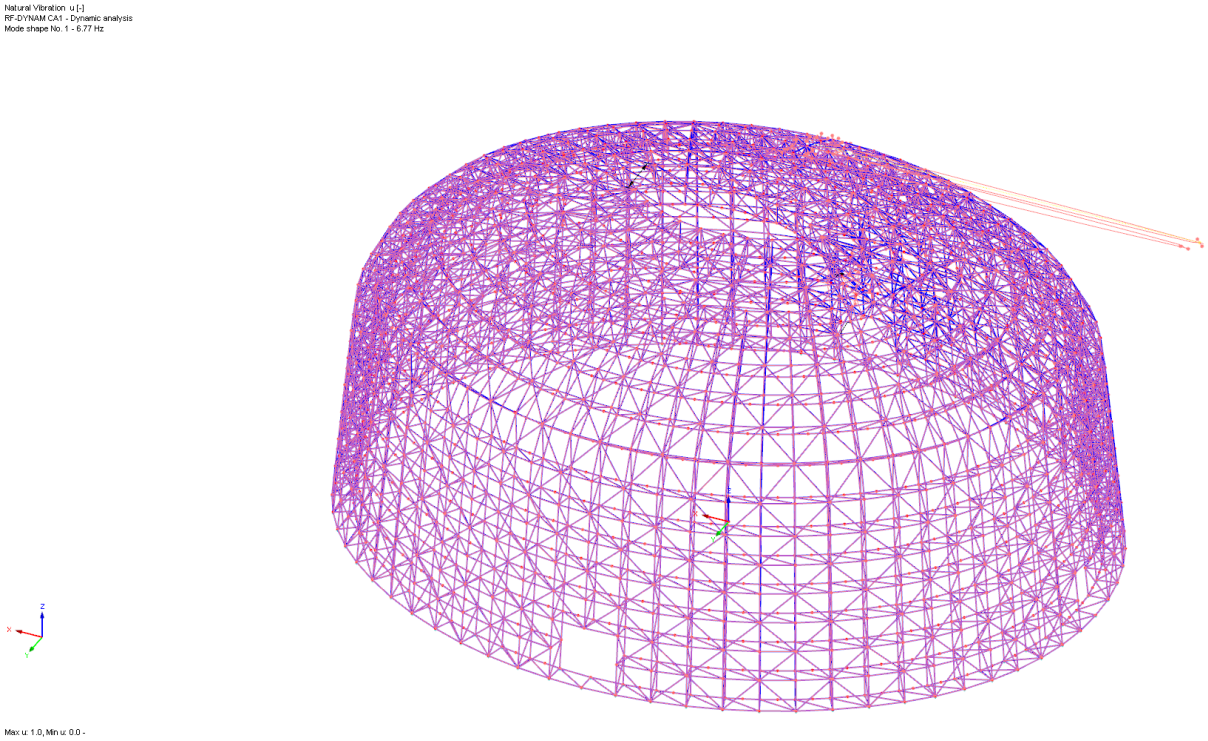

Mode no. 4 - sway

Natural Vibration u [-]
RF-DYNAM CA1 - Dynamic analysis
Mode shape No. 4 - 8.05 Hz

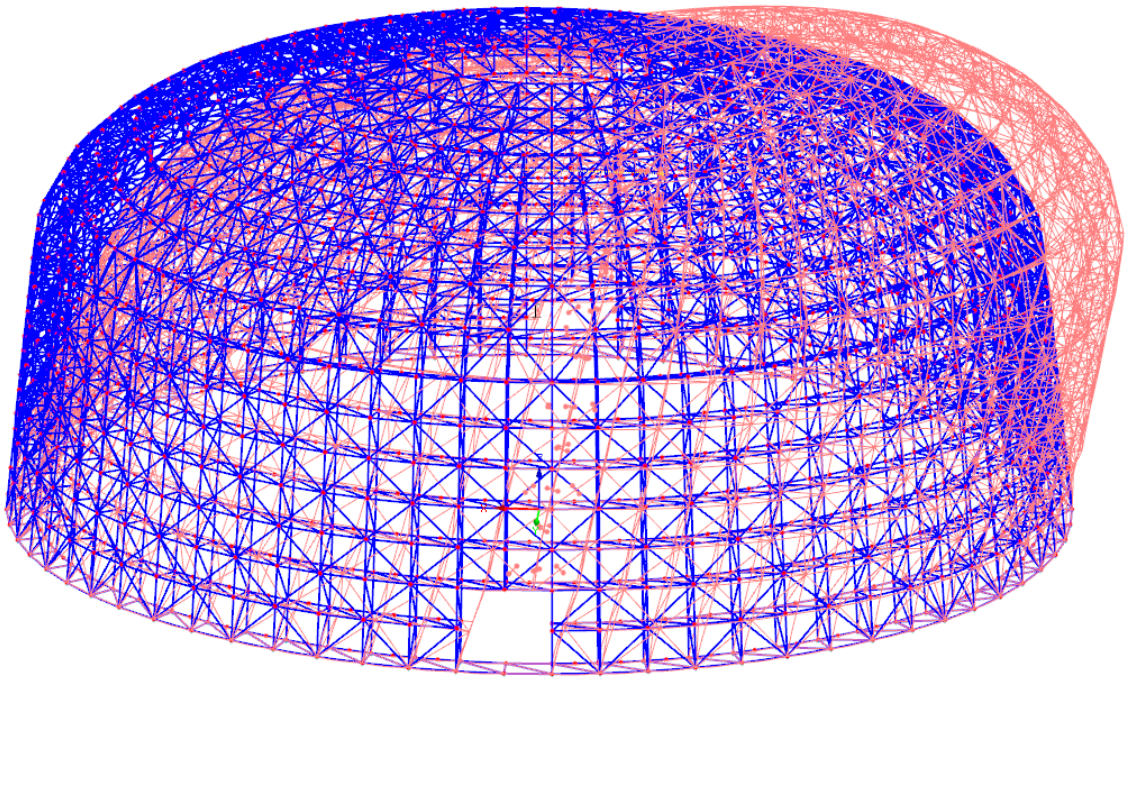


Max u: 1.0, Min u: 0.0 -

Mode no. 7

Natural Vibration u [-]
RF-DYNAM CA1 - Dynamic analysis
Mode shape No. 7 - 10.93 Hz

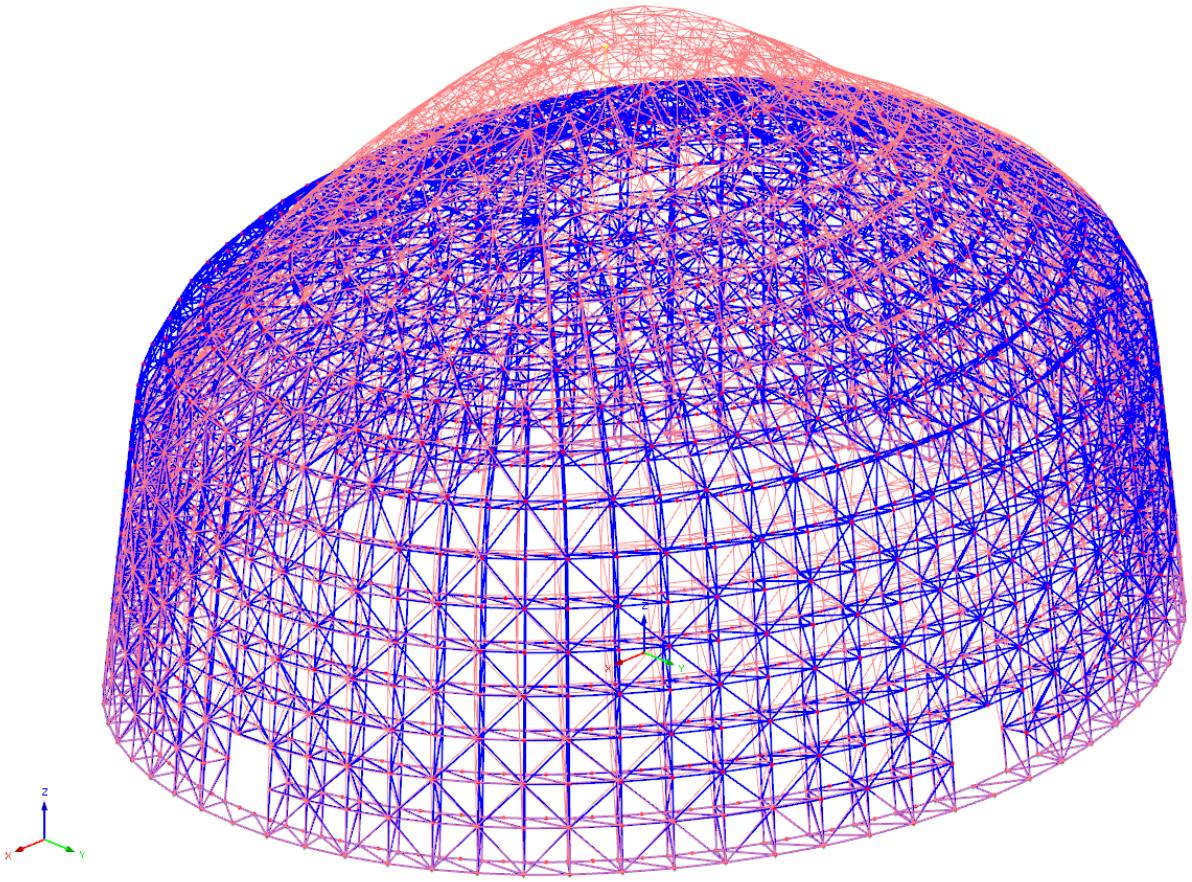


Max u: 1.0, Min u: 0.0 -

Mode no.11

Natural Vibration u [-]
RF-DYNAM CA1 - Dynamic analysis
Mode shape No. 11 - 15.21 Hz

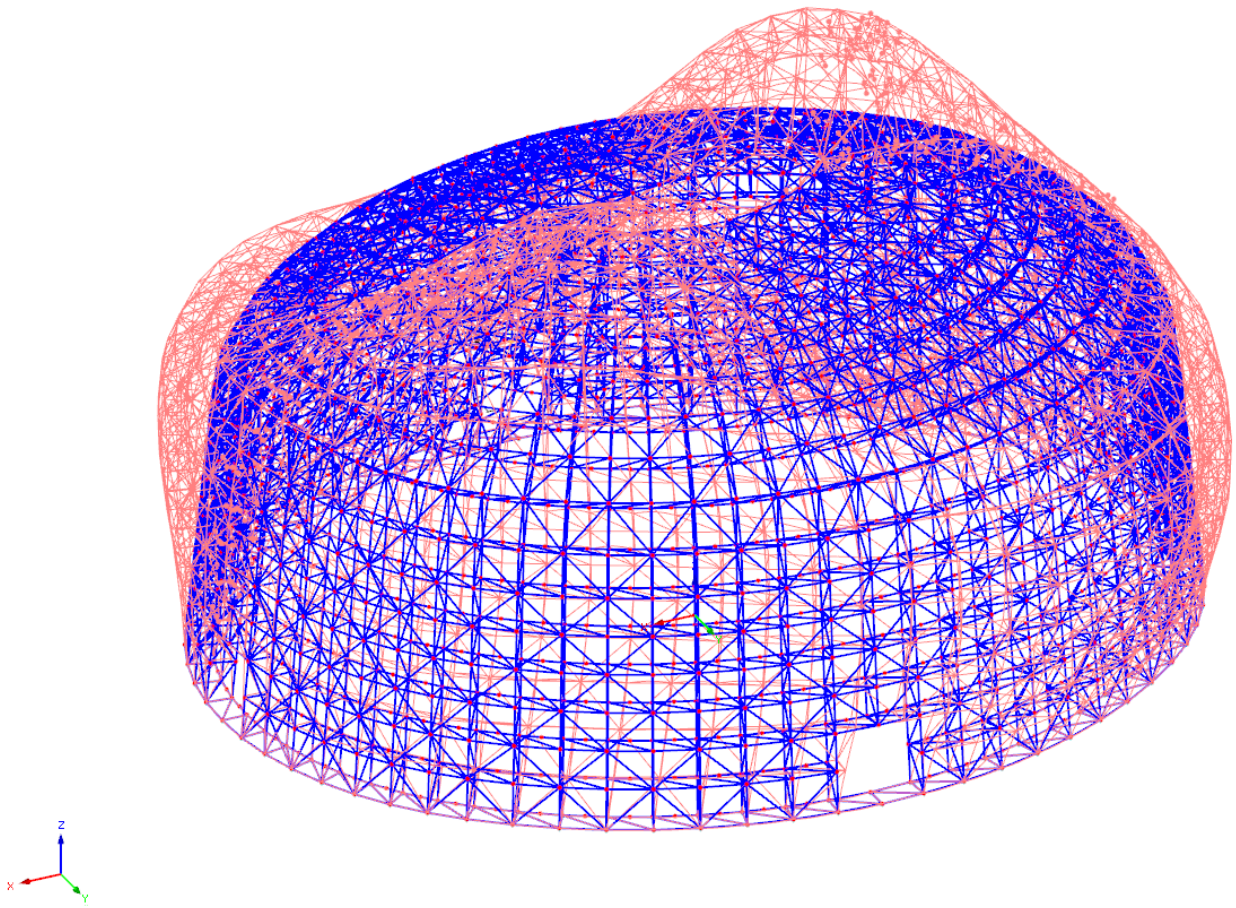


Max u: 1.0, Min u: 0.0 -

## 2. Temperature loading

Node deformation under 30 ºC temperature load;